FACULTY OF TEXTILE ENGINEERING TUL

Dissertation Thesis

Development of Flame Retardant Cotton Fabrics with Multifunctional Properties

Study programme:	P3106 Textile Engineering
Study branch:	Textile Technics and Materials Engineering
Author:	**Asif Javed, M.Sc.**
Thesis Supervisor:	Ing. Jana Šašková, Ph.D. Department of material engineering

Liberec 2024

Declaration

I hereby certify, I, myself, have written my dissertation as an original and primary work using the literature listed below and consulting it with my thesis supervisor and my thesis counsellor.

I acknowledge that my dissertation is fully governed by Act No. 121/2000 Coll., the Copyright Act, in particular Article 60 – School Work.

I acknowledge that the Technical University of Liberec does not infringe my copyrights by using my dissertation for internal purposes of the Technical University of Liberec.

I am aware of my obligation to inform the Technical University of Liberec on having used or granted license to use the results of my dissertation; in such a case the Technical University of Liberec may require reimbursement of the costs incurred for creating the result up to their actual amount.

At the same time, I honestly declare that the text of the printed version of my dissertation is identical with the text of the electronic version uploaded into the IS/STAG.

I acknowledge that the Technical University of Liberec will make my dissertation public in accordance with paragraph 47b of Act No. 111/1998 Coll., on Higher Education Institutions and on Amendment to Other Acts (the Higher Education Act), as amended.

I am aware of the consequences which may under the Higher Education Act result from a breach of this declaration.

May 6, 2024 Asif Javed, M.Sc.

ACKNOWLEDGEMENT

First and foremost, I am thankful to the Almighty ALLAH for giving me the strength and capability to successfully accomplish this research work. I am thankful to the administration of the Faculty of Textile Engineering at the Technical University of Liberec for granting me a scholarship to pursue my Ph.D. and for providing the necessary resources to conduct this research. Upon the completion of this dissertation, I am indebted to numerous individuals for their invaluable assistance. I would like to commence by expressing my deepest gratitude to Prof. Ing. Jiří Militký, CSc. Euring, as well as my supervisor Ing. Jana Saskova, PhD and Prof. Ing. Jakub Wiener, PhD for their support, motivation, encouragement, guidance, and collaboration throughout my doctoral studies. Their expert guidance helped me in every stage of my research and the writing of this thesis.

Furthermore, I would like to acknowledge the kind support and esteemed guidance of Ing. Blanka Tomkova, Ph.D. (Head of the Department of Materials Engineering). I am also immensely grateful to all the individuals at the Department of Material Engineering who consistently provided valuable assistance throughout the course of my dissertation. I am deeply appreciative of the regular help and support provided by Ing. Bohumila Keilová, Ing. Hana Musilová, Kateřina Nohýnková, Martina Čimburová, and Ing. Marie Kasprova, Ph D. I am truly thankful to the following individuals at The Institute for Nanomaterials, Advanced Technologies and Innovation: Dr. Jana Müllerová, and Dr. Pavel Hrabák for their provision of research facilities and assistance in my research work.

Additionally, I am forever grateful to my parents, sisters, and brothers for their support and motivation throughout my life.

Asif Javed

TABLE OF CONTENTS

ABSTRACT

Cotton's unique qualities, such as hydrophilicity, biodegradability, durability, high dye-ability, and comparatively low cost, make it a popular textile fabric. However, in contemporary times, people desire cotton fabric to possess multifunctional qualities that can provide safety based on the work place environment and weather conditions. The demand in the market has shifted towards flame retardant, UV protection, self-cleaning, antibacterial, permanently stiff textiles, and extensive studies are being conducted in these fields. Nanoparticles (NPs), for example, zinc oxide (ZnO), titanium dioxide (TiO_2), magnesium oxide (MgO), copper oxide (CuO), carbon nanotubes, silicon dioxide (SiO_2), and silver (Ag), exhibit remarkable functional properties. Among the various nanoparticles, zinc oxide (ZnO) emerges as the most environmentally friendly and relatively cost-effective option. ZnO can be applied to diverse substrates, including textile polymers and fabrics. Researchers have utilized different approaches for the deposition of ZnO NPs onto the fabric surface, such as in-situ synthesis and ex-situ deposition. However wash durability of the coated fabric is of great concern, moreover environmentally friendly, ecological functionalization of fabrics is the main demand of the present era.

The aim of the present research work is to develop a halogen and formaldehyde free ecological and durable flame retardant fabric along with multifunctional properties and to find the optimal conditions and parameters. In this research work, ZnO NPs were grown onto 100 % cotton fabric using the sonochemical method. Zinc acetate dihydrate ($Zn(CH_3COO)_2.2H_2O$) and sodium hydroxide (NaOH) were used as precursors. After ZnO NPs growth N-Methylol dime-thylphosphonopropionamide (MDPA) flame retardant was applied in the presence of 1, 2, 3, 4-butanetetracarboxylic acid (BTCA) as a cross linker and sodium hypophosphite (SHP) as a catalyst by conventional pad dry cure method. Induced coupled plasma atomic emission spectroscopy (ICP-AES) was used to determine the deposited amount of Zn contents % and phosphorous (P) contents %. Scanning electron microscopy (SEM), X-ray powder diffraction (XRD), and Fourier-transform infrared spectroscopy (FTIR) were employed to determine the surface morphology and characterization of developed samples. Furthermore, the thermal degradation of untreated

sample and treated samples was investigated by thermo gravimetric analysis (TGA). Furthermore, the vertical flame retardant test, limiting oxygen index (LOI), ultraviolet protection factor (UPF), antibacterial activity, self-cleaning ability, and wash durability of samples were examined. The developed samples showed excellent results for self- cleaning, flame retardancy (i.e. 39 mm char length, 0 second after flame time, 0 second after glow time), 32.23 LOI, 143.76 UPF, 100 % antibacterial activity. The developed samples showed good wash durability. Additionally, the bending rigidity, air permeability and tensile strength of the developed samples were measured. The developed samples showed an increase in bending rigidity while a decrease in air permeability and tensile strength. Statistical analysis of obtained data revealed that all process parameters have a significant effect on the properties of the developed samples.

Keywords: Flame retardants, antibacterial, ZnO, nanoparticles, metal oxide

ABSTRAKT

Jedinečné vlastnosti bavlny, jako hydrofilita, biodegradabilita, trvanlivost, dobrá barvitelnost a relativně nízká cena, z ní činí oblíbenou textilii. V současné době však lidé touží po tom, aby bavlněná tkanina měla multifunkční vlastnosti, které mohou poskytnout větší komfort na základě pracovního prostředí a povětrnostních podmínek. Poptávka na trhu se posunula směrem k nehořlavosti, UV ochraně, nemačkavosti, samočisticím a antibakteriálním vlastnostem - v těchto oblastech probíhají rozsáhlé studie. Nanočástice (NP), například oxid zinečnatý (ZnO), oxid titaničitý (TiO_2), oxid hořečnatý (MgO), oxid měďnatý (CuO), uhlíkové nanotrubice, oxid křemičitý (SiO_2) a stříbro (Ag), vykazují pozoruhodné funkční vlastnosti. Mezi různými nanočásticemi se využití oxidu zinečnatého (ZnO) jeví jako nejekologičtější a nejekonomičtější možnost. Zároveň jej lze aplikovat na různé substráty včetně textilních polymerů a tkanin. Vědecké práce popisují různé přístupy k depozici nanočástic oxidu zinečnatého na povrch taniny, jako například syntéza in-situ a depozice ex-situ. Hlavním požadavkem dnešní doby je ekologická a přírodu nezatěžující funkcionalizace tkanin a u povrchově upravených tkanin je důležitá I stálost v praní.

Cílem této výzkumné práce je vyvinout ekologicky upravenou a trvale nehořlavou tkaninu bez obsahu halogenů a formaldehydu s multifunkčními vlastnostmi a nalézt optimální podmínky a parametry. V této výzkumné práci byly nanočástice oxidu zinečnatého vyvíjeny na 100% bavlněné tkanině pomocí sonochemické metody. Jako prekurzory byly použity dihydrát octanu zinečnatého ($Zn(CH_3COO)_2.2H_2O$) a hydroxid sodný (NaOH). Po růstu nanočástic ZnO byl metodou pad-dry aplikován zpomalovač hoření N-methyloldimethylfosfonopropionamid (MDPA). Jako zesíťující činidlo byla použita 1, 2, 3, 4-butantetrakarboxylová kyselina (BTCA) a jako katalyzátor fosfornan sodný (SHP). Pro stanovení množství procentuálního obsahu zinku a fosforu byla použita atomová emisní spektroskopie s indukovaným vázaným plazmatem (ICP-AES). Pro charakterizaci vyvinutých vzorků a sledování povrchu byly použity rastrovací elektronová mikroskopie (SEM), prášková rentgenová difrakce (XRD) a infračervená spektroskopie s Fourierovou transformací (FTIR). Dále byla zkoumána tepelná degradace neupraveného vzorku a ošetřených vzorků termogravimetrickou analýzou (TGA). Byly též provedeny vertikální testy retardéru hoření, a

stanoveno limitní kyslíkové číslo (LOI), byl zkoumán UPF faktor (ochrana proti ultrafialovému záření), antibakteriální aktivita, samočisticí schopnost a stálost v praní. Vyvinuté vzorky vykazovaly vynikající výsledky pro samočištění, zpomalení hoření (tj. 39 mm délka spáleného vzorku, 0 s doba dohoření, 0 s doba dosvitu), 32,23 LOI, 143,76 UPF, 100% antibakteriální aktivita. Vyvinuté vzorky vykazovaly i dobrou stálost v praní. Dále byla měřena tuhost v ohybu, propustnost vzduchu a pevnost v tahu vyvinutých vzorků. Bylo prokázáno zvýšení ohybové tuhosti při současném snížení propustnosti vzduchu a pevnosti v tahu. Statistická analýza získaných dat ukázala, že všechny parametry procesu mají významný vliv na vlastnosti vyvinutých vzorků.

Klíčová slova: Zpomalovače hoření, antibakteriální, ZnO, nanočástice, oxidy kovů

LIST OF FIGURES

LIST OF TABLES

LIST OF ABBREVIATIONS/ SYMBOLS

Abbreviations

UV	Ultra Violet
NPs	Nanoparticles
MDPA	N-Methylol Dimethylphosphonopropionamide
BTCA	Butanetetracarboxylic Acid
SHP	Sodium Hypophosphite
ICP-AES	Induced Coupled Plasma Atomic Emission spectroscopy
SEM	Scanning Electron Microscopy
XRD	X-Ray Powder Diffraction
FTIR	Fourier-Transform Infrared Spectroscopy
TGA	Thermo Gravimetric Analysis
LOI	Limiting Oxygen Index
UPF	Ultraviolet Protection Factor
NFPA	National Fire Protection Association
PBDEs	Polybrominated Diphenyl Ethers
PBB	Polybrominated Biphenyls
EU	European Union
USA	United States of America
DHHS	Department of Health and Human Services
DMDAEP	N,N-Dimethyl Di(acryloyloxyethyl) Phosphoramide
DMF	N,N-Dimethylformamide
PLA	Poly Lactic Acid
EMI	Electromagnetic Shielding
IARC	International Agency for Research on Cancer

FDA	Food and Drug Administration
UVR	Ultraviolet Radiations
UVA	Ultraviolet Radiations A
UVB	Ultraviolet Radiations B
UVC	Ultraviolet Radiations C
TBBPA	Tetrabromobisphenol A
FR	Flame Retardants
APP	Ammonium Polyphosphate
CNTs	Carbon Nanotubes
ROS	Reactive Oxygen Species
DNA	Deoxyribonucleic Acid
DLS	Dynamic Light Scattering
ATR	Attenuated Total Reflectance
ASTM	American Society for Testing and Materials
AATCC	American Association of Textile Chemists and Colorists
JCDPS	Joint Committee on Powder Diffraction Standard
CA	Citric Acid

Symbols

%	Percentage
$	Dollar
eV	Electron volt
µm	Micrometer
N	Newton

mN	Millinewton
°C	Degree centigrad
kHz	Kilohertz
W	Watt
M	Mole
g	Gram
g/L	Gram per liter
mL	Milliliter
ϴ	Theta
s	Second
Pa	Pascal
mm/s	Millimeter per second

CHAPTER 1

Introduction

Fire has claimed more deaths in the United States than all other natural incidents combined. The National Fire Protection Association (NFPA) disclosed that there were 1.35 million fires in the United States in 2009, which resulted in 3010 fatalities, 17,050 human injuries, and a $12.53 billion loss of assets. Surprisingly, residential structures accounted for 28% of all fires and caused the majority of the damage[1]. According to reports, furniture with upholstery, mattresses, and bedding fires caused 70% of the fatalities associated with household smoking material flames[2]. Thus, the flame retardant coating of textile-based items can greatly help to save lives as well as property in residential buildings[3], [4].

Cotton fiber is among the most plentifully used fibers all over the world. It is comfortable, cozy, and breathable when used in garment form [5], [6]. However, it is one of the most combustible and very susceptive to thermal decomposition. It exhibits a very lower limiting oxygen index (approximatelty 17-18), as well as it is a highly flammable fiber. It burns very quickly with a hot flame and little spark [7], [8]. Moreover, with flammability and combustibility, cotton fabric provides an indigent defence to human skin against UV radiation and bacterial growth. Wearable cotton textile goods effectively absorb perspiration, sebum, and other skin secretions, a property that makes it easier for bacterial growth. This bacterial breeding is directly linked to a number of newly developing infections or diseases that are currently gaining attention in the global public health arena. Therefore these are the fundamental problems for the cotton fabric, limiting its use in industrial work wear, housing, and technical applications [9], [10].

Flame retardant treatment on textile fabrics has gained significant importance because flame retardant fabrics can be used as safety work wear in industry, firefighting wears, in hospitals, and as in household upholstery [11], [12]. Various chemical applications are involved in producing flame retardant fabrics, but most of the flame retardant chemicals contain halogen compounds that are not environmentally friendly [13], [14]. Halogen-based compounds produce hazardous fumes and gases that affect the endocrine system. The findings of some

studies caused the manufacturing of two main classes, notably polybrominated diphenyl ethers (PBDEs) and polybrominated biphenyls (PBB), to be banned in the EU and the USA. All of this occurred as a result of increasing findings that PBDEs accumulate in biological organisms and remain in the environment. Additionally, toxicological tests revealed that these compounds may be hazardous to the neural systems and cause deleterious effects on the thyroid, and liver. PBBs have been reported to be carcinogenic to the liver of mice and rats. As per the findings of the Department of Health and Human Services (DHHS) PBBs could be harmful to human health in terms of cancer. Phosphorous based durable flame retardant chemicals are alternatives to halogen compounds. These phosphorous based compounds are ecological, environmentally friendly and economical for cotton textile applications [15]. In a study Cheema *et al.* treated cotton fabric with N,N-dimethyl di(acryloyloxyethyl) phosphoramide (DMDAEP), a halogen free phosporous and nitrogen based chemical for flame retardancy. They achieved excellent flame retardancy along with increased char formation[7]. In one more study Gall *et al*. fabricated cotton, cotton/polyester, and cotton/polyamide surfaces by coating water soluble cyclophosphazene as a flame retardant finish and reported the increase in flame retardancy, increase in limiting oxygen index, as well as the formation of the glassy insulating layer on the substrate [8]. In an other study Zhang *et al.* achieved improved flame retardancy of cellulose fibers by grafting zinc ion along with N,N-dimethylformamide (DMF) application[11]. Li *et al*. synthesized a halogen free flame retardant for cotton fabric containing –P–O–NH_4^+ groups and achieved excellent results for flame retardancy[16]. Chen *et al.* synthesized poly lactic acid (PLA) and phosphazene/triazine bi-group composite along with doping of zinc oxide nanoparticles (ZnO NPs) and achieved excellent flame retardancy, higher limiting oxygen index, and increased char residues[17].

N-methylol dimethyl phosphonopropion amide (MDPA) is one of the most promising and ecological flame retardant compounds due to its durability, low toxicity, environmentally friendly nature and convenient application. When it is applied along with a cross linker onto the cotton fabric, it makes the covalent bond with a hydroxyl group of cotton cellulose, hence enhancing its durability[18], [19].

Nanotechnology is another most important field that has been utilized successfully and efficiently in the industry to achieve desired fruitful results. Nanomaterials in the textile

industry have earned great importance due to their multipurpose uses [20]. Nanomaterials in the form of nanoparticles are being used in the textile industry for antibacterial textile [21], UV protection, to increase flame retardancy, self-cleaning, electromagnetic shielding (EMI), conductive textiles, etc. [22]–[24]. Among the nanoparticles used in industry, metal oxides are of the great importance because of their multipurpose properties [25]. Zinc oxide (ZnO) and titanium dioxide (TiO_2) are the most commonly used inorganic metal oxides in the textile industry. TiO_2 has just been categorized as an IARC group 2B carcinogen, probably harmful to humans, by the International Agency for Research on Cancer (IARC). The IARC findings are based on data demonstrating that exposure to large concentrations of pigment-grade and ultrafine TiO_2 dust results in cancer of the respiratory tract in rats. The discoveries were deemed relevant to humans by the IARC because several biological processes that result in lung cancer in rats appear to be similar to those that occur in people who work in dusty environments. However, ZnO is "generally identified as safe" by the US Food and Drug Administration (FDA). ZnO is n-type semiconductor white in color, having a high refractive index with a wide band gap of 3.37 eV [26], [27]. Along with UV protection, antibacterial, and self-cleaning properties, zinc oxide nanoparticles (ZnO NPs) are being used in flame retardant coating [28], [29]. ZnO NPs are used as co-catalyst in flame retardant finishing and are very effective in char formation during the burning of fabric [14]. Researchers showed that ZnO NPs as co-catalyst increase the flame retardancy of cotton fabric by forming a protective layer on the fabric and restricting the supply of oxygen to the fabric which is necessary for burning, as well as it also increases the durability of flame retardant [30], [31].

The main challenges in the flame retardant/ZnO NPs system are the use of formaldehyde free cross linker, homogeneous, even, and stable deposition of ZnO NPs. BTCA is a formaldehyde free cross linker that can be used for cotton flame retardant systems[32]. Javed *et al*. reported that sonochemical is an advanced and economical method for the in-situ synthesis of ZnO NPs onto the cotton fabric[33]. This technique controls the nanoparticle size, as well as ultrasonic waves disperse and deposit the nanoparticles onto the fabric more stably, homogeneously and evenly[34].

Among all properties, the integration of UV protection on flame retardant surfaces is of great concern in the present work. This is because the risks of UV radiation to induce acute and

chronic illnesses when they interact with skin increased significantly in recent years. UV radiations in sunlight are a natural threat to human skin and can result in major medical issues. Additionally, certain artificial medical lights produce UV radiation. Human body exposed to UV radiation without protection can suffer from major health issues such as melanoma (skin cancer), rash, erythema (skin redness), and skin ageing. Moreover, industrial workwears along with flame retardancy, also require UV protection and protection against various bacteria. Workers related to welding are exposed to hazardous radiation along with flame sparks. During arc welding, strong ultraviolet radiations (UVR) are released into the air. These radiations contain ultraviolet radiations A (UVA), ultraviolet radiations B (UVB), and ultraviolet radiations C (UVC). Human skin is harmed worsely by the exposure to ultraviolet radiations A (UVA), ultraviolet radiations B (UVB), and ultraviolet radiations C (UVC) from a short distance in the absence of a barrier. So there is a need to develop protective work wear with multifunctional properties[35], [36].

In this research study, ZnO NPs were in-situ synthesized onto the cotton fabric by ultrasonic irradiation method. After that, MDPA flame retardant in the presence of formaldehyde free ecological cross linker BTCA was applied onto the cotton fabric by pad dry cure method. The main goal of the present work is to find the optimized parameters for in-situ sonochemical synthesis of ZnO NPs, and investigate the role of ZnO NPs in flame retardant finishing and their influence on functional properties.

To the best of the author's knowledge, this is the first study on the flame retardant application in combination with MDPA along with formaldehyde free cross linker, and ZnO NPs by sonochemical method. The finding of this study could be beneficial for application in safety textiles (welding work wear, electrical work wear, industrial work wear etc.).

CHAPTER 2

Aim and Objectives

The production of flame retardant fabrics on a wide scale using affordable, simple, and environmentally friendly methods still faces several difficulties. Research on environmentally friendly preparation techniques should be prioritized, along with studies on textile durability and mechanical stability. The general goal of this research project is to utilize halogen and formaldehyde free ecological phosphorous based chemical N-methylol dimethyl phosphonopropion amide (MDPA) and deposition of ZnO NPs on cotton textiles to create flame retardant textiles with additional capabilities (such as UV protection, self-cleaning, antibacterial, etc.).

The specific objectives are as follows;

- Deposition of ZnO NPs by ultrasonic irradiation method to achieve increased flame retardancy and multifunctional properties.
- Application of N-methylol dimethyl phosphonopropion amide (MDPA) to modify the surface of fabric.
- Different parameters, such as precursor concentrations and sonication time, significantly affect the deposition of ZnO NPs on the fabric. Furthermore, concentration of N-methylol dimethyl phosphonopropion amide (MDPA) affects the flame retardancy. The purpose is to optimize process parameters and to evaluate the effect of process parameters and conditions upon flame retardancy as well as other functional properties.
- Content analysis of coated fabrics by induced coupled plasma atomic emission spectrometer (ICP AES).
- Evaluation of surface morphology of nanoparticles coated fabrics by scanning electron microscopy (SEM).
- Characterization of coated fabrics by X-ray diffraction (XRD) and the fourier transform infrared spectroscopy (FTIR)
- Evaluation of thermal stability of coated fabrics by thermo gravimetric analysis.

- Evaluation of flame retardant properties from vertical flame test and limiting oxygen test (LOI).
- Evaluation of antibacterial efficacy of coated cotton fabrics against gram positive and gram negative bacteria.
- Evaluation of UV protection of coated cotton fabrics.
- Evaluation of photo catalytic self-cleaning ability by degradation of coffee stain under UV light.
- To do the statistical analysis of obtained results.
- Evaluation of coated cotton fabric against washing.

CHAPTER 3

Literature Review

3.1. Prologue

This section provides a general review of the area of research, including background, basic theories, and current study. The readers will become acquainted with the experimental methodologies in the next part.

3.2. Textile fibers

Polymers with a variety of structural configurations make up textile fibers, giving them a wide range of mechanical, chemical, physical, thermal, and biological characteristics[37], [38]. To create yarns, threads, textiles, and a variety of textile items, thin, flexible, spinnable strands or filaments known as textile fibers are utilized. They are the fundamental building units of textiles and can be either natural, man-made (synthetic or regenerated), or a combination of both[39], [40]. Individual textile fiber can range in diameter from 10 to 50 micrometer. Filaments are continuous (very long) having indefinite length, while the staple fibers have significantly shorter lengths[41]. The length of natural fibers differs based on their source[42]. In general, filaments are joined and then twisted to create yarns, whereas staple fibers are spun to produce yarns[43]. Fabrics are typically created by weaving or knitting yarns. Numerous fibers make up each piece of fabric. One small swatch of thin cloth, for instance, may have nearly 100 million fibers in it[44]. Despite the fact that there are many different types of fibers in nature, only those fibers that have ability to be spun into yarns are acceptable for use in the production of textile fabrics. Natural fibers and man-made fibers are the two primary categories of textile fibers. Cellulosic fibers like cotton; and protein fibers like wool are the most significant types of natural fibers[42]. Man-made fibers, on the other hand, can be further broken down into regenerated fibers such as rayon and synthetic fibers such as polyester. Figure 1 shows the classification of essential textile fibers[40].

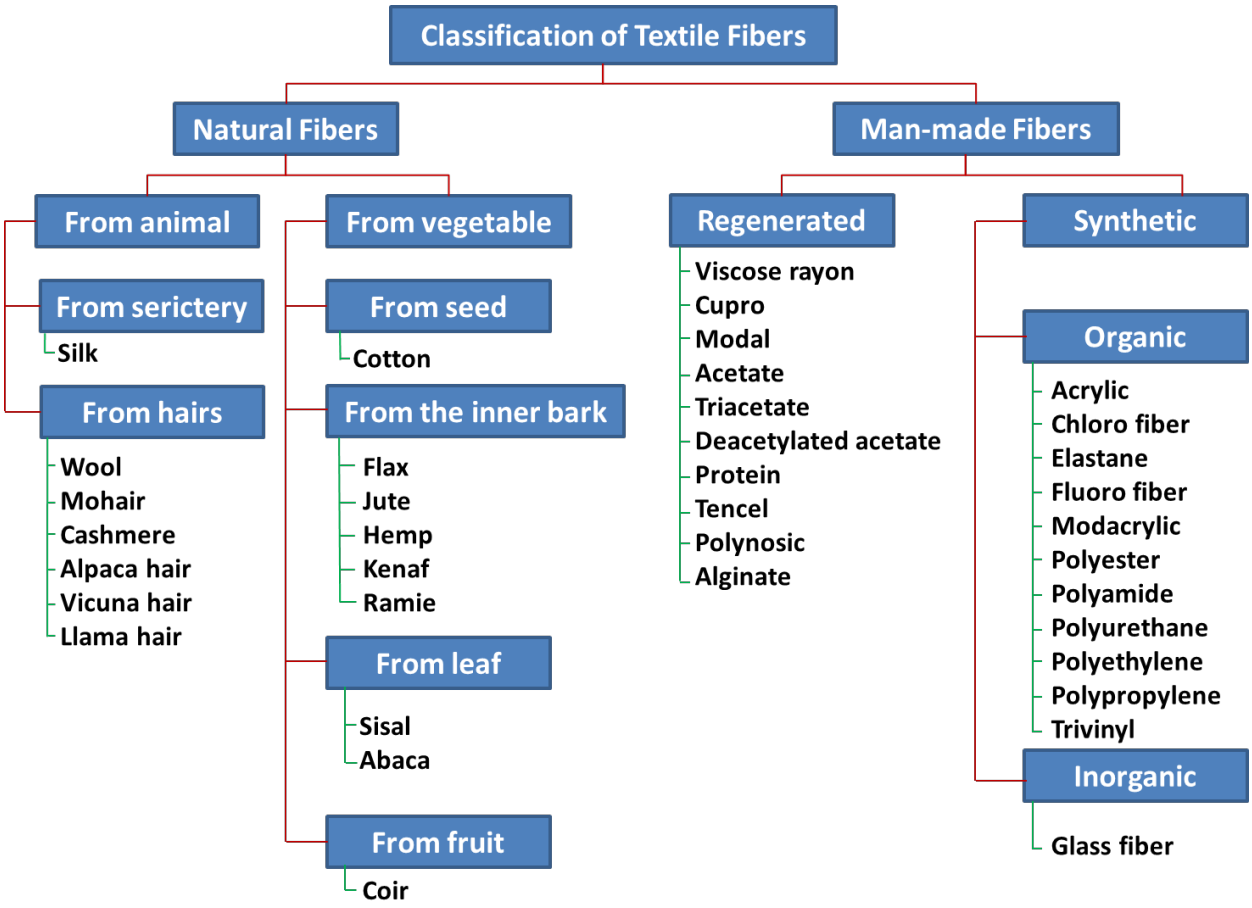

Figure 1. Classification of textile fibers.

3.3. Cellulose

The fundamental structural unit in the cell wall of plants is cellulose, a very complex carbohydrate. With a water contact angle of about 20 to 30 degrees, cellulose is hydrophilic, tasteless, and odorless. It is a naturally occurring organic compound and has the chemical formula $(C_6H_{10}O_5)_n$. It is a kind of linear polymer made up of glucose units connected by 1,4-glycosidic linkages. The polymerization degree of cellulose exhibits significant variation and is roughly 10,000 glucose units to 15,000 units[45], [46]. The lengthy, fibrous chains that cellulose forms are insoluble in water and give plant cells stiffness and strength. Hydrogen bonds between cellulose chains help to generate microfibrils, which can then come together to

form longer fibers. These hydrogen linkages enable the chains to form highly ordered molecular structures, which lead to a variety of structured crystalline configurations. The higher cellulose crystallinity is due to structural order, uniformity, symmetry, and hydrogen bonds. Plant tissues are stabilized and strengthened by these cellulosic structures[47], [48].

Cellulose belongs to a class of natural biodegradable polymers and can be decomposed by various environmental bacteria and enzymes. This characteristic makes cellulose an environmentally friendly material and adds to the natural carbon cycle. Numerous applicable uses for cellulose can be found in various industries[49], [50]. Cellulose fibers are treated and made into sheets, which are then used to make paper and cardboard. Additionally, cellulose is used in the production of textiles made from plant materials like rayon, acetate, and lyocell. Cotton, linen, and jute fibers are examples of naturally occurring cellulose fibers, that are used in the production of textile products[51]. Cellulose in cotton is notable for having a high level of crystallinity and degree of polymerization. Crystallinity shows that the molecules in cotton fiber are parallel to each other and very closely packed, and a higher levels of degree of crystallinity and polymerization correspond to stronger fibers. The main constituents in the cotton cellulose polymer chain are β-1, 4-D glucopyranose and are connected by l, 4- glucodic linkages. Steric effects prevent the anhydrogluco-pyranose C-O-C bond from freely rotation. Each anhydroglucose has three hydroxyl groups connected to it. Three groups are joined at C-2, C-3, and C-6, separately. There are several additional bonds possible because of the hydroxyl groups that are present and the polymer chain shape[52].

In alkaline conditions, carbon disulfide is the most significant solubilizing agent for cellulose. Other solubilizing substances are N-methylmorpholine N-oxide, Schweizer's reagent, and also lithium chloride in the presence of dimethylacetamide. Generally speaking, these substances modify the cellulose, making it soluble. Additionally, cellulose is soluble in a variety of ionic liquids. Various reagents can be used to partially or completely react with the hydroxyl groups (OH) of cellulose to produce derivatives with beneficial qualities, most notably cellulose esters and cellulose ethers[53], [54]. Figure 2 shows the structure of cellulose.

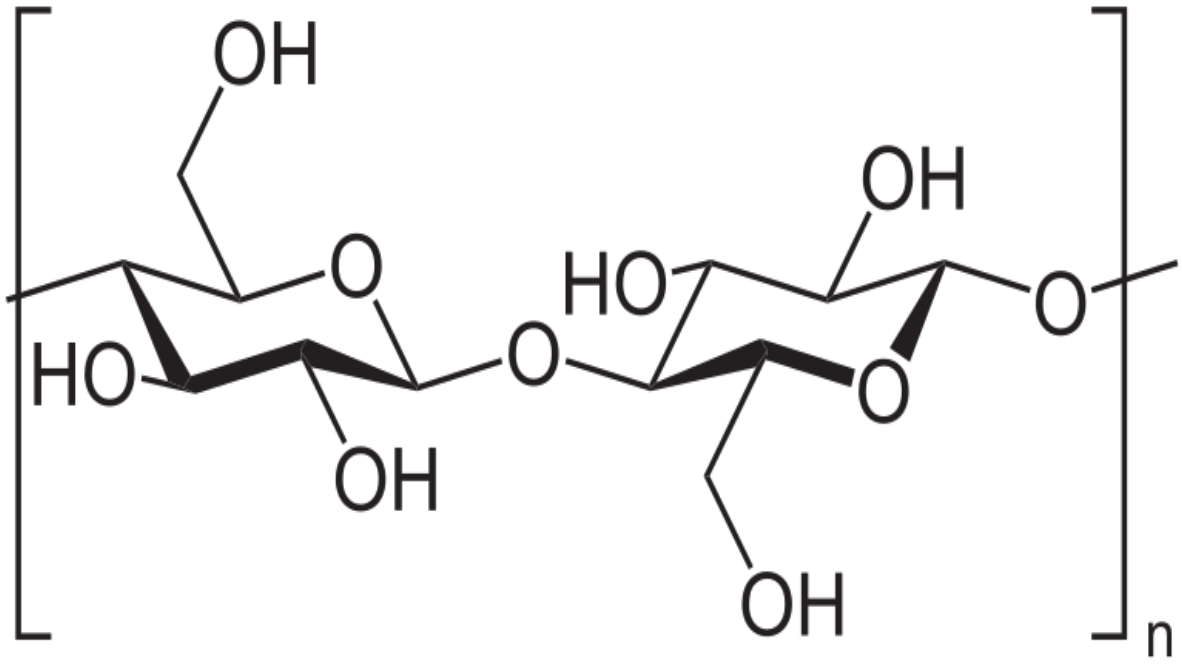

Figure 2. Structure of cellulose[55].

3.4. Cotton

Humans have been using cotton for thousands of years, and its history is broad and complex. Around 3000 BC, cotton was being grown in India, where it is thought to have been started across the valley of the Indus river in present-day Pakistan. Ancient Egyptians also grew cotton, which they used to create fabrics and garments. Cotton was first brought to Europe during the Middle Ages and quickly became a prominent crop in countries like Spain and Italy. Cotton was introduced to the American continent by European invaders in the 1600s, and it quickly established itself as a significant crop across the southern areas of the United States. Although cotton consumption decreased after the advent of man made fibers in the 20th century, it is still a significant crop in several countries in the present day. Overall, cotton's history is strongly connected to the evolution of global civilization, the expansion of the world's economic status, and the political and cultural disputes that have driven these changes[56], [57].

Natural, fluffy, and silky cotton fiber develops in the cotton plant's seed pods (Figure 3). It is a significant commodity crop and one of the most popular natural fibers in the world. The shrub-like plant is indigenous to many tropical as well as subtropical areas of the world, inclusive of the American areas, Africa, Egypt, Pakistan, and India. Most types of wild cotton are found in Mexico, with Australia and Africa coming in second and third. Cotton has four commercially produced species, all of which were domesticated in antiquity[58], [59]:

Gossypium hirsutum, which is alternatively referred to as Upland cotton is a native of Central America, many parts of Mexico, the Caribbean islands, and also southern Florida and accounts for 90% of global production[60].

Gossypium barbadense, a tropical South American native and producer of 8% of the world's cotton, is also called extra-long staple fibre cotton[61].

Tree cotton, known as Gossypium arboreum is only 2% endemic to the subcontinent (India and Pakistan)[62].

Gossypium herbaceum, sometimes known as Levant cotton, accounts for less than 2% is indigenous to southern Africa and the Arabian Peninsula[63].

Each individual cotton fibre represents a fully formed cell that originates in the outermost layer of the cotton seed. These fibres consist of several distinct components: cuticle, primary wall, secondary wall, and a lumen (depicted in Figure 4 b). The cuticle, known as the 'outermost' or 'skin' layer of the cotton fibre, is composed of a layer of cotton wax that possesses a waxy nature. The lumen, on the other hand, is a hollow canal that extends throughout the length of the fibre and serves as a conduit for supplying essential nutrients during the plant's growth phase. Depending on the stage of maturity, the lumen's dimensions can vary significantly. In mature fibres, the secondary wall contains a substantial amount of cellulose, resulting in a relatively small lumen, whereas immature fibres possess a thin wall structure and a larger lumen. The dimension of cotton fiber exhibits a reasonably consistent pattern, fluctuating within the range of 12 to 20 μm. The configuration of cotton fiber, in general, is commonly alluded to as possessing a structure resembling that of a kidney (Figure 4a)[64].

Cotton fibers generally measure 20 to 30 mm in length and 20 microns in diameter[65]. They are comprised of essentially pure cellulose, a durable and complex carbohydrate. The primary wall, cuticle, secondary wall, and lumen make up cotton fiber (Figure 4). Whereas, the secondary wall is the predominant source of cellulose in nature, with the primary wall and cuticle containing roughly 55 percent lower molecular weight cellulose[66], [67]. Single fiber tensile strength ranges from around 127.5 to 313.7 mN (Tex)[68]. Cotton fiber, unlike most other textiles, acquires strength as humidity increases. The surface gets smoother as the temperature rises, while fiber strength diminishes[69]. The twisted, ribbon-like configuration of the fibers provides them their distinctive flexibility and strength. The number of twists present in the fiber and the direction of convolution are important factors in fiber strength. Cotton fibers have between 3.9 and 6.5 twists per millimeter of length and have a change in a spiral reversal from 1-3 times per millimeter of length. The angle of convolution has been observed to vary with variety. There are differences in reversal frequency between cotton varieties and different species, between lint and fuzz obtained from the same ovule, as well as within a single fiber. In the cotton fiber structure, molecular density differs greatly. As compared to other locations, it has been observed that the molecular packing is particularly thick close to the reversal. The shape of cotton fiber is tapered. In comparison to the bottom, it is thinner at the top. Another important factor is cotton fiber maturity, which the end user takes very seriously. The cell wall's proportion to the total area of a circle, which is equal to an un-collapsed fiber, is a measure of cotton's maturity. Its ratio of 0.85 is adequate. If this number is less than 0.5, it means that there is a lot of immature cotton available, which makes it difficult to produce high-quality goods. When grading cotton, parameters like fiber length, cotton fineness, and cotton fiber maturity level are taken into consideration[65], [70]. Figure 5 shows the microscopic images of cotton fibers.

Cotton is an excellent choice for clothes along with various textile based products because of being breathable, durable, porous, and absorbent[71], [72]. Additionally, It is extremely versatile, as it has compatibility to be blended with many other fibers like polyester, linen, spandex, or rayon to enhance performance attributes like flexibility and/or moisture wicking[73]–[76].

Figure 3. Open cotton fiber boll [77].

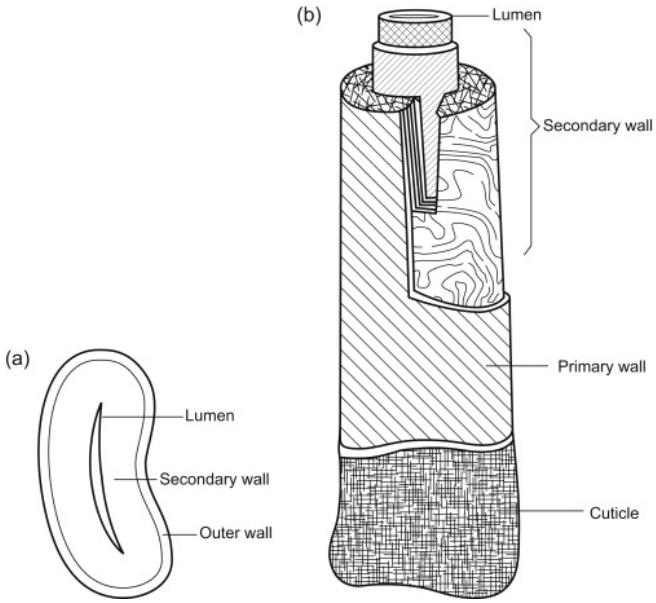

Figure 4. Structure of cotton fiber. (a) cross-section of fiber, (b) vertical section of fiber [64].

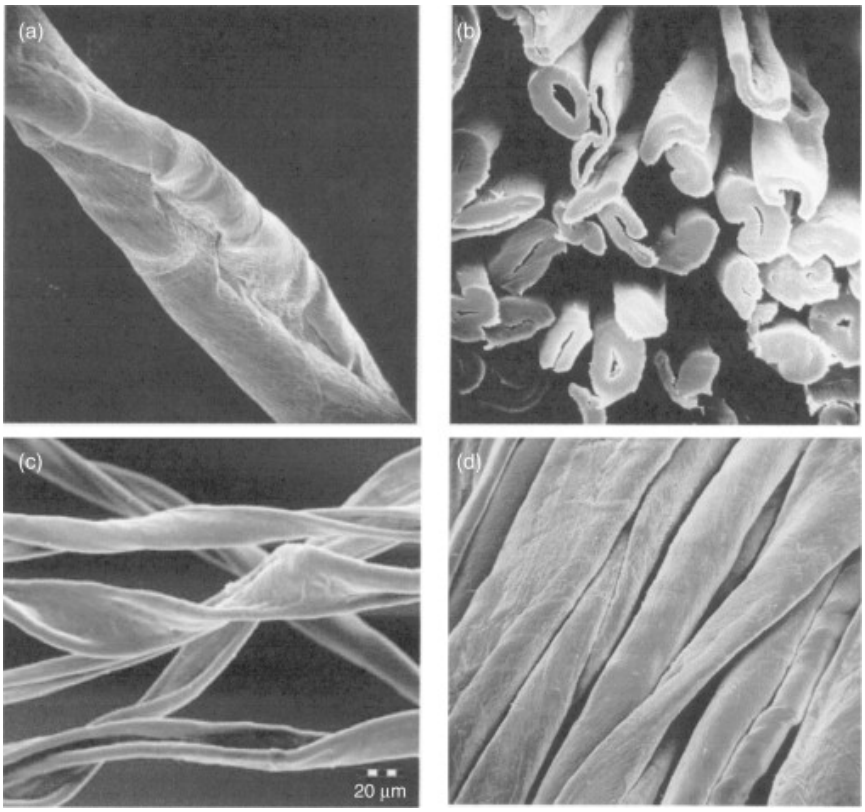

Figure 5. Microscopic views of cotton fibers[65].

3.5. Functional cotton fabrics

Among the most popular and commonly utilized natural organic fibers all over the world is cotton. Cotton's use has expanded from clothing to technical applications in textiles because of its superior absorption properties, large specific surface area, porous structure, lower cost, as well as biodegradability[78]. However, certain traits, such as the hydrophilic nature, ineffective antibacterial activity, high flammability, lower strength, and very poor defence against UV radiation, limit their range of applications, particularly in several high-end fields for medical, use in personal healthcare, as functional textile, safety clothing and self-cleaning[79]–[82]. Because of their potential for application in physical defense, thermal protection, biological shielding, and medical safety, as well as to satisfy the constantly changing demand from end users for innovative products, the functionalization of cotton has

attracted significant scientific, industrial, and commercial attention. Cotton serves more than just aesthetic purposes; value-added cotton textiles are now the foundation for several industrial and technological uses[83]. Recently, research has focused on cotton fabrics with functional properties. Numerous studies have looked into various techniques for giving cotton textiles particular qualities.The term "functional cotton fabric" relates to cotton textile fabrics and clothings that have undergone various functional finishing processes to improve their performance characteristics. These finishes could possess resistant to stains, anti-bacterial efficacy, anti-static capability, protection against UV radiations, water-repellency, flame retardancy and moisture-wicking properties[84]. Fabrics that have undergone a treatment process to enhance their level of ease in care have been specifically formulated to exhibit resistance against the formation of wrinkles, shrinkage, and fading, thereby endowing them with the highly desirable qualities of being low-maintenance and possessing increased durability[85]. Another technique utilizes fluorescent molecules to give cotton fabrics hydrophobic and fluorescent properties. One example of such a dye is 1,8-naphthalimide fluorescent dye[86]. Additionally, inorganic additives and sol-gel-based treatments have been investigated as potential means of improving the flame-retardant behaviors of cotton textiles[87]. Cotton textiles can be engineered to offer improved thermal insulation, which enables them for usage in cold climates. This is accomplished by the incorporation of insulating materials or technology[88]. Certain textiles are treated with fragrances that are microencapsulated and release gradually during wear, leaving a delicate and subtle scent. This may enhance the sensory experience in textile fabrics[89]. Cotton possesses inherent breathability; however, specific treatments or interlacing techniques may augment this attribute, thereby stimulating improved air circulation and ventilation[90]. Fabrics specifically engineered for active or sports-oriented purposes have the potential to undergo a treatment process that expedites the drying process, effectively aiding in the regulation of perspiration and moisture levels while engaging in physical activities[91].

Because of their versatility, excellent performance and developed characteristics, functional cotton fabrics are getting more and more popular. They have a wide range of uses, including in bedding, apparel, safety clothing, upholstery, and other areas[92]. Figure 6 shows some types of functional finishing of cotton fabrics.

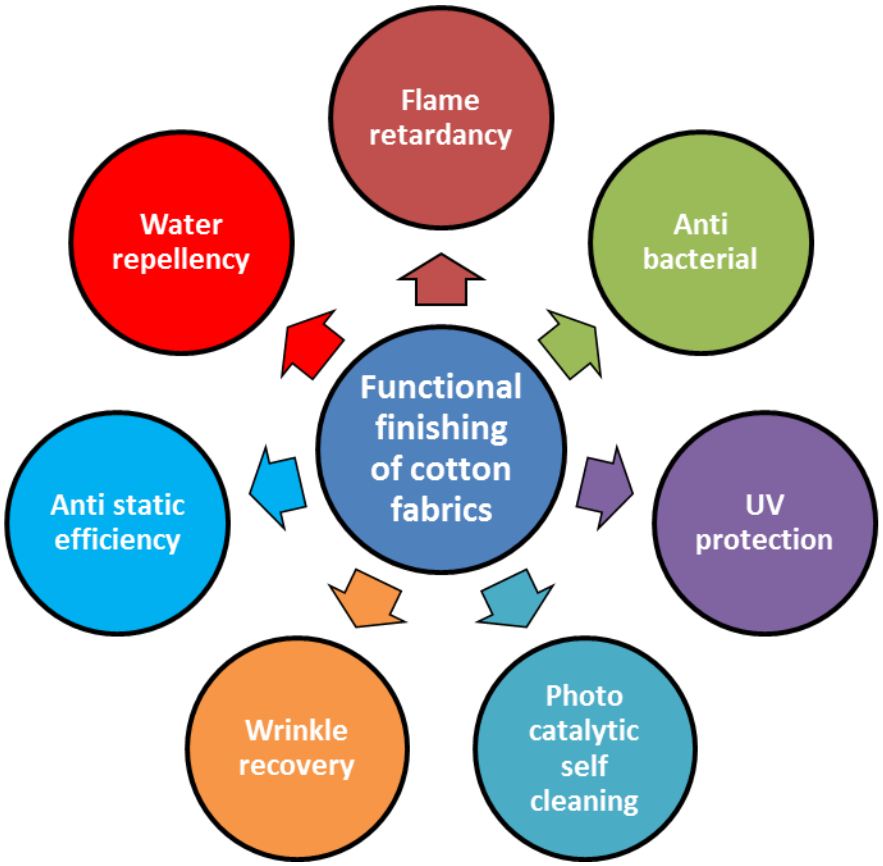

Figure 6. Types of functtional finishing of cotton fabrics.

3.6. Fire resistance

Cotton is recognized as a highly combustible substance with low flame resistance since it burns easily[93]. To create appropriate flame resistance, it is critical to comprehend the chemical and physical transformations that occur during the burning of cellulose. Cellulosic materials burn with certainty because cellulose is made up of carbon and hydrogen, which serve as fuel, and oxygen, which supports burning. By taking into account two quite different processes, flaming combustion and smoldering combustion, the burning of cellulosic materials might be associated with a flame or glow[94].

Fabric that loses its ability to support a flame when the ignition source is removed is referred to as flame retardant fabric. When an ignition source is removed, a fabric is said to be glow resistant if it doesn't burn through smoldering or glowing processes[95].

3.7. The thermal decomposition of cellulose

When a fire happens at elevated temperatures, polymers break down into combustible and incombustible species and components through physical and chemical changes[96]. The breakdown kinetics and end products are influenced by the chemical composition, structure of polymeric materials, rate of heating and the quantity of available oxygen. Degradation generally starts in the bonds with the lowest dissociation energy and in the more accessible areas[97]. Polymers, both natural and synthetic undergo heat degradation via processes such as chain fragmentation, chain elimination, and chain stripping. Instead of melting, cellulosic materials behave similarly to thermoset materials, undergoing irreversible chemical alterations during their decomposition[98]. Using thermal gravimetric analysis, a technique that measures changes in weight as a function of heat, a great number of research have been published on the process and mechanisms of cellulose decomposition and pyrolysis[99]. A moderate temperature of 200–300 °C usually results in a decline in the degree of polymerization of cellulose, leading to the generation of volatiles like levoglucosan, or 1,6-anhydro-β-D-glucopyranose, and a liquid pyrolysate. As the temperature rises to 400–600 °C, cellulose continues to degrade, giving rise to flammable gases and highly boiling compounds. A polymeric substance needs to first degrade and split down into free radicals and lower molecular weight combustible volatiles in order to experience ignition and burning. These breakdown products burn with air oxygen at high temperatures (above the point of ignition) or in the vicinity of a source of ignition. We must first look into the decomposition of cellulose in order to find out why it is combustible[100]. According to Shafizadeh *et al*., cellulose breaks down into a species known as "activated" cellulose, which is a reactive intermediate. It has been proposed that this activated" cellulose is created during the first stage of degradation, during which there is no loss in mass but a decrease in the degree of polymerization[101]. An advanced mechanism for the creation and subsequent assessment of the activated cellulose throughout cellulose burning was proposed by Liu *et al*[102]. Price *et al.* also investigated the degradation of cellulose via activated cellulose containing species. This activated cellulose

stage further degrades as the temperature rises[103]. Physical and chemical parameters like temperature, atmosphere type, crystallinity, impurities being present, and cellulose sample size and texture all affect the thermal degradation pathway and the chemical structure of the products that result from degradation[104]–[106]. It is commonly acknowledged that there are two distinct processes by which cellulose degrades: dehydration and depolymerization (also known as decomposition). Anhydrocellulose and water are formed during the degradation processes of dehydration (300–400 °C). During degradation process, aliphatic char is formed. This aliphatic char is converted to aromatic char by further oxidation along with the successive release of carbon monoxide and carbon dioxide (400–600 °C). Up to 800 °C, this aromatic char shows thermal stability. Levoglucosan is produced through an unzipping mechanism where the chain separation of acetal linkages of the glycosidic groups results in the creation of levoglucosan. The depolymerization happens in both crystalline and amorphous regions. Levoglucosan undergoes further degradation to produce low molecular weight compounds, such as furan and its derivatives[107]–[109]. Figure 7 shows the thermal and thermo-oxidative cellulose degradation process.

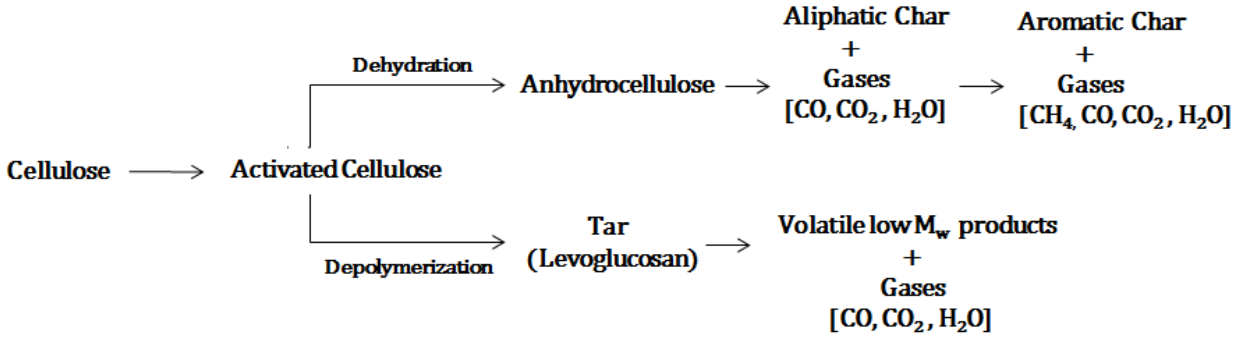

Figure 7. Diagram showing the thermal and thermo-oxidative cellulose degradation process. From left to right, the temperature is rising[110].

3.8. Combustion theory

The chemical reaction among substances that typically involves oxygen and produces light and heat in the shape of flames is known as combustion. It is a quick, exothermal (heat

evolving), and redox (oxygen adding) chemical process. In this reaction the fuel must be heated to a temperature higher than the ignition point. The steps involved are as follows: first, the substrate is heated, and moisture evaporates; after that, more heating causes the substrate to break down and generate small in size, organic compounds (volatile in nature). Finally these small size compounds are burned, and char is produced. When there is a balance between the total thermal energy of both reactants and products, the combustion process comes to an end[111], [112].

The most common kind of combustion is an open flame fire. The fuel must be in its gaseous condition for this chemical reaction to occur with an oxidizing agent. Since the reaction is gas to gas, the fuel, whether solid or liquid must first experience a phase transition or chemical change to turn into a gas in order to participate in an exothermic combustion process. In the event of a flame fire, there must be at least 10% oxygen present as an oxidizer[113], [114].

Smoldering combustion (also known as glowing combustion) is the one more form of combustion. This kind of combustion is a solid-to-gas chemical reaction that results in the direct oxidation of the combustible solid's surface, chars, and other nonvolatile breakdown products without the production of flames. Sustainable glowing combustion requires a lower proportion of oxygen. This typically happens at temperatures below the substrate's ignition temperature[115]–[117].

3.9. Polymer combustion

The process of polymer combustion is started by heating and involves endothermal decomposition[118]. As the combustible gases are produced, they combine with oxygen gas in the atmosphere to form a mixture that is ignited, which encourages the spread of flames (exothermic reactions) and the production of heat. Endothermic processes are involved in the heating, degradation, and pyrolysis of polymers; exothermic reactions are started upon ignition, which is followed by thermal feedback that strengthens the polymer's decomposition. Flame propagation is supported by highly energetic H and OH radicals[119]. Figure 8 shows the exothermic and endothermic processes involved in polymer combustion, while the polymer combustion cycle is depicted in Figure 9.

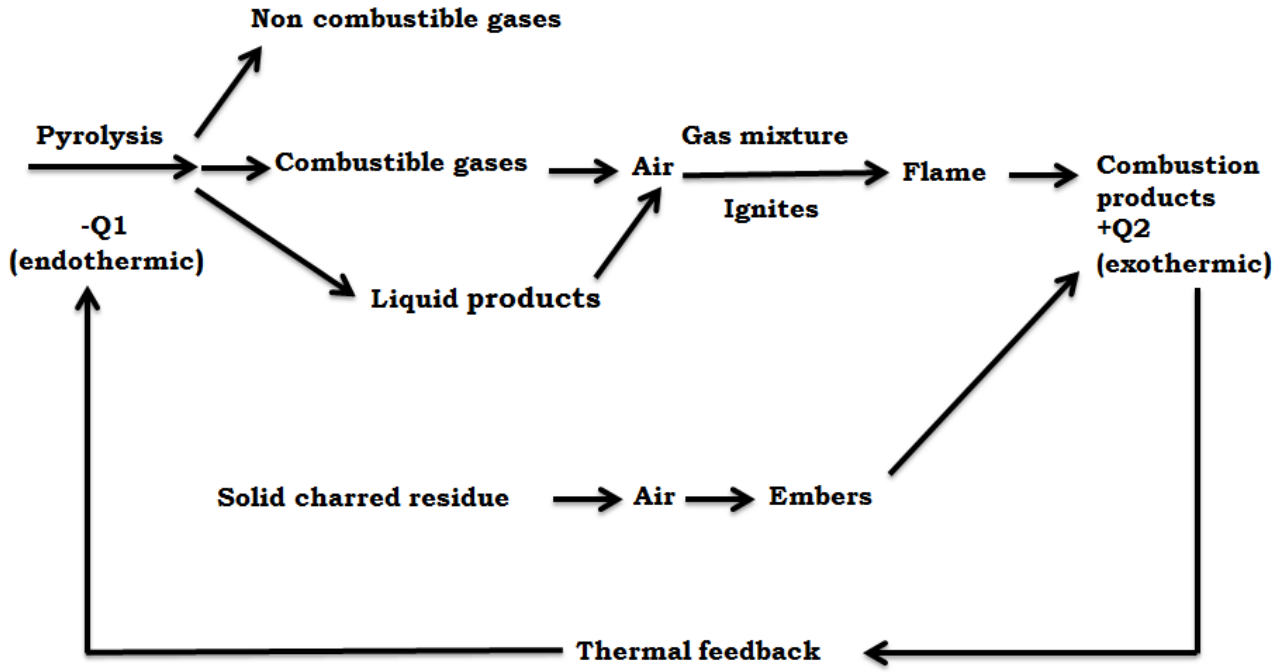

Figure 8. Exothermic and endothermic processes involved in polymer combustion[120].

The use of textile and polymeric products, which are mostly made of organic compounds and have been produced with both conventional and modern techniques, is restricted due to their flammability[121]. It has been found through research on polymer combustion that both chemical and physical processes play a role in this complicated procedure. These occurrences happen in the transition between the gaseous and condensed phases, and polymer pyrolysis produces flammable volatiles. The volatiles subsequently undergo oxidation in the presence of oxygen, and the resultant thermal degradation products produce a significant amount of heat[122].

Enough heat must be applied to the polymer to break it down and ignite the by-products of pyrolysis in order for the combustion cycle to be self-sustaining, as well as the proper amount of heat to be returned to the matter to support the burning cycle and induce additional degradation. Depending on the flammable species, multiple byproducts from the combustion process are obtained. Water vapor (H_2O), carbon dioxide (CO_2), and carbon monoxide (CO) are produced when polymers are burned. Ash and carbon (C) make up the residual solid residue[123].

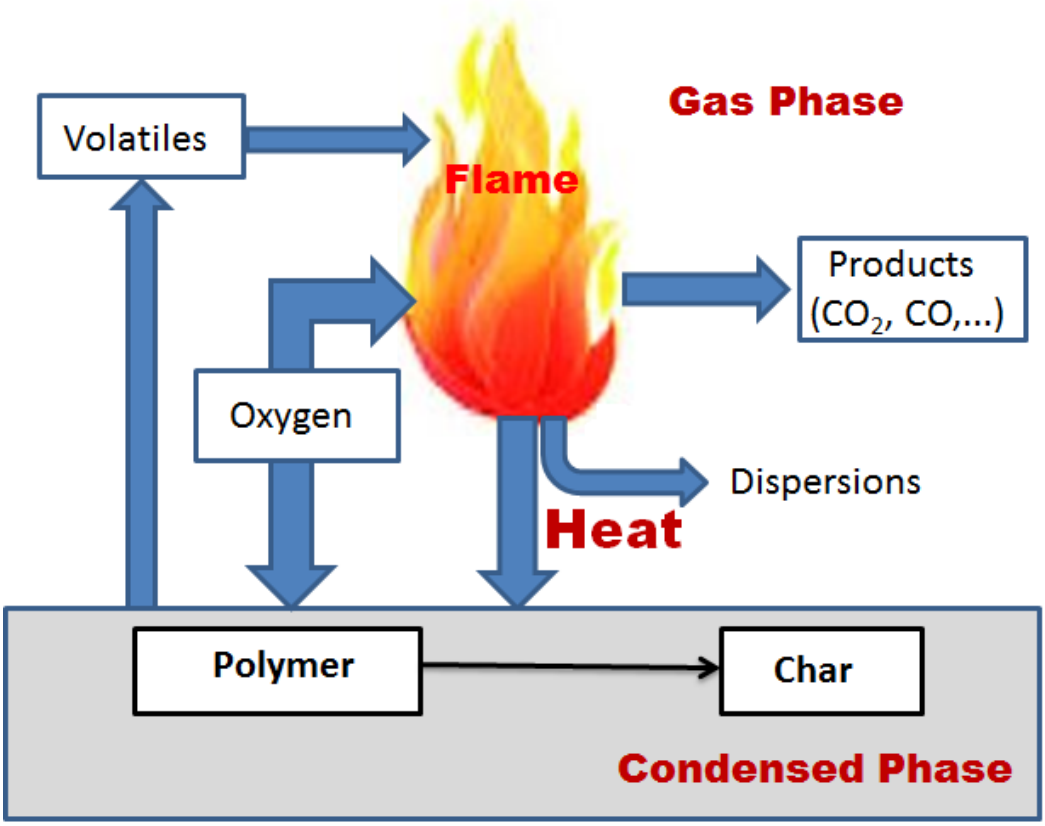

Figure 9. Polymer combustion cycle[124].

Since the two subsequent decomposition and oxidation reactions have a cyclic relationship (Figure 10), there is another model to characterize the combustion of polymers that is based on the kinetics of those reactions. Thus, there is a mutual influence between these two reactions. Polymer pyrolysis yields volatile substances that influence the pace of oxidation-combustion. Additionally, through the generation of heat during the combustion phenomenon, this oxidation-combustion influences pyrolysis. A non-charring polymer's combustion can be schematically represented (equations 1 and 2) as two successive overall reactions that take place in the condensed and gas phases[125].

$$P \xrightarrow{k_G} G \quad (1)$$

$$G + O_2 \xrightarrow{k_{OX}} OX \quad (2)$$

In the above equations k_G and k_{OX} represent, respectively, the total specific rates of the oxidation and pyrolysis of polymer molecules (P) to create volatile compounds (G).

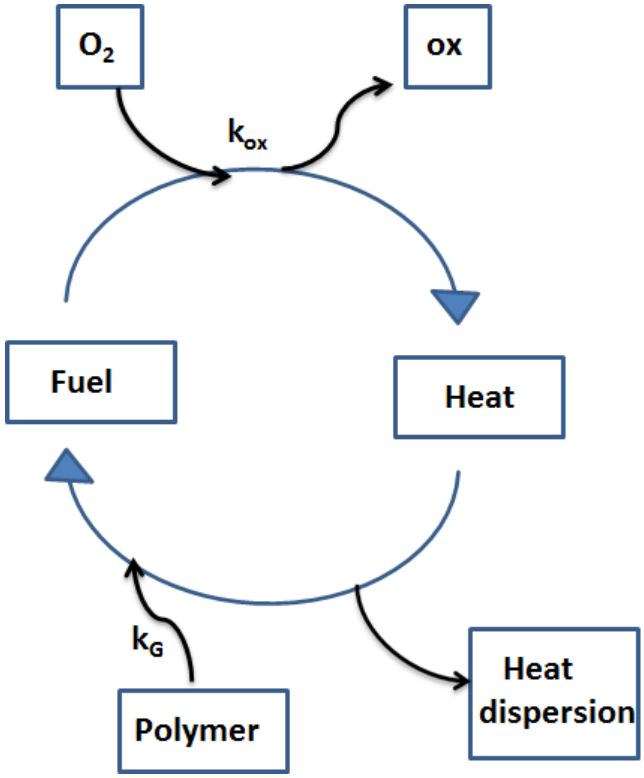

Figure 10. The cyclic fire loop[125].

3.10. Flame retardants

It is important to understand the meaning of "flame retardants" in order to properly label products that extinguish or suppress flames when tested in standard laboratory conditions. "The agents that, when combined with combustible material, postpone the material's ignition and decrease its flame spread when subjected to flame source"[126]. Flame retardants can be defined as substances that impede or even inhibit or decelerate the process of combustion, by altering the chemical reactions of degradation or oxidation involved in the burning process[122]. Flame retardants can function chemically or physically to achieve their desired

effects. These processes can take place in the condensed phase or, in some cases, in the gas phase. They are especially relevant when radicals are trapped or when they dilute flammable gasses, particularly when their actions trap radicals or dilute flammable gasses[127]. As previously indicated, the combustion procedure encompasses many stages; the introduction of flame retardant additives may impede this procedure at a specific stage or processes, such as heating, degradation, ignition, pyrolysis or breakdown, and propagation of flame[122].

Flame retardant materials work physically in the following ways:

- Since heat is consumed during the endothermic breakdown of some additives, they influence the pyrolysis process by cooling. As a result, the temperature drops and the substrate or media for reaction cools to a temperature lower than what is required to keep the burning process going. Water vapor is released by some flame retardants at approximately 200°C to 550 °C[128], [129].
- By the emergence of gaseous or solid protective layer which inhibits the release of flammable species and separates the process of combustion and thermal decomposition phase[16], [130], [131].
- Fuel is diluted in both the gaseous and solid phases. Certain flame retardants produce inert gases during their breakdown, for example H_2O, CO_2, NH_3, etc., which dilutes the flammable gaseous mixture[132].

The term "chemical actions" describes how flame retardants affect the combustion processes chemically and alter the fire process[133]. Condensed and gaseous phases are possible for them to act in. With an approach of radical trapping, flame retardants can impede the free radical mechanism during the burning process. As the combustion process progresses, free radicals might interact with the flame retardant chemicals. Less reactive compounds are created when flame retardants in the gas phase release certain radicals, like Br or Cl, and combine with extremely reactive radicals, such H• and OH•[127], [128], [134].

When a polymer or textile is subjected to a flame or other heat source, flame retardants can cause two different types of chemical reactions that inhibit the combustion process: they can generate an intumescent protective layer or a char (carbon-based) layer on the surface of the material. This char serves as a solid physical insulating barrier and divides the gas phase from

the condensed phase. Certain flame retardants also exhibit another chemical mechanism that includes the breaking of polymer chains at a faster rate. This causes the polymer to drip and escape the flame action region[135]–[137]. Mechanism of thermal transfer during materials combustion is depicted in Figure 11.

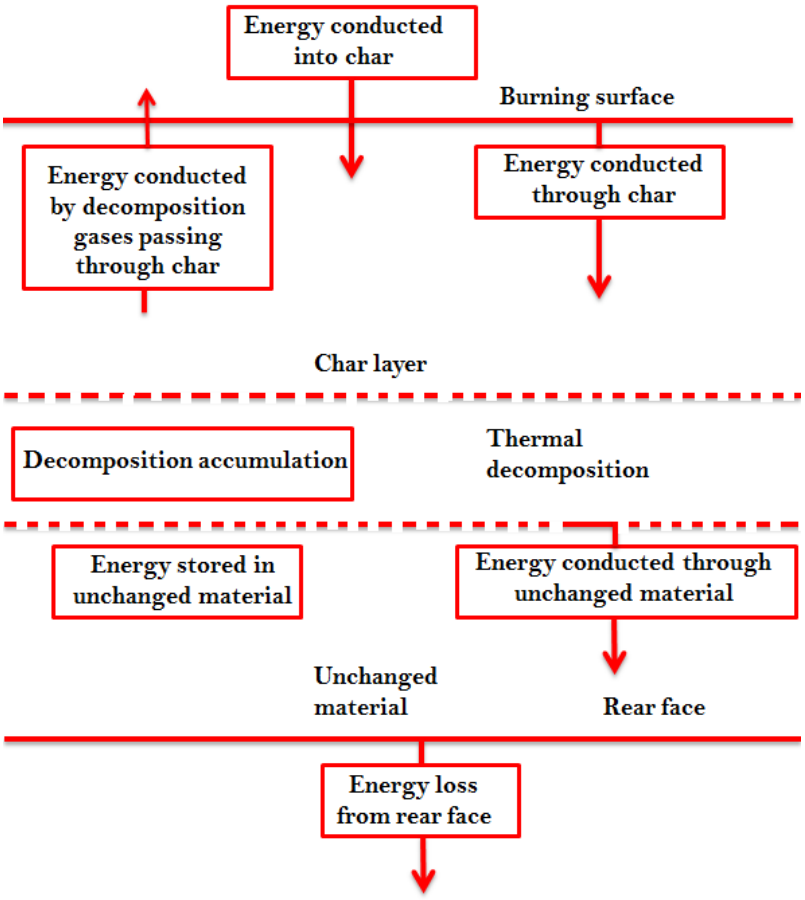

Figure 11. Mechanism of thermal transfer during materials combustion [128].

Reactive and additive flame retardants are two categories into which they can be divided[138].

The term "reactive flame retardants" refers to substances which are combined into the chains of polymers. These can be added chemically during polymer production or through post-reaction procedures, such as chemical grafting[136].

During the polymer transformation process, additive flame retardants can be physically added to the polymer. However, during combustion, when the temperature reaches a certain point, the flame retardant reacts with the polymer. This class includes hybrids and mineral fillers[139].

3.11. Intumescence

Intumescence is the mechanism by which materials retard the flames. These intumescent materials have the ability to swell, expand and create a carbonized layer when exposed to a heat source or fire. This expanded layer acts as a barrier to insulate against heat while simultaneously reducing fuel transfer and restricting the diffusion of oxygen into the material[140], [141].

A carbonizing or char-forming agent, an acid source that encourages the production of char, and a blowing agent (foaming agent) are needed for the development of intumescent materials. This blowing agent decomposes and releases gas, resulting in the creation of a swollen multicellular layer[142].

3.12. Types of flame retardants

Mineral flame retardants, halogenated flame retardants, phosphorus-based flame retardants, nitrogen-based flame retardants, silicon-based flame retardants, and nanoparticles are examples of widely used flame-retardant additives[128].

3.12.1. Mineral flame retardants

Mineral-based compounds called "mineral flame retardants" are included in materials to lessen their flammability and increase their resistance to fire. These compounds function by either physically interfering with combustion or they break down endothermically at higher temperatures, absorbing energy in the process. Additionally, they produce non-flammable molecules (CO_2, H_2O), which can help to form a protective vitreous or ceramic coating and dilute combustible gasses[143].

Aluminum hydroxide and magnesium hydroxide are one example of minerals used as flame retardant. Heat causes these minerals to emit water vapor, which cools the surrounding

environment and dilutes flammable gasses. Aluminum hydroxide and magnesium hydroxide may potentially exert a catalytic influence on the process of burning of the carbonized residues that are generated. The observed incandescence phenomena witnessed in various flame retardant tests can be explained by this[129]. The following equations (3 and 4) show the water emission mechanism of aluminum hydroxide and magnesium hydroxide upon heat[128].

$$2Al(OH)_3 \rightarrow Al_2O_3 + 3H_2O \quad (1050\, kJ/kg) \tag{3}$$

$$2Mg(OH)_2 \rightarrow 2MgO + 2H_2O \quad (1300\, kJ/kg) \tag{4}$$

Borates represent an additional category of inorganic additives that possess flame retardant characteristics. Among this group, zinc borates, exemplified by $2ZnO{\cdot}3B_2O_3{\cdot}3.5H_2O$, are the most commonly employed. Through their endothermic decomposition (503 kJ/kg) that occurs within the temperature range of 290 to 450 °C, water, boric acid, and boron oxide (B_2O_3) are released. The B_2O_3 that emerges subsequently softens at temperature 350 °C and exhibits a propensity to flow at temperatures surpassing 500 °C, thereby giving rise to the creation of a protective vitreous layer. In situations where polymers contain oxygen atoms, the presence of boric acid induces dehydration, which in turn fosters the generation of a carbonized layer. This particular layer serves to safeguard the polymer against the influences of both heat and oxygen. Consequently, the liberation of combustible gases is mitigated as a result[128], [144], [145].

Hydroxycarbonates is one more example of mineral based flame retardants[128], [146]. All carbonates discharge CO_2 at elevated temperatures; however, solely magnesium carbonates and calcium carbonates discharge it under 1000 °C, whereby magnesium carbonate exhibits the most minimal temperature of release (550 °C). Although hydroxycarbonates are less extensively utilized in comparison to other conventional flame retardants, they persist as a substitute for metal hydroxides. Furthermore, in addition to the emission of water, both natural magnesium carbonate and synthetic magnesium hydroxycarbonate degrade endothermically owing to the release of CO_2 at elevated temperatures[128], [147]. The following equations (5-7) describe the thermal decomposition of magnesium hydroxycarbonate in air[128].

$$4MgCO_3.Mg(OH)_2.4H_2O \rightarrow 4MgCO_3.Mg(OH)_2 + 4H_2O \quad (5)$$

$$4MgCO_3.Mg(OH)_2 \rightarrow 4MgCO_3.MgO + H_2O \quad (6)$$

$$4MgCO_3.MgO \rightarrow 5MgO + 4CO_2\ (associated\ heat = 800\ kJ/kg) \quad (7)$$

Magnesium hydroxycarbonate liberates both water and carbon dioxide within the temperature range of 200 °C to 550 °C, thereby implying a potential comparable or superior flame resistance efficacy in comparison to aluminum trihydrate and magnesium hydroxide[128].

3.12.2. Halogenated flame retardants

Flame retardants containing halogen elements, like chlorine or bromine, are known as halogenated flame retardants. These chemicals are frequently employed to increase the flame resistance of a variety of products, such as electronics, polymers, textiles, and plastics[148]. In order to prevent flames from igniting, halogenated flame retardants release radicals that obstruct the chemical processes that lead to burning. The primary factor influencing the effectiveness of halogen based flame retardants can be attributed predominantly to the cleavage of the carbon-halogen bond. The efficacy of halogen based flame retardants relies on the specific halogen utilized[122], [149]. Fluorine and iodine containing compounds are not employed due to their lack of interference with the combustion process of polymers. Fluorinated compounds exhibit greater thermal stability than the majority of polymers and do not generate halogen radicals within the same range of temperature or below the pyrolysis temperature of the polymers. Iodine containing compounds, on the other hand, possess lower thermal stability as compared to the majority of commercial polymers, thus leading to the release of halogen containing species during the processing of the polymer. Bromine and chlorine, due to their diminished bonding energy with carbon atoms, can be easily liberated and participate in the process of combustion, particularly in conjunction with the aforementioned gas-phase free-radical mechanism. Thermal decomposition of polymers results in the generation of highly reactive species (free-radical), for example H• and OH•. These species effectively support the combustion process in the gaseous phase through a cascading chain mechanism. Halogen based flame retardants have the ability to react with these reactive species, thereby halting the decomposition of the chain and subsequently extinguishing the polymer combustion[122], [150], [151]. The following equations (8-11)

show the reaction mechanism of halogen based flame retardants with highly reactive species (free- radical)[149].

$$RX \rightarrow R^{\bullet} + X^{\bullet} \quad (X\ can\ be\ Br\ or\ Cl) \tag{8}$$

$$X^{\bullet} + R'H \rightarrow R'^{\bullet} + HX \tag{9}$$

$$HX + H^{\bullet} \rightarrow H_2 + X^{\bullet} \tag{10}$$

$$HX + OH^{\bullet} \rightarrow H_2O + X^{\bullet} \tag{11}$$

Tetrabromobisphenol A (TBBPA) represents the prominent halogenated flame retardant employed in a broad range of applications. Its primary use lies in its function as a reactive flame retardant, particularly in epoxy resins[152]. In terms of halogenated flame retardant families, the polybromodiphenylether (PBDE) compounds rank second in terms of popularity. Up to ten bromine atoms bound to a diphenyl ether molecule can be found in the polybromodiphenylether (PBDE) compounds. These polybromodiphenylethers compounds, which have been developed as flame retardant additives, include penta- (5), octa- (8), and deca- (10) bromodiphenylethers[153], [154]. Figure 12 illustrates the chemical structure of tetrabromobisphenol A (TBBPA) and polybromodiphenylether (PBDE) compounds.

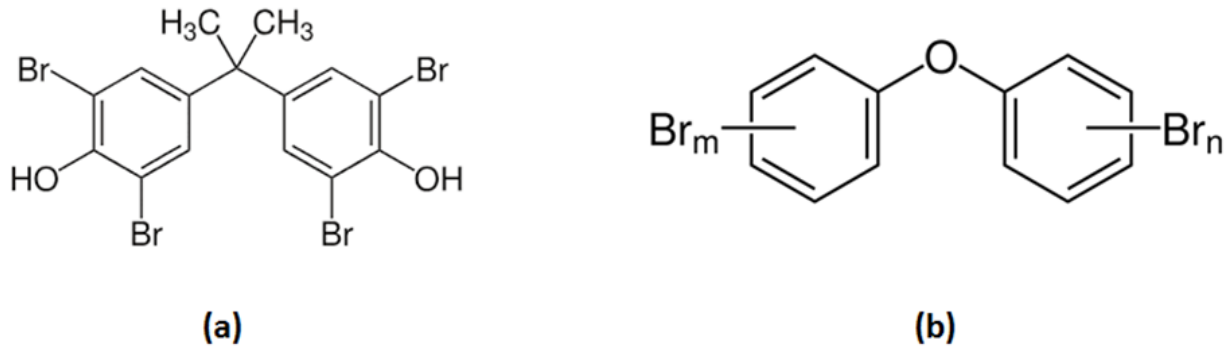

Figure 12. Chemical structure of halogen containing flame retardants (a) TBBPA (b) PBDE [128], [155].

Halogenated flame retardants, although effective in improving fire resistance, have given rise to apprehensions regarding the environment and health. Upon reaching the end of their life cycle, products containing these flame retardants pose a potential threat of chemical leaching into the surrounding environment. Certain halogenated flame retardants exhibit persistence and have the capability to accumulate within organisms, thereby giving rise to the possibility of long-lasting ecological and health consequences. As a result of these concerns, there has been a notable transition towards the development of substitute flame retardants that exhibit reduced detrimental effects on both the environment and human well-being[146], [156].

3.12.3. Nitrogen-based flame retardants

Nitrogen compounds constitute a relatively modest yet swiftly growing assemblage of flame retardants (FR), which have attracted substantial public attention owing to their eco-friendliness[157]. These substances are currently mostly used as dicyandiamide, melamine, or melamine phosphates in polyolefins; melamine cyanurate in nylons; and melamine for polyurethane flexible foams along with other intumescent paints. In addition, guanidine phosphates are used in fabrics, while guanidine sulfamate is used in wall coverings[158]. Melamine-based flame-retardant additives function similarly to a combination of inorganic and halogenated flame-retardants when they degrade over heat. Melamine's crystalline structure is thermally stable and experiences endothermic sublimation at temperatures around 350°C, which lowers the temperature during the combustion process[159]. The melamine breaks down at high temperatures, releasing non-flammable volatiles like ammonia that dilute the mixture of combustible gases and cause thermally stable condensates to form. In addition, melamine salts also function as flame-retardants in the condensed phase[160]. One of the notable advantages of nitrogen-based flame-retardants is their inherent low toxicity, low emission of smoke, and their ability to be recycled. They are frequently employed in conjunction with other flame-retardants, such as phosphorus-based flame-retardants[161]. Figure 13 shows the structural formula of melamine.

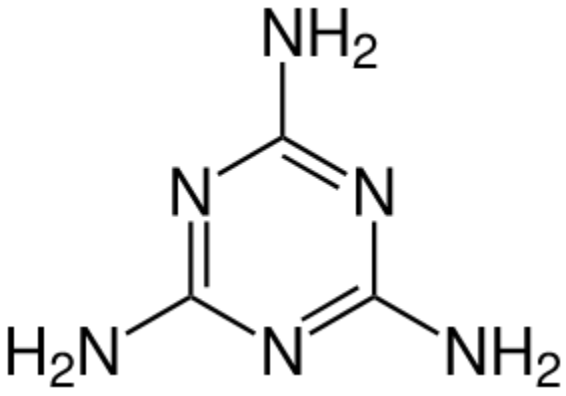

Figure 13. Structural formula of melamine [128].

3.12.4. Phosphorus-based flame-retardants

There is an enormous variety of phosphorus-based flame retardant compounds available, such as red phosphorus, phosphates, phosphonates, phosphinates, and phosphate oxides. These phosphorated flame retardants, which have been proven to be effective in the condensed and/or vapor phase, can be added to other substances or integrated into the polymeric chain during its production[162], [163]. The flame retardants that are based on phosphorus display a high level of efficacy in a condensed phase when used with polymers that are composed of oxygen, such as polyesters, polyamides, and cellulose. In the case of the majority of these flame retardants, the process of thermal decomposition results in the generation of phosphoric acid. This acid has a propensity to readily condense, thereby giving rise to the formation of pyrophosphate structures and the release of water[135]. The reaction mechanism of the formation of pyrophosphate structure through condensation of phosphoric acid is shown in Figure 14.

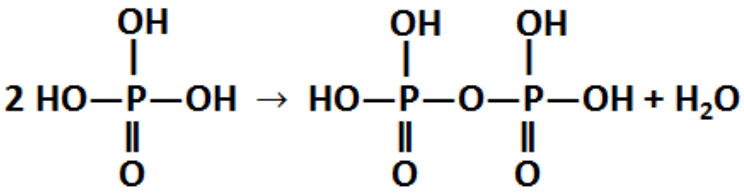

Figure 14. Formation of pyrophosphate structure through condensation of phosphoric acid[128].

The liberation of water leads to the dilution of the oxidizing gas phase. Additionally, the dehydration reaction of the terminal alcohols, resulting in the creation of carbocations and carbon–carbon double bonds, can be catalyzed by phosphoric acid and pyrophosphoric acid (Figure 15). This, in turn, at elevated temperatures, can subsequently lead to the production of crosslinked or carbonized structures[135], [162].

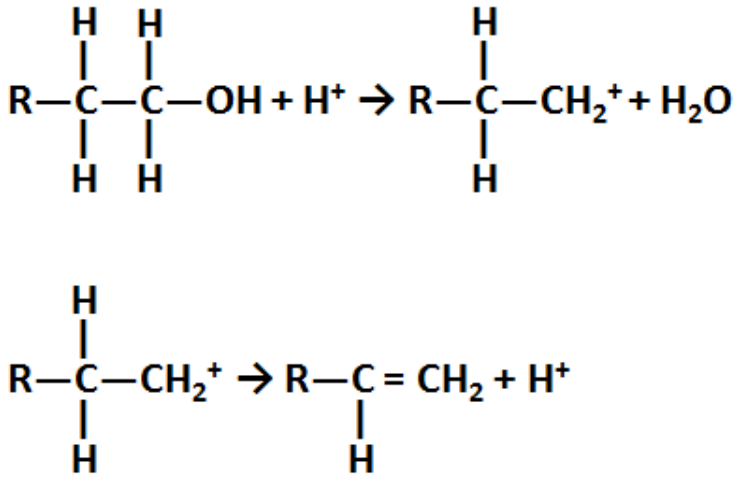

Figure 15. Formation of double carbon–carbon bonds after dehydration of alcohol end groups. [128]

At elevated temperatures, ortho- and pyrophosphoric acids undergo a transformation into metaphosphoric acid "(O)P(O)(OH)" and their associated polymers "$(PO_3H)_n$". Subsequently, the phosphate anions (pyro- and polyphosphates) engage in char formation alongside the carbonized residues. This resulting carbonized layer, known as char, acts as a shield, effectively insulating and safeguarding the polymer from the flames while also impeding the diffusion of oxygen. Additionally, the presence of char hinders the volatilization of fuel and serves as a barrier against the generation of new free radicals[128].

Phosphorus containing compounds are also capable of undergoing volatilization and into the gaseous state, thus leading to the creation of active radicals (such as PO_2•, PO•, and HPO•) and serve as scavengers for H• and OH• radicals. Volatile phosphorated flame retardant compounds are regarded as some of the most potent inhibitors of combustion due to the fact that, on average, phosphorus containing radicals are 5 times more efficacious than bromine radicals and ten times more efficacious than chlorine radicals. Phosphorus containing flame

retardants exhibit a significantly enhanced efficacy in polymers that contain either oxygen or nitrogen. Consequently, the presence of oxygen or nitrogen atoms within the polymer's molecular structure is of utmost importance. In instances where the polymer lacks suitable reactive groups that can contribute to the charring process, it becomes crucial to introduce a co-additive alongside the phosphorus-based flame retardant to facilitate highly efficient charring[130], [131]. This co-additive can potentially take the form of a polyol, for example pentaerythritol. Moreover, certain polymers like polyamides or polyurethanes can also serve as effective charring agents within intumescent flame retardant systems[164].

Ammonium polyphosphate (APP) (Figure 16) is a compound that consists of an inorganic salt formed from polyphosphoric acid and ammonia[165]. The length of the chain in this polymeric compound, whether it is branched or unbranched, can vary. The value of the chain length, denoted as "n," can exceed 1000. APPs with shorter, linear chains (known as crystalline form I or APP I) have a greater sensitivity to water (hydrolysis) and exhibit lower thermal stability in comparison to APPs with longer chains (known as crystalline form II or APP II), which have a chain length greater than 1000. APP II also displays very poor water solubility, measuring less than 0.1 grams per 100 milliliters. It is commonly known that APP is incorporated into oxygen and/or nitrogen possessing polymers such as polyesters, polyamides, and polyurethane is widely recognized as leading to the charring of the polymer. Upon thermal breakdown, APP generates free acidic hydroxyl groups, which undergo thermal dehydration to produce a crosslinked ultraphosphate and a highly crosslinked polyphosphoric acid. The polyphosphoric acid then interacts with the oxygen or nitrogen possessing polymers, catalyzing their dehydration reaction and promoting the formation of char[128], [166], [167]

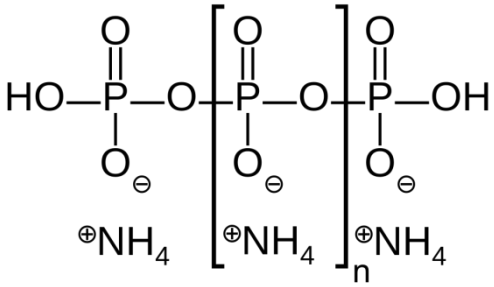

Figure 16. Structure of ammonium polyphosphate[128].

Despite the fact that numerous organic phosphorus derivatives exhibit flame-retardant characteristics, the quantity of those possessing commercial significance is constrained by the temperature at which processing occurs and the inherent properties of the polymer that is to be altered. Moreover, organic phosphorus derivatives have the capability to function as additives or as reactive (co)monomers/oligomers. The primary classifications of organophosphorus compounds encompass phosphate esters, phosphonates, and phosphinates (Figure 17)[128], [168].

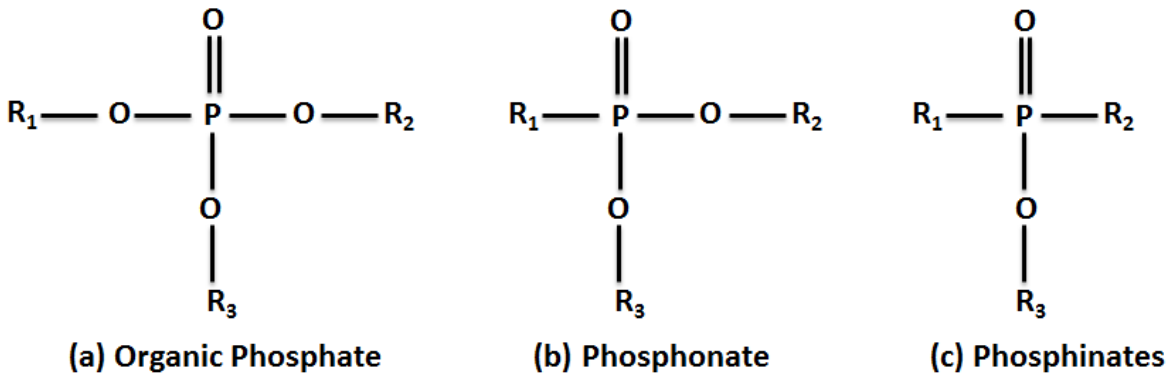

Figure 17. Chemical structures of some phosphorus based flame retardant[128].

N-methylol dimethylphosphonopropionamide (MDPA) is organophosphorus based durable flame retardant compound for cellulose fabrics[168]. Huong *et al.* conducted an assessment on the efficacy of an innovative flame retardant system comprising of N-methylol dimethylphosphonopropionamide (MDPA), citric acid, and sodium hypophosphite catalyst on cotton fabric. They discovered that a rise in the concentration of N-methylol dimethylphosphonopropionamide (MDPA) resulted in an escalation of the limiting oxygen index (LOI) and a reduction in char length values. Collectively, MDPA has demonstrated potential as an additive for flame retardancy in diverse applications. Figure 18 indicates the chemical structure of MDPA[18].

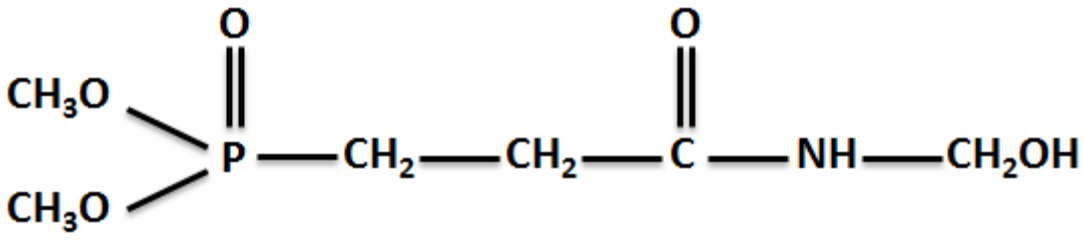

Figure 18. Chemical structure of MDPA[169].

3.12.5. Silicon-based flame-retardants

Silicon-based compounds that are appropriate for use as flame retardants include silica, silicones, organosilanes, silicates, and silsesquioxanes[170]. Because silicon is plentiful and may be modified to have desirable qualities for particular applications, silicon-based flame retardants are appealing. They may appear in the shape of copolymers or be incorporated as fillers into the polymer. When silicones with high heat resistance and excellent thermal stability break down, a small amount of harmful gasses is released[128]. Silicones were used in polycarbonate (PC) as flame retardants. Because of the combined effect of polysiloxane and condensed aromatic compounds, they are easily distributed in polycarbonate and migrate towards the surface after combustion to generate a highly persistent char[171]–[173]. The flame-inhibiting principle for additives that retard flames in silicon-based materials involves the movement of silicone derivatives towards the surface of the material as it degrades during the process of combustion. This movement results in the creation of a partially protective char layer that is thermally stable, and that provides some level of protection to the underlying material. The formation of this char layer is primarily influenced by the viscosity of both the degrading polymer and the flame-retardant complex that is based on silicon[174].

Silica, a naturally found compound comprised of silicon and oxygen (SiO_2), is frequently employed as a flame inhibiting filler in various substances. When subjected to elevated temperatures, silica has the ability to facilitate the creation of a stable char layer, which functions as a barricade against flames[175]. Figure 19 shows the chemical structure of silicon dioxide.

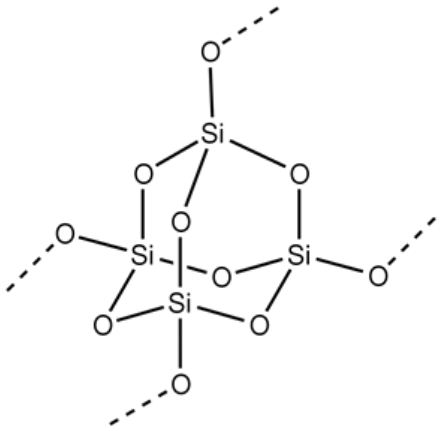

Figure 19. Chemical structure of silicon dioxide[176].

Siloxanes are substances that encompass silicon-oxygen (Si-O) bonds. Certain siloxanes have undergone examination due to their flame-restraining attributes. These compounds may potentially operate via the emission of water vapor during combustion, which aids in the cooling of the material and the dilution of combustible gases[177], [178]. Chemical structure of siloxane is shown in Figure 20.

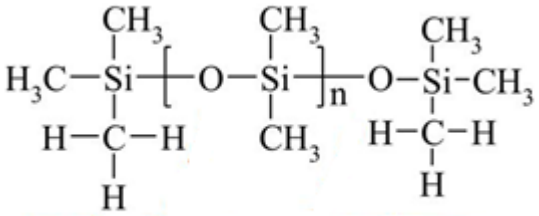

Figure 20. Chemical structure of siloxane[179].

3.12.6. Nanoparticles as flame retardants

Nanoparticles are currently under investigation for their potential application as flame retardants on account of their distinct characteristics and potential advantages. The rationale behind the utilization of nanoparticles as flame retardants lies in capitalizing on their

diminutive dimensions and extensive surface area, which can result in improved efficacy in diminishing flammability. Numerous categories of nanoparticles have been examined for their flame retardant attributes[180], [181].

Nanoparticles of metal oxides, namely zinc oxide (ZnO), magnesium oxide (MgO), aluminum oxide (Al_2O_3) and titanium dioxide (TiO_2), have been the subject of extensive investigation due to their inherent flame-retardant properties[182]–[185]. Metal oxides act as a physical barrier and have the potential to promote the formation of a substantial char layer when the polymer is combusted, thereby impeding the material's exposure to thermal sources and enabling the apprehension of the smoke produced during the burning process, creating a labyrinth effect, and suppressing molecular mobility. Consequently, these metal oxides act as a safeguard, shielding the interior substances from combustion[186], [187].

Carbon nanotubes (CNTs) and other structures composed of nanotubes has been the subject of investigation due to their properties as flame retardants. These materials are capable of acting as physical obstacles, thereby restricting the entry of oxygen to the substance. Furthermore, they have the potential to augment the generation of char[188], [189].

Non-combustibility constitutes a pivotal characteristic of nano-clays. The incorporation of nano-clays into polymers has been observed to diminish the flammability of said polymers. The substitution of conventional halogen-containing flame retardants with nano-clays has become prevalent due to their cost-effectiveness, wide accessibility, environmentally friendly nature, and enhanced physical properties. The mechanism underlying the non-combustibility properties of nano-clay-based materials involves the creation of a carbonaceous layer that shields the underlying material during combustion. The non-flammable nature of nano-clays holds great promise in a multitude of contemporary applications, including aerospace, automotive, textile, electronic, construction, and environmental domains[190]–[192].

3.13. Zinc oxide nanoparticles (ZnO NPs)

Zinc oxide (ZnO) is a powder, white in color that can be synthesized from the rarely found mineral zincite, available in nature or produced from several precursors[193]. Zinc oxide (ZnO) is classified as an n-type semiconductor with excellent electron mobility, possessing a

direct and broad band gap (≥3.37 eV) located near the UV spectrum region[194], [195]. It comprises Zn^{2+} and O^{2-} ions bound together with a significant degree of ionicity and a lower degree of covalency[23]. In general, ZnO has been found in three primary crystalline structures: cubic rocksalt structure, cubic zinc blende, and wurtzite hexagonal crystalline structure. Of these, the wurtzite hexagonal crystalline form is the most abundant because it is thermally stable in ambient environments[196]. Zinc oxide (ZnO) has been widely acknowledged as a chemical agent for the functionalization of textiles due to its distinctive physical and chemical attributes, ecological compatibility, biocompatibility, and economical cost[33], [197]. The primary benefit of this material is found in the aspect that the US Food and Drug Administration (FDA) have generally acknowledged bulk ZnO as a substance that is safe for consumption[197].

There are mainly two approaches for producing ZnO nanoparticles: the top-down method, also known as the metallurgical procedure, involves roasting the precious mineral zincite. Second approach is the bottom-up method employs a range of physical and chemical synthesis techniques, such as mechanochemical, electrochemical techniques, sonochemical, hydrothermal process, solvothermal, ultrasonic irradiation, microwave irradiation, sol-gel method, microemulsion, coagulation processes, and controlled precipitation methods[23], [33], [193], [198]. ZnO can generally be applied as a ZnO salt solution or suspension that has already been manufactured, or it can be applied by creating ZnO nanoparticles (ZnO NPs) in-situ onto a textile substrate[199], [200]. ZnO nanoparticles (ZnO NPs) are among the most effective photocatalytic self-cleaning, antibacterial, and UV-protective agents due to their exceptional photocatalytic activity, chemical stability during the exposure of UV radiation, thermal stability, and ability to absorb a wide range of UV radiation. Moreover, ZnO NPs have recently been incorporated into textile fibers to enhance their hydrophobicity, electrical conductivity, moisture management, thermal stability, and flame retardancy[193], [201]–[211]. Due to their photocatalytic qualities, ZnO NPs can also be employed as degradation reagents for various contaminants, including dyes and surfactants found in effluent from the textile sector[212], [213].

3.13.1. Flame retardancy of ZnO NPs

A condensed phase mode of action through the heat barrier effect has been suggested as the foundation for flame retardancy of ZnO NPs[124]. Due to exceptional thermal stability, ZnO NPs can shield the insulating layer on the surface of the fiber, minimizing the amount of heat, fuel, and oxygen that are transferred from the flame to the fibers and, as a result, lowering the intensity as well as rate of burning. Additionally, ZnO is already classified as a substance that suppresses the production of smoke[214].

The research on ZnO NPs based flame-retardant fabrics is quite limited[215]. The researchers applied ZnO NPs either alone or jointly with phosphorus containing organic compounds to cotton, polyester, or a blend of cotton and polyester; nevertheless, for technical purposes, sisal and jute fibers containing textile substrate were also utilized[204], [216], [217]. The outcomes demonstrated that replacing bulk ZnO with ZnO NPs greatly increased the flame retardancy of the ZnO NPs loaded cellulosic fibers[204]. ZnO NPs suppressed smoke, lowered the rate of heat release, and enhanced the limiting oxygen index of the cellulosic fibers[31], [204], [217]. Furthermore, ZnO NPs greatly enhanced the amount of char residue, decreased the char length, and reduced the after flame time as well as afterglow time[201], [214], [215]. However, ZnO NPs coating was unable to achieve the self-extinguishing properties of cellulose fiber, even at excessive mass loadings[214].

3.13.2. Photocatalytic self-cleaning properties of ZnO NPs

Because of its electrical structure, zinc oxide (ZnO) exhibits extraordinary multifunctional features, including photocatalytic activity[218]. When exposed to radiation with energy equivalent to or higher than the band, excitable electrons in ZnO migrate to the conducting band (e^-_{CB}), while holes remain behind in the valence band (h^+_{VB})[219]. At the top surface of ZnO, two different photochemical processes occur simultaneously when water and oxygen are present. The initial process involves oxidation, where photo-induced holes participate, while the subsequent process involves reduction, with the participation of photo-induced electrons. These reactions lead to the formation of reactive oxygen species (ROS), specifically $\bullet OH^+$ and $\bullet O^-_2$, which play a pivotal role in the efficient photocatalysis of ZnO. Conversely photocatalytic efficiency of ZnO is reduced by the recombination of the photo-excited

negative electrons present within the conduction band with the photo-induced positive holes present within the valence band, which causes heat to be dissipated [193]. When ZnO NPs exist on the top of textile fabrics, ZnO NPs has the ability to react and degrade different organic dirt stains, both colorful and colorless[220]. In this scenario, the organic compounds can undergo direct photo-oxidation through a reaction with h^{+}_{VB}, as well as indirect photo-oxidation through a reaction with reactive oxygen species (ROS). As a result, organic chemicals breakdown and are removed from textile fabrics[221]. This phenomenon is known as photocatalytic self-cleaning since it cleans the textile surface without the need for washing procedures[193].

3.13.3. Antibacterial properties of ZnO NPs

The antibacterial efficacy of ZnO is ascribed to the production of reactive oxygen species (ROS) via ZnO photocatalysis and the liberation of Zn^{2+} cations from the surface of ZnO nanoparticles[222]. Despite extensive investigation conducted in this domain, the precise mechanism underlying the antibacterial effectiveness of ZnO NPs remains incompletely comprehended. The divergence in findings is likely attributable to the utilization of distinct zinc precursors, variances in synthesis conditions, differing concentrations of ZnO NPs, structures of ZnO crystal, sizes, shapes, dissimilar surface textures, various types of defects, and functionalization, all of which exert an influence on the antibacterial mechanism[193]. Under visible as well as ultraviolet exposure, it is thought that the photocatalytic production of ROS, particularly H_2O_2 and •OH, is essential for antibacterial action of ZnO NPs. ZnO NPs have the ability to adsorb directly to the surface of bacterial cells; thereafter, they can cause disruption of the cell wall (Figure 21). The membrane of bacterial cells can be readily penetrated by the highly reactive ROS produced, leading to oxidative stress and the deterioration of cellular constituents (i.e. proteins, lipids, and DNA). Moreover, Zn^{2+} cations that are liberated by ZnO dissolution have the ability to enter bacterial cells and stop respiratory enzyme activity there. Under conditions of low light intensity, the antibacterial effectiveness of ZnO NPs is hypothesized to be less dependent on the production of reactive oxygen species (ROS). Instead, it is primarily associated with the adherence of ZnO NPs to the walls of bacterial cells, as well as the accumulation of higher amount of Zn^{2+} ions within the cytoplasm of these bacteria[223]–[225].

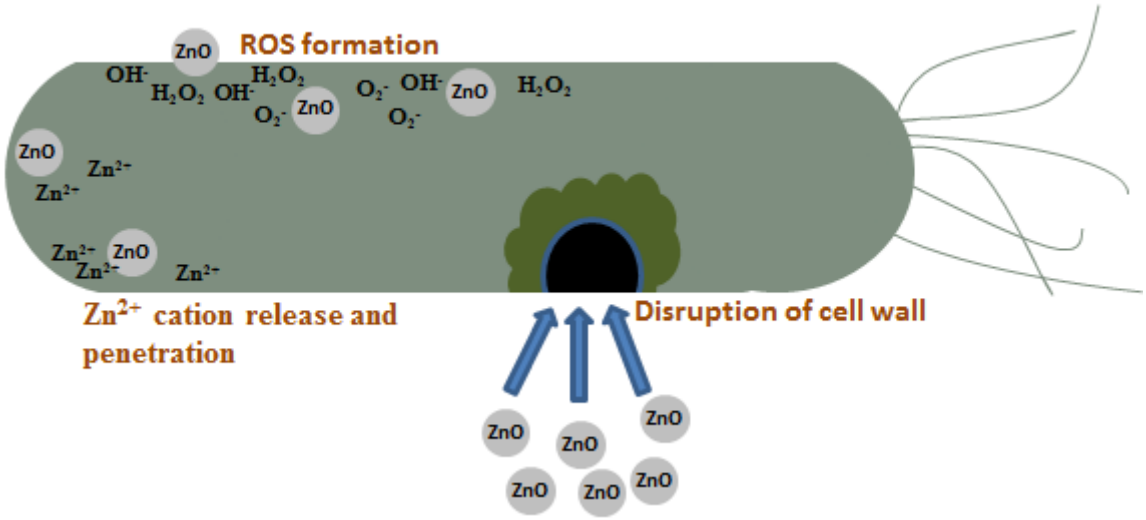

Figure 21. Mechanism of antibacterial activity of ZnO NPs[193].

3.13.4. UV protection of ZnO NPs

The spectrum of sunlight encompasses ultraviolet (UV) radiations, which can be classified into three primary types: ultraviolet A, B, and C radiation, denoted as UVA, UVB, and UVC, respectively. UVC radiation spans the wavelengths ranging from 100 to 280 nm, while UVB radiation covers the range from 280 to 315 nm, and UVA radiation extends from 315 to 400 nm[23]. It is important to note that UVC radiation is predominantly absorbed by the ozone layer in the atmosphere and, therefore, does not reach the surface of the earth. Among the mentioned types, UVA radiation poses the greatest risk, leading to skin cancer, sunburn, acne, and deoxyribonucleic acid (DNA) damage[226]. The fabric's capacity to shield the skin against harmful radiation is measured by the UV protection factor (UPF). The UPF value quantifies the extent to which the fabric transmits UV rays[227]. The Australian Standardization Institute has established UPF values and protection categories for different fabrics, which are presented in Table 1[228].

Table 1. UPF value and protection category of the fabric categorized by The Australian Standardization Institute.

UPF value	Protection level
Below 15	Not good
15-24	Good
24-39	Very good
40 and above	Excellent

Zinc oxide (ZnO) is renowned for its remarkable ultraviolet (UV) protection characteristics[229]. These attributes arise from its exceptional chemical resilience when exposed to UV radiation and its remarkable efficacy in obstructing both UVA and UVB rays. Zinc oxide nanoparticles possess the capability to absorb ultraviolet (UV) radiation, primarily within the UVA and UVB spectra. When exposed to UV rays, ZnO NPs absorb the corresponding energy through the interaction with their electrons, impeding the penetration of such radiation from the fabric into the skin. This absorption phenomenon plays a pivotal role in safeguarding the integrity of DNA within skin cells, thereby reducing the likelihood of both sunburn and long-lasting skin harm[230]. Apart from absorption, ZnO NPs also disperse UV radiation via the process of scattering. This scattering effect disperses UV rays in diverse directions, thus preventing their penetration from the surface of fabric to the skin. Consequently, this scattering effect contributes significantly to the comprehensive UV protection offered by ZnO NPs against both UVA and UVB rays[231]. Furthermore, ZnO NPs exhibit reflective attributes within the UV range, effectively deflecting a proportion of the incident UV radiation away from the surface of the fabric. This reflective mechanism imparts an additional layer of protection against harmful UV exposure[193].

CHAPTER 4

Materials and Methods

4.1. Materials

The 100 percent cotton fabric with a plain weave texture, 155 g/m^2 density, 52 ends/inch, 28 picks/inch, and 20 tex warp count, 20 tex filling count, was acquired from the Technical University of Liberec, Czech Republic. Citric acid $C_6H_8O_7$, zinc acetate dihydrate ($Zn(CH_3COO)_2.2H_2O$), sodium hydroxide (NaOH), sodium hypophosphite (SHP), and 1, 2, 3, 4-butanetetracarboxylic acid (BTCA) chemical reagents were procured from Merk, Prague, Czech Republic. N-Methylol dimethylphosphonopropionamide (MDPA) was obtained from the Huntsman Corporation. Acramin SW acrylic-based binder was obtained from Tanatex Chemicals, The Netherlands. All the obtained chemical reagents were of analytical grade and utilized as purchased without further purification.

4.2. Surface activation of cellulose

To obtain maximum adherence of ZnO NPs and MDPA on the cellulosic structure of the cotton fabric, the cotton fabric was pretreated with a 0.5% aqueous solution of citric acid in the presence of 0.5% sodium hypophosphite as a catalyst for cellulosic surface activation. As the citric acid and cotton fibers were added to deionized water, both were ionized, as shown in equations (12) and (13). In a further reaction, carboxylic groups of citric acid were easily attached to the hydroxyl groups on the cotton fabric, as shown in equation (14).

$$C_6H_8O_7 + H_2O \leftrightarrow C_6H_7O_7^- + H_3O^+ \quad (12)$$

$$Cellulose\text{-}OH + H_2O \leftrightarrow Cellulose\text{-}O + H_3O^+ \quad (13)$$

$$C_6H_7O_7^- + Cellulose\text{-}OH + H_2O \leftrightarrow Cellulose\text{-}CA + H_3O^+ \quad (14)$$

4.3. In-situ sonochemical synthesis of ZnO NPs on cotton fabric

ZnO NPs were synthesized and stabilized onto the cotton fabric concomitantly by hydrolysis of zinc acetate dihydrate ($Zn(CH_3COO)_2.2H_2O$) and sodium hydroxide (NaOH) in deionized

water. Table 2 shows the experimental variables used in this research. Full factorial experimental design was applied to develop the samples. The precursors, zinc acetate dihydrate ($Zn(CH_3COO)_2.2H_2O$) and sodium hydroxide (NaOH) with different molar concentrations, were dissolved separately in deionized water under vigorous magnetic stirring (300 rpm) conditions. After that, the cotton fabric piece was dipped into the zinc acetate dihydrate solution for 10 min under vigorous magnetic stirring (300 rpm). After 10 min, the NaOH solution was poured dropwise into that solution at ambient temperature and under vigorous magnetic stirring (300 rpm). For absolute completion of the reaction mechanism, the obtained solution containing the immersed cotton fabric piece was sonicated for different sonication times (Table 2). The Branson sonication probe (20 kHz, 50% efficiency, 150 W) was utilized in this experimental procedure. The reaction temperature was maintained at 80 °C by utilizing a hot plate. Then, the treated fabric pieces were washed thoroughly with deionized water to remove any impurities. Eventually, the obtained fabric pieces were placed in an air oven at 90 °C for 120 min. In order to compare the sonochemical process and to accentuate the critical influence of ultrasound irradiation waves, one sample was developed using a conventional magnetic stirring method using the same precursor concentrations (0.1 M $Zn(CH_3COO)_2.2H_2O$, 0.3 M NaOH) and temperatures (80 °C) as the optimized sample (will be discussed in next section), under vigorous magnetic stirring (300 rpm) for 90 min. In this research work, this sample was named sample A.

Equations (15–17) show the proposed mechanism of ZnO NPs synthesis on the cotton fabric.

Table 2. Experimental variables for the synthesis of ZnO NPs.

Zinc acetate dihydrate (M)	Sodium hydroxide (M)	Sonication time (minute)
0.05	0.1	30
0.1	0.2	60
0.15	0.3	90
		120

$$Zn(CH_3COO)_2.2H_2O + 2NaOH \rightarrow 2CH_3COONa + Zn^+ + 2OH^- + 2H_2\,O \quad (15)$$

$$Zn^+ + 2OH^- \rightarrow Zn(OH)_2 \quad (16)$$

$$Zn(OH)_2 \rightarrow ZnO + H_2O \quad (17)$$

4.4. Extraction of solid powder

After removing the fabric, the solution was centrifuged at 5000 rpm for 3 min to separate the solid ZnO NPs from the liquid. The centrifuged solid was thoroughly washed with deionized water to remove any impurities and finally dried in an air oven at 90°C for 120 min.

4.5. MDPA application

MDPA application was performed with the help of a laboratory padder (Werner Mathis AG Switzerland) at 80% wet pick up. The bath formulation used 300 g/L MDPA, 60 g/L BTCA crosslinker, 50 g/L SHP catalyst, and 5 g/L acramin SW binder. Various preliminary trials were conducted to determine the best compatible concentrations of MDPA and BTCA with optimized ZnO NPs loaded samples. ZnO NPs loaded samples were impregnated in MDPA and BTCA solution, padded and dried at 110 °C for 3 min, and cured at 150 °C for 2 min. In order to determine the crucial role of ZnO NPs in flame retardancy, a cotton fabric sample was treated with MDPA and BTCA without ZnO NPs treatment. In this research work, that sample was named sample B.

Figure 22 shows the schematic diagram for surface activation of cellulose; in-situ synthesis of ZnO NPs on the cotton fabric and MDPA application and the Figure 23 indicates reaction mechanism of MDPA and BTCA with cellulose.

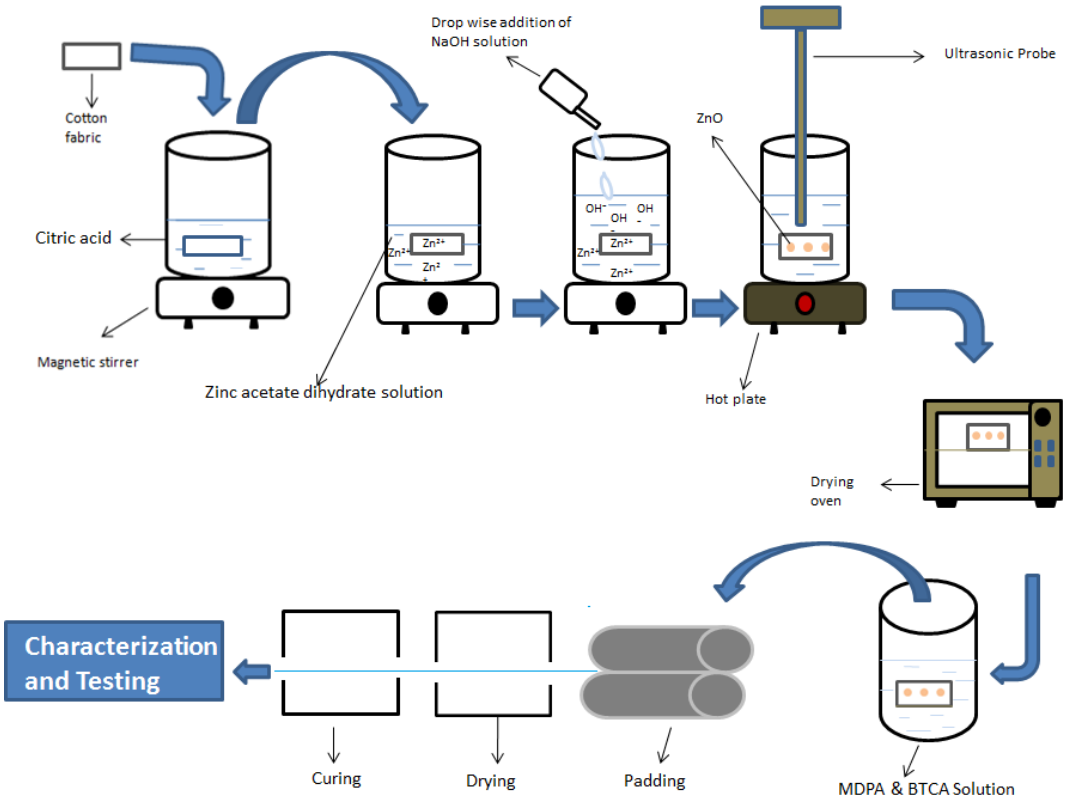

Figure 22. Schematic diagram for surface activation of cellulose, in-situ synthesis of ZnO NPs on the cotton fabric and MDPA application.

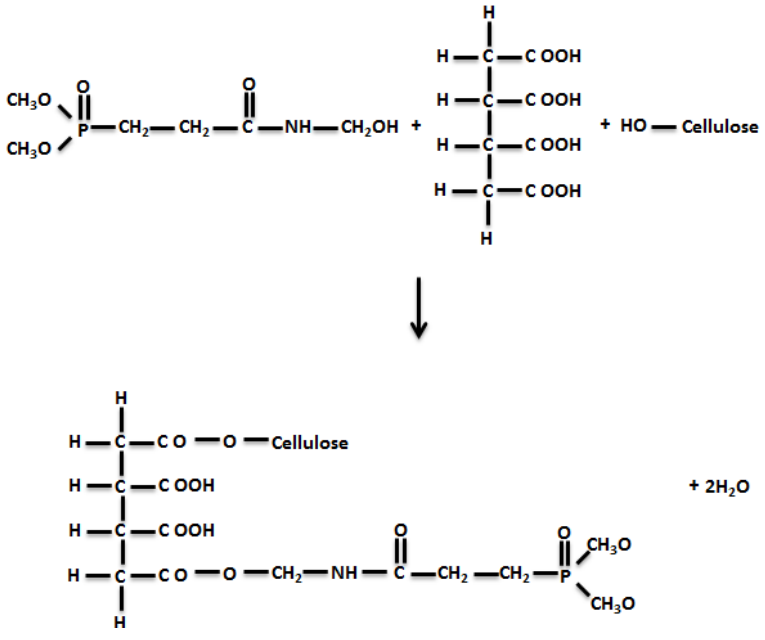

Figure 23. Reaction mechanism of MDPA and BTCA with cellulose.

4.6. Characterization and testing

4.6.1. Content analysis

The induced coupled plasma atomic emission spectrometer (ICP AES, Optima7300 DV, Perkin-Elmer Corporation, Waltham, MA, USA) was utilized to analyze the Zinc (Zn) contents and phosphorous (P) contents. The developed fabric sample of weight 0.1 g was treated with 8 mL of concentrated nitric acid (HNO_3) (65 %) until the fabric was wholly dissolved. Then the obtained solution was shifted to a volumetric flask of 100 mL capacity, and finally, dilution was done with deionized water.

4.6.2. Add-on %

The add-on % (uptake) was calculated according to equation (18).

$$Add\ on\% = \frac{wf-wi}{wi} \times 100 \quad (18)$$

In equation (18)

wf= final weight of the developed sample

wi= initial weight of the untreated sample

4.6.3. Surface morphology

The surface of the pristine cotton and developed samples was visualized using a Quanta 200 FEG scanning electron microscope (SEM) (FEI Company, Hillsboro, OR, USA). The specimens underwent a process of gold sputter coating in order to enhance the electrical conductivity of their surface.

4.6.4. Particle size analysis

The particle size of the synthesized ZnO NPs was examined by employing dynamic light scattering (DLS) technology using the Malvern zeta sizer (Malvern Panalytical Ltd, United Kingdom). Extracted solid ZnO NPs from the synthesis solution were dispersed in deionized water with the help of an ultrasonic probe. Eventually, the DLS technique was employed.

4.6.5. XRD analysis

The XRD patterns were measured using an X-ray diffraction system (Powder X-ray diffraction system, ARL, X,TRA, Thermo Scientific USA). The measurements were recorded in the range of diffraction angle 2Θ=10°-70°, with step size 0.02, and scan rate 2 [°/m], and 0.6 integration duration.

4.6.6. FTIR analysis

The fourier transform infrared spectroscopy (FTIR) was employed on the developed samples and pristine cotton to investigate the surface chemical structure. The measurements were performed at room temperature with the help of a Perkin Elmer spectrometer equipped with Thermo Scientific Nicolet IS50 FT-IR USA attenuated total reflectance (ATR) technology. The spectra were recorded in the range of 4000 to 400 cm^{-1} using ZnSe crystal at a resolution of 4 cm^{-1} with 32 scans.

4.6.7. Thermogravimetric analysis

The thermal stability of the developed and untreated samples was examined with the help of thermo gravimetric analysis (TGA) using a TGA/SDTA 851 METLER TOLEDO analyzer. The untreated and developed samples were subjected to heat in a synthetic air atmosphere from 30 °C to 700 °C with a 10 °C/min heating rate. Finally, the weight loss percent of the samples was measured.

4.6.8. Vertical flame test

To evaluate the flammability of untreated cotton samples and developed samples, vertical flame test (ASTM D6413-2015) was employed. This particular methodology aims to ascertain the reaction of textile materials when exposed to a prescribed source of ignition. It intends to derive quantitative data regarding the duration of after flame, after glow, and the length of the resulting char. Samples with dimensions (300 × 70 mm) that have been cut from the fabric for the purpose of testing are affixed to a frame, which is suspended in a vertical position within the flame chamber. Subsequently, a regulated flame 38 mm in size is directed towards the sample for a predetermined period of time (i.e. 12 seconds). Following the removal of the burner, the duration for which the material continues to burn, known as the after flame time, is documented. Additionally, the length of time the material continues to emit a glow after the

flame has been extinguished, referred to as the after glow time, is also recorded. Lastly, the specimen is torn apart using weights, allowing for the measurement of the char length. This refers to the distance from the fabric's exposed edge, which was subjected to the flame, to the end of the area that has been impacted by the flame.

4.6.9. Limiting oxygen index

The LOI values were recorded for untreated and developed samples according to the standard test method ASTM D2863-97. In this method, sample is ignited with combustible flame in an oxygen/nitrogen environment. The LOI measurement is conducted on specimens with dimensions (80 × 10 mm), which are positioned vertically within a glass chimney at its center. In order to achieve homogenization, the gas mixture is passed through layers of glass beads as it moves upstream through the chimney. Following a 30 seconds column purge, the specimen's upper part is ignited, resembling the lighting of a candle. Then the oxygen concentration in the oxygen/nitrogen environment is decreased until the flame is extinguished. The minimum concentration of oxygen which supports the combustion is recorded. LOI is expressed as volume percent and calculated according to the following equation (19).

$$LOI = (100 \times O_2)/(O_2 + N_2) \quad (19)$$

4.6.10. UV protection

Pristine cotton sample and treated samples were analyzed for their UV protective properties on a Varian CARY 1E UV/VIS spectrophotometer equipped with a DRA-CA-301 integration sphere and solar screen software. The samples were measured in the UV range 280 nm to 400 nm. The transmittance measurements and calculations of the UPF were carried out in accordance with the AATCC 183-2000 standard. The UPF value was calculated according to equation (20).

$$UPF = \frac{\sum_{280nm}^{400nm} E_\lambda S_\lambda \Delta_\lambda}{\sum_{280nm}^{400nm} E_\lambda S_\lambda T_\lambda \Delta_\lambda} \quad (20)$$

E_λ= solar spectral irradiance

S_λ= relative erythemal spectral response

Δ_λ= measured wavelength interval in nanometers

T_λ= average spectral transmittance from the sample

4.6.11. Antibacterial activity

The quantitative method AATCC 100-2012 was used to analyze the antibacterial performances of the samples. According to this standard, 1 mL of bacterial inocula was taken in a conical flask, and fabric pieces (4.8±0.1 cm diameter) were added into that flask and let to remain in contact with bacterial inocula for 24 hours. After that, the solution was subjected to serial dilution up to 10^{-7} in nutrient broth. Then, the 0.1 mL of the dilution was transferred to the agar plate and finally incubated for the duration of 24 hours at a temperature of 37 °C. The no. of bacterial colonies that appeared were counted. The bacterial reduction % was calculated according to the following equation (21).

$$R\% = \frac{A-B}{A} \times 100 \quad (21)$$

Where

R= bacterial reduction %

A= no. of bacterial colonies appeared from the untreated sample

B= no. of bacterial colonies appeared from the treated sample

4.6.12. Self-cleaning

The photocatalytic self-cleaning activity of the untreated and chemically modified samples was determined based on the photodegradation of a coffee stain under UV light. For this purpose, the samples were immersed in coffee (10 g ground coffee/100 mL water) for 30 s; the stained samples were irradiated under the UV light of Philips TL 6W UV tubes (315-400 nm) and the stain degradation performance was evaluated as a function of exposure to UV light. Later, the fabric surfaces discolored after the tests were scanned with 300 dpi and the scanned images were analyzed to calculate the color intensity by Image J software (Figure 24).

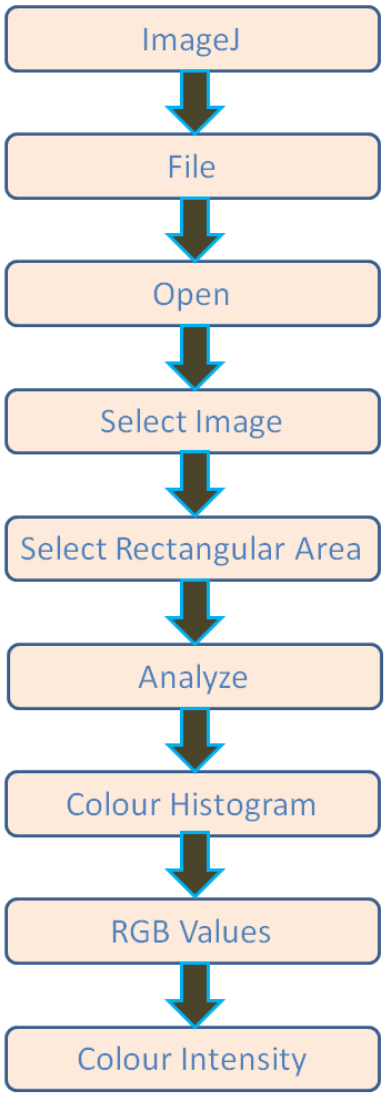

Figure 24. Method to calculate color intensity by ImageJ.

4.6.13. Bending rigidity

Bending rigidity was measured using the TH-7 instrument. This equipment produces a bending force from which we can compute bending rigidity. The measuring range of this device for bending force is 40 mN to 4000 mN. This device is identical to the standard Kawabata KES-FB 2 device, which is used for assessing low stress mechanical properties. The mean of five readings for each sample was calculated.

4.6.14. Air permeability

The Textest FX 3300 equipment was used to assess the air permeability of untreated and developed samples in accordance with ČSN EN ISO 9237 standard. The measuring principle relies on the measurement of the airflow passing through the fabric at a specific pressure. The airflow passing through at 200 Pa pressure on an area of 20 cm^2 at a range of 6 was measured. Five measurements were taken at various sites for each sample, and their averages were computed.

4.6.15. Tensile strength

Tensile strength of the samples was measured according to the test method ASTM D5034. The procedure outlined in the ASTM D5034 test method pertains to the determination of the maximum force at break for textile fabrics utilizing a grab method. The grab test, which is a form of tensile strength assessment, involves clamping the center of the specimen using mechanical clamps. Subsequently, force is applied, and the force at which the sample breaks is recorded. The Zweigle F-425 tensile tester was utilized in this research work.

4.6.16. Wash durability

The home laundering washing durability of the treated samples was examined as per ISO 105-CO6 standard. Each wash cycle of this method is equal to five home laundering. The treated samples were washed at 50 °C for 45 minutes with 4 g/L washing detergent. Finally, the washed samples were rinsed and then dried at 80 °C. Eventually, the washed samples were investigated for their functional properties.

CHAPTER 5

Results and Discussion

All the results present in this research study are the mean of five replications.

5.1. Content analysis

The ICP-AES technique was employed to analyze the Zn and P contents of the developed samples and tabulated in Table 3. Zn contents analysis was done to decide the most productive and optimized sonication time and concentrations of chemical reagents. It can be seen from Table 3 and Figure 25 (3D surface plots) that with an increased sonication time of up to 90 minutes the synthesized mass of Zn contents also increased. However, after 90 minutes the synthesized mass of Zn contents decreased. After a critical time of 90 minutes, ultrasonic waves might be led to remove the ZnO NPs from the fabric. While the higher molar concentration of NaOH leads to the higher synthesized amount of Zn contents. In the case of zinc acetate with increased concentration up to 0.1 M zinc acetate synthesized mass of Zn contents also increased. However, at 0.15 M zinc acetate synthesized mass of Zn contents tends to decrease. The maximum synthesized mass of Zn contents was achieved for sample 23, which exhibited Zn contents of 13.14 %. So, the optimal sonication time for this experiment is 90 minutes, and the optimal concentrations of the reagents are 0.1 M zinc acetate, and 0.3 M NaOH. Table 3 shows that optimized sample 23 has 3.44 phosphorous (P) contents % and 30.47 add on %. Furthermore, it can be seen from Table 3 that add on % shows the same trend as Zn contents %.

Equation (22) shows the regression model for the prediction of Zn contents %. R-squared value can be used to evaluate how well the model fits the data; the R-squared value presented in the model summary shows that the fitted model could explain 73.58 % of total variations , while the p-value = 0.00 and F-value = 80.30 presented in the model summary indicate that the model is significant.

Table 3. Experimental results for Zn contents, P contents, and add-on %.

Sample	Zinc acetate (M)	NaOH (M)	Sonication time (minutes)	MDPA (g/L)	Zn contents		P contents		Add on	
					(%)	Std. dev.	(%)	Std. dev.	(%)	Std. dev.
1	0.05	0.1	30	300	1.69	0.07	3.88	0.08	16.92	0.15
2	0.05	0.1	60	300	1.84	0.04	3.86	0.07	17.11	0.12
3	0.05	0.1	90	300	2.13	0.09	3.83	0.06	17.45	0.15
4	0.05	0.1	120	300	1.91	0.08	3.84	0.07	17.22	0.16
5	0.05	0.2	30	300	2.83	0.11	3.81	0.08	18.31	0.18
6	0.05	0.2	60	300	3.19	0.09	3.79	0.05	18.61	0.14
7	0.05	0.2	90	300	3.34	0.13	3.78	0.09	18.91	0.22
8	0.05	0.2	120	300	3.27	0.07	3.79	0.06	18.78	0.14
9	0.05	0.3	30	300	4.64	0.10	3.75	0.05	20.38	0.17
10	0.05	0.3	60	300	4.86	0.06	3.73	0.08	20.70	0.13
11	0.05	0.3	90	300	5.09	0.10	3.72	0.06	20.96	0.15
12	0.05	0.3	120	300	5.01	0.05	3.72	0.06	20.84	0.13
13	0.1	0.1	30	300	5.34	0.07	3.71	0.05	21.23	0.12
14	0.1	0.1	60	300	5.47	0.08	3.70	0.07	21.43	0.16
15	0.1	0.1	90	300	5.65	0.05	3.70	0.06	21.60	0.12
16	0.1	0.1	120	300	5.53	0.05	3.70	0.06	21.51	0.11
17	0.1	0.2	30	300	8.78	0.07	3.63	0.07	25.32	0.16
18	0.1	0.2	60	300	9.07	0.06	3.61	0.05	25.65	0.14
19	0.1	0.2	90	300	9.31	0.04	3.58	0.05	25.48	0.19
20	0.1	0.2	120	300	9.17	0.07	3.60	0.07	25.77	0.20
21	0.1	0.3	30	300	11.23	0.06	3.50	0.04	28.24	0.16
22	0.1	0.3	60	300	12.09	0.07	3.47	0.03	29.21	0.18
23	0.1	0.3	90	300	13.14	0.06	3.44	0.06	30.47	0.12
24	0.1	0.3	120	300	12.54	0.05	3.46	0.05	29.79	0.11
25	0.15	0.1	30	300	5.39	0.06	3.72	0.06	21.31	0.13
26	0.15	0.1	60	300	5.61	0.07	3.69	0.04	21.54	0.10
27	0.15	0.1	90	300	5.73	0.04	3.69	0.05	21.72	0.11
28	0.15	0.1	120	300	5.57	0.05	3.70	0.07	21.52	0.13
29	0.15	0.2	30	300	8.89	0.05	3.62	0.05	25.42	0.11
30	0.15	0.2	60	300	9.21	0.02	3.59	0.03	25.82	0.08
31	0.15	0.2	90	300	9.43	0.04	3.55	0.04	26.11	0.10
32	0.15	0.2	120	300	9.29	0.03	3.58	0.06	25.91	0.11
33	0.15	0.3	30	300	9.63	0.06	3.54	0.02	26.31	0.09
34	0.15	0.3	60	300	9.91	0.03	3.53	0.03	26.65	0.09
35	0.15	0.3	90	300	10.13	0.05	3.52	0.05	26.91	0.12
36	0.15	0.3	120	300	9.97	0.08	3.53	0.04	26.57	0.14
A	0.1	0.3	90 (magnetic stirring)	300	7.83	0.10	3.67	0.06	24.09	0.18
B	-	-	-	300	-	-	3.92	0.0	14.93	0.93

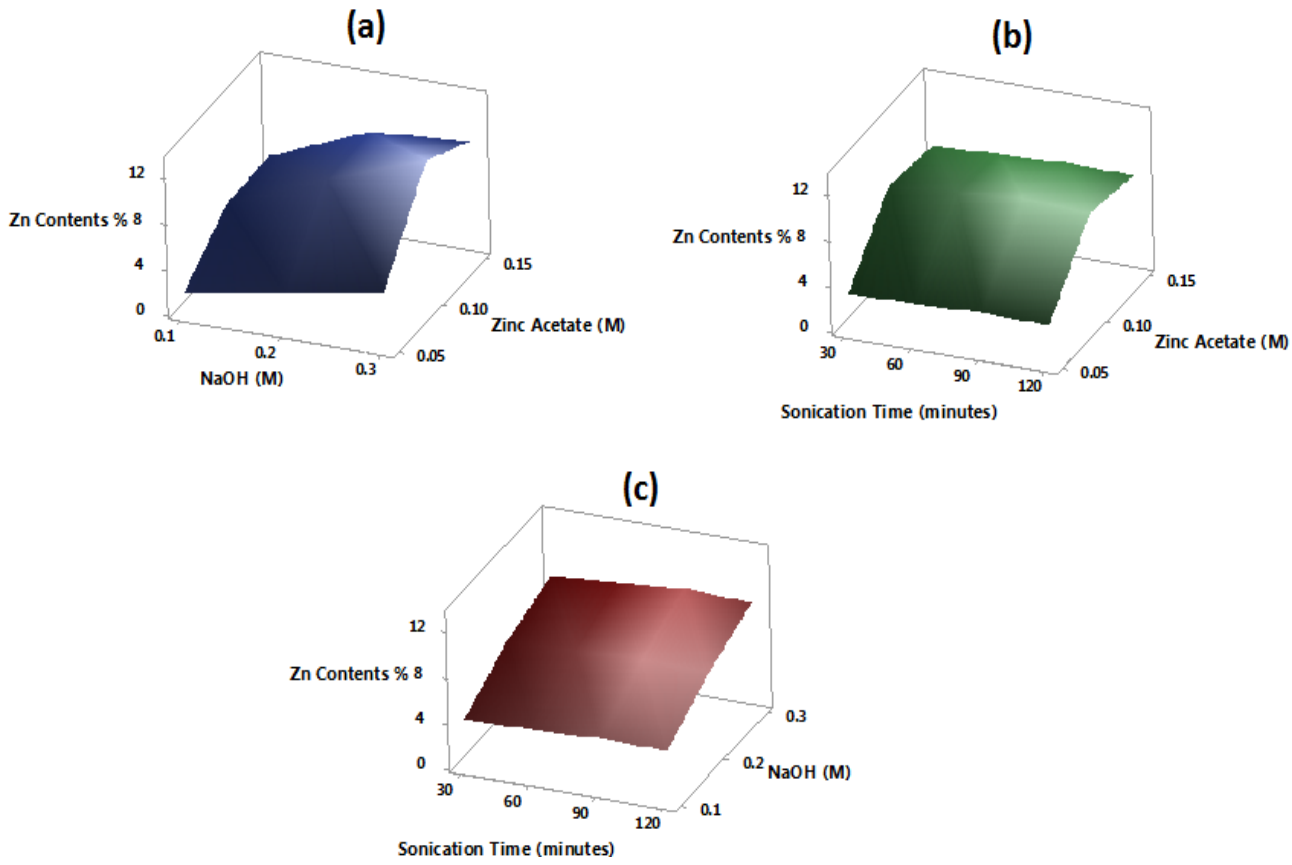

Figure 25. 3D surface plots the relative synthesized amount of Zn contents %.

$$Zn\ contents\ \% = -1.45 + 36.2\ zinc\ acetate\ (M) + 14.69\ NaOH\ (M) + 0.00001 sonication\ time\ (minutes) + 66.4\ zinc\ acetate\ (M) \times NaOH\ (M) - 0.0049\ zinc\ acetate\ (M) \times sonication\ time\ (minutes) + 0.0289\ NaOH\ (M) \times sonication\ time\ (minutes) \quad (22)$$

Model summary of Zn contents %

S = 1.7058 R-squared = 73.58% R-squared (adj) = 72.66% R-squared (pred) = 71.69%

F-Value = 80.30 p-value = 0.0000

The analysis of variance subjected to data regarding the synthesized amount of Zn contents % under the effect of zinc acetate (M), NaOH (M), and sonication time (minutes) are presented in Table 4, which revealed highly significant effects for all the variables and there interactions upon the synthesized amount of Zn contents % with p-value <.001.

Table 4. Analysis of variance for the synthesized amount of Zn contents %.

Source of variation	Sum of squares	df	Mean square	F-value	p-value
A-Zinc acetate (M)	1126.181	2	563.091	107854.55	<.001
B-NaOH (M)	671.350	2	335.675	64295.32	<.001
C-Sonication time (minutes)	8.959	3	2.986	571.97	<.001
A×B	92.845	4	23.211	4445.88	<.001
A×C	1.139	6	.190	36.35	<.001
B×C	1.627	6	.271	51.94	<.001
A×B×C	2.587	12	.216	41.29	<.001
Error	0.752	144	.005		
Total	1905.440	179			

The main effects plots for fitted mean values of the synthesized amount of Zn contents % under different experimental variables are shown in Figure 26. The plots elaborate that all the values are distinct from one another. In the case of zinc acetate (M) the maximum mean value of the synthesized amount of Zn contents % is 8.94 which is obtained at 0.1 molar concentration of zinc acetate, while for the NaOH (M) the maximum mean value of synthesized amount of Zn contents % is 9.02 which is obtained at 0.3 molar concentration of NaOH. The plots show that the maximum mean value of Zn contents % for sonication time (minutes) is 7.11 which is obtained at 90 minutes of sonication time.

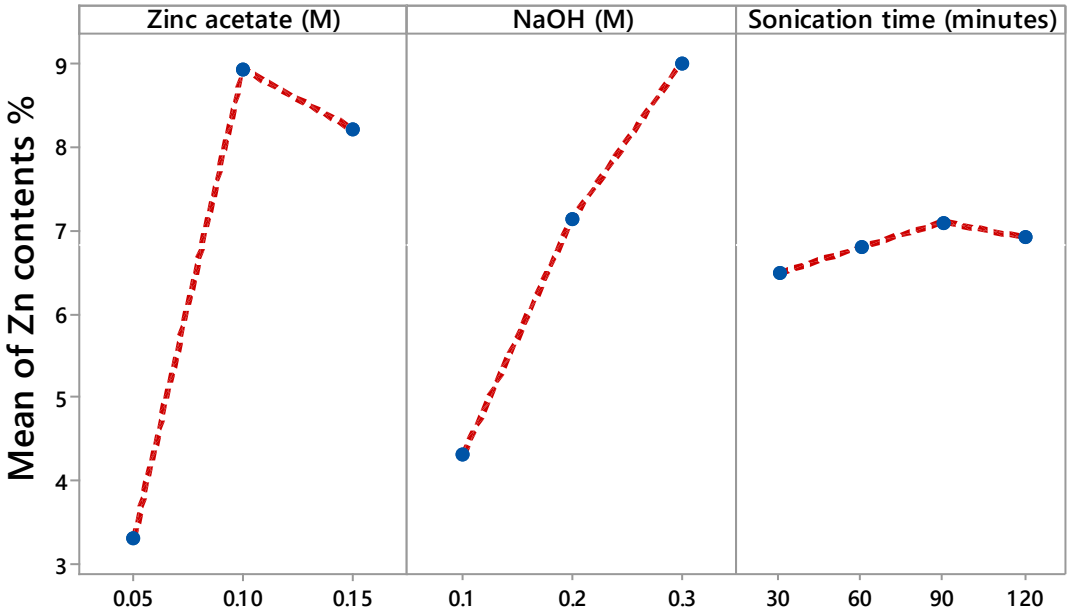

Figure 26. Main effects plots for Zn contents %.

5.2. SEM analysis

SEM Images were measured to investigate the surface morphology of the pristine cotton fabric and ZnO NPs coated samples. It can be seen from Figure 27 (a) and Figure 27 (b) that pristine cotton has a clean and smooth surface. Figures 27 (c) and 27 (d) show the SEM images for optimized sample 23, which reveals that after optimized sonochemical treatment ZnO NPs are spread onto the cotton fabric surface homogeneously, finely, and evenly. Figures 27 (c) and 27 (d) show that the surface of the fabric is entirely covered by the ZnO NPs. The deposition of ZnO NPs onto the cotton fabric surface results from attractive forces between cellulosic functional groups and ZnO NPs [232]. SEM images show that the deposition of ZnO NPs created roughness on the surface of fibers. Figure 27 (f) SEM image for sample A indicates that there is a deposition of ZnO NPs onto the cotton fabric surface after the conventional magnetic stirring method, but as compared to the sonochemical method, the ZnO NPs are not spread smoothly, finely and homogeneously. Figure 27 (e) shows the SEM image for optimized sample 23 at high resolution, showing that ZnO particles

are deposited onto the cotton surface at a nano scale with narrow size distribution. Moreover, Figure 27 (e) reveals that most of the ZnO NPs have round and spherical shapes.

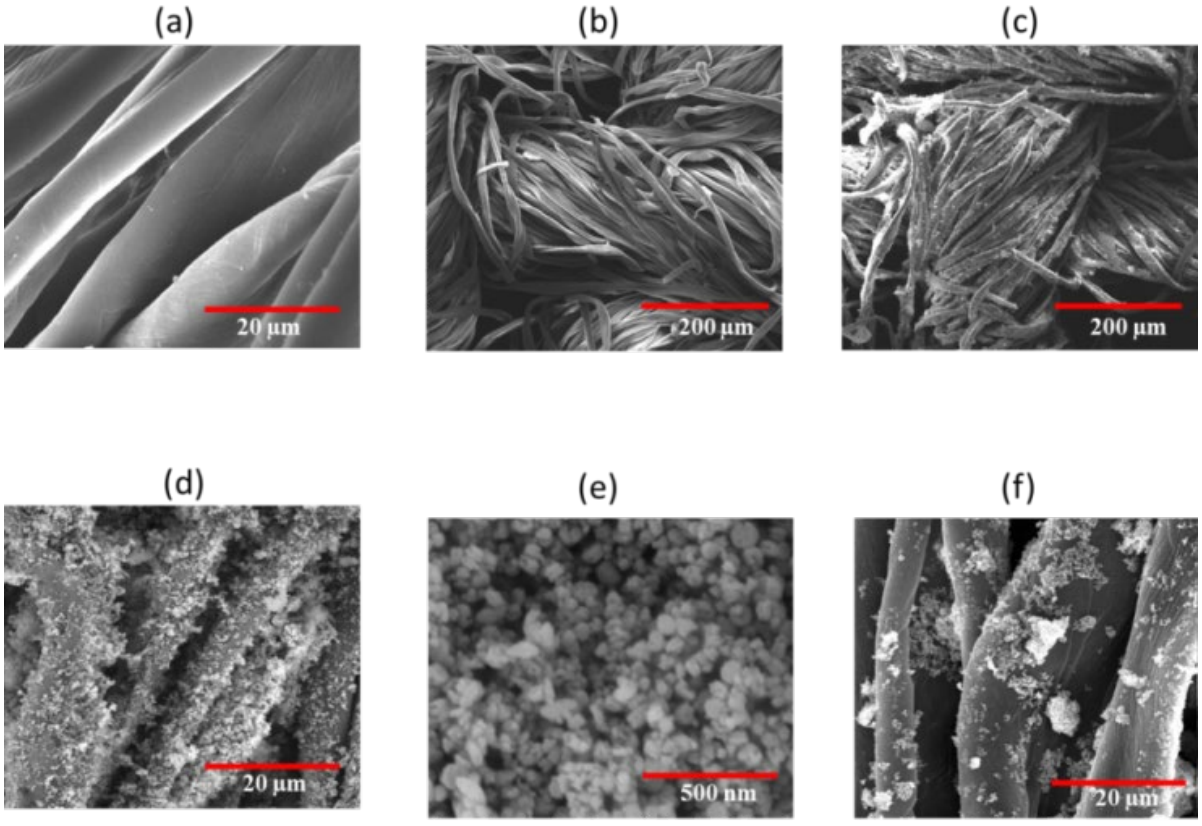

Figure 27. SEM images (a,b) pristine cotton, (c,d,e) sample 23 and (f) sample A.

5.3. Particle size

Figure 28 shows the particle size distribution of sonochemical in-situ synthesized ZnO NPs (optimized sample 23). It can be seen from Figure 28 that nanoparticle size distribution is uni-modal with an average particle size of 30.89 nm. At the nano scale the particles have increased surface areas, allowing the nanoparticles to be utilized in many technical applications [233], [234]. Dodd *et al.* reported that a decrease in particle size results in an augmentation of the specific surface area. Consequently, this augmentation also leads to an increase in the quantity of active surface sites. These sites facilitate the reaction between the

photogenerated charge carriers and absorbed molecules, thereby giving rise to the formation of hydroxyl and superoxide radicals[235].

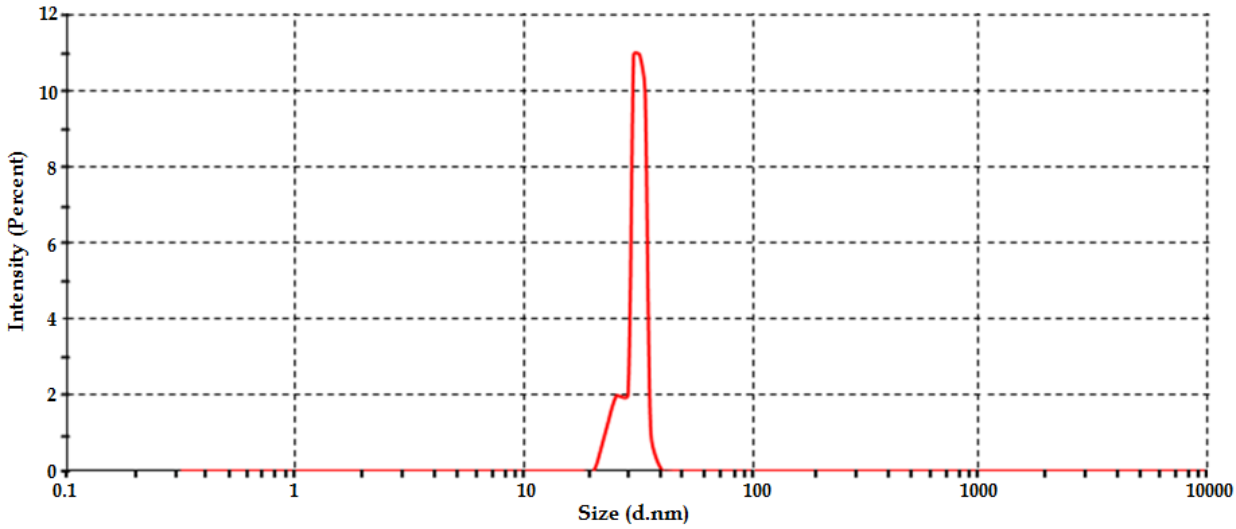

Figure 28. Particle size distribution sample 23.

5.4. XRD analysis

XRD diffractograms of pristine cotton fabric and optimized sonochemically treated sample 23 are presented in Figure 29. It is evident from Figure 29 that the pristine cotton fabric has only the characteristic peaks of cellulose (at 2Θ= 14.8, 16.5 and 22.7) (JCDPS No.03-0226) [236]. While the sample 23 has some additional peaks (at 2Θ= 32.1, 34.7, 36.5, 47.8, 56.7, 63.1, 68.1, 69.2) in the diffraction planes (100), (002), (101), (102), (110), (103), (200), and (112). These are characteristic peaks of ZnO NPs (as per diffraction standard No.36-1451 defined by the joint committee on powder diffraction standard (JCDPS)) [237]. The additional peaks are evidence of the presence of crystalline hexagonal wurtzite structure of ZnO NPs [210], [238]. The peak in plane (101) has the highest intensity, which shows that the (101) plane direction is the main dominant and leading growth direction for ZnO NPs. Moreover, in the case of sample 23, the peak intensity of the cellulose has decreased due to ZnO NPs loading. Furthermore, there is no extra peak in the diffractogram of sample 23 other than cellulose and ZnO NPs, which shows the purity of the ZnO NPs.

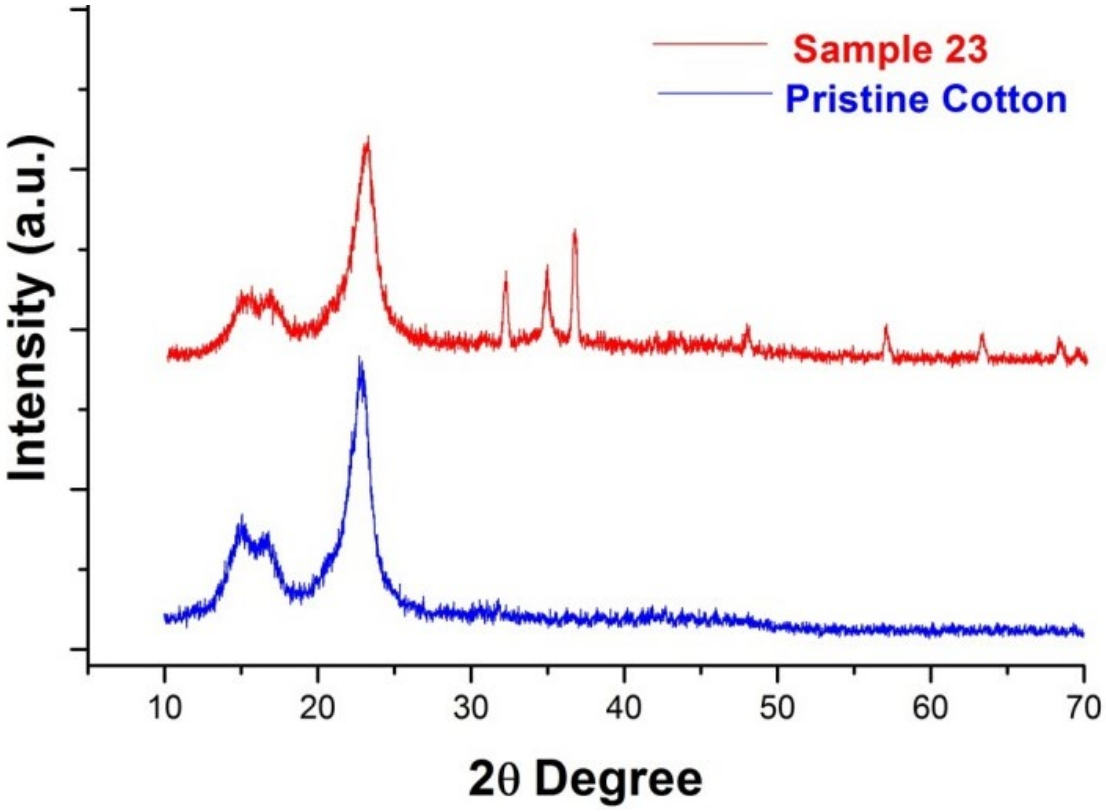

Figure 29. XRD diffractogram of pristine cotton and sample 23.

5.5. FTIR analysis

The FTIR spectra for pristine cotton, cotton-CA, sample 23, sample A, and sample B are presented in Figure 30. The pristine cotton has an O-H stretching band at 3300 cm^{-1}, which contains hydrogen bonding, a band at 2900 cm^{-1} is the result of C-H stretching, a band at 1310 cm^{-1} is due to the C-H wagging, while the peak at 1640 cm^{-1} shows the presence of absorbed H_2O molecules. The band at 1030 cm^{-1} was attributed to C=O stretching. The C-H bending is evident from the peak available at 1314 cm^{-1} [239], [240]. After citric acid treatment, a new absorption peak appeared at 1729 cm^{-1}, which can be attributed to the absorption of the carboxyl group from citric acid [241]. In the case of treated samples, there are some new peaks. The peak due to P=O is centered at 1250 cm^{-1}, while the peak centered at 884 cm^{-1} is associated with the P-O bond. Furthermore, the presence of the amide group can be confirmed by the peaks at 1624 cm-1 (amide vibration) and 1528 cm^{-1} (amide vibration), which are

evidence of flame retardant treatment onto the cotton fabric [242]. Moreover, in the case of sample A and sample 23, there is a significant shift of FTIR spectra in the wavenumber range of 400 cm^{-1} to 500 cm^{-1}, which is attributed to the presence of ZnO NPs on the cotton fabric. In the case of sample 23, the intensity of spectra shift is more than that of sample A, which can be attributed to the high amount of ZnO NPs available in the case of sample 23. The shift of spectra in that wavenumber range can be attributed to the formation of the $–CH_2$-O-Zn structure [238], [243].

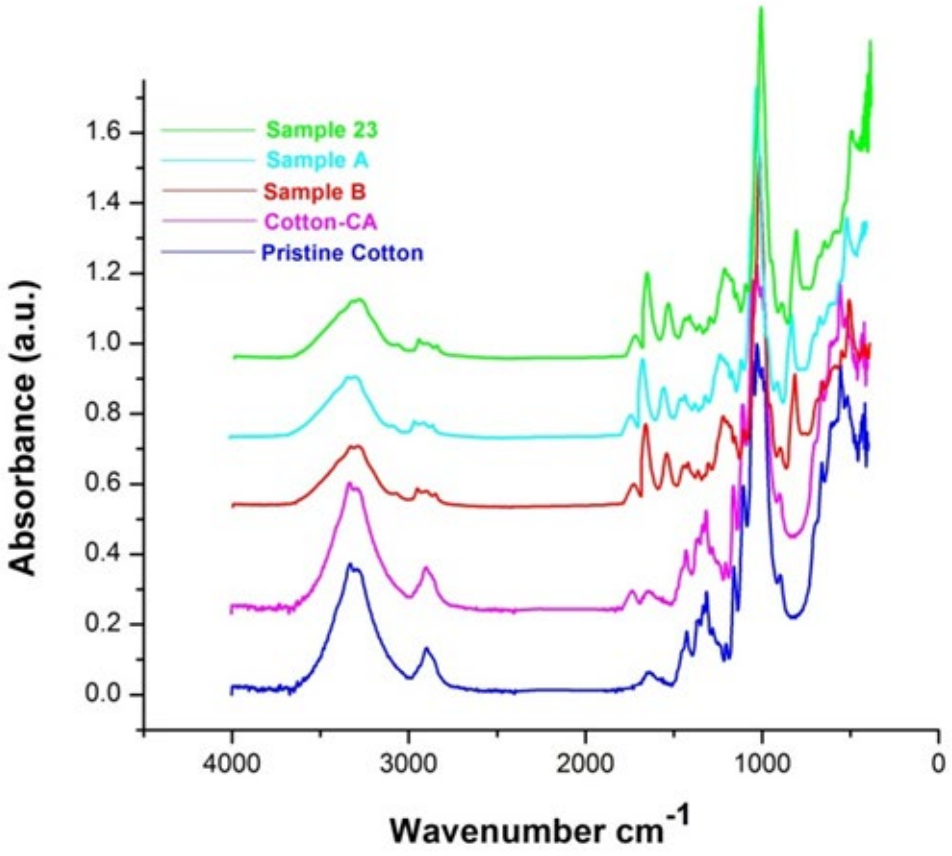

Figure 30. FTIR spectra of pristine cotton and sample A, sample B and sample 23.

5.6. Thermo gravimetric analysis

The thermal degradation trend of the fabric can be used to evaluate the flammability behavior of cotton fabric. So, the thermo gravimetric analysis of pristine cotton and developed samples

was performed in a synthetic air environment. Figure 31(a) shows the weight loss percentage with the rise of temperature, Figure 31(b) shows the weight loss rate with the rise of temperature, whereas Table 5 shows the values of decomposition temperatures for pristine cotton and developed samples. In the case of the TGA curve for pristine cotton, there is only little weight loss below 343 °C, which corresponds to the evaporation of water molecules. In this region, the decarboxylation and dehydration process of cotton cellulose occurred, forming the aliphatic char and combustible gasses. The region 350 °C to 550 °C corresponds to the transformation of aliphatic char into an aromatic form of carbon dioxide and carbon monoxide [244]. Citric acid treated cotton fabric showed the same degradation behavior as pristine cotton but with little increase in residue. From Table 5, it can be seen that the $T_{onset\ 10\%}$ values have shifted towards lower temperatures after MDPA and ZnO NPs coating. For pristine cotton, $T_{onset\ 10\%}$ is 319.23 °C, while for sample 23, $T_{onset\ 10\%}$ is 266.07 °C, which is the lowest than all the samples. This attributes to the stronger performance of MDPA and ZnO NPs for the decomposition of cellulose as compared to pristine cotton. This T_{onset} mass loss is due to the evaporation of moisture contents from the fabric. Loading of MDPA and ZnO NPs tends to escalate the fabric's moisture, hence lowering the T_{onset} for developed samples than pristine cotton [245]. T_{max} for pristine cotton was observed at 343.15 °C, while after treatment, T_{max} decreased, and the lowest T_{max} was observed for sample 23 (i.e. 280.19 °C). From Table 5, it can be seen that the char residue at T_{max} and 600 °C increased after treatment compared to pristine cotton. This improvement can be explained as phosphorous components in MDPA were turned into phosphoric acid, which caused the fabric's dehydration, hence leading to the lower degradation temperature and higher char residues [246]. The high char residual amount in the case of sample 23 corresponds to ZnO NPs [247]. The quantitative amount of char residue produced is associated with flame retardance performance [248]. The reduction in degradation temperature after MDPA treatment might be due to the fact that the O-P-C bond in MDPA is less stable than the C-O-C bond in cotton, and MDPA produced the phosphorous derivatives at lower temperature that might be accelerated cellulose degradation to char at lower temperature[249], [250]. While after ZnO NPs treatment, degradation temperature further decreased, which can be attributed to the loss of fiber strength during sonochemical process (will be discussed at next pages) which led to degradation of cellulose at lower temperature. The results are in accordance with Dhandapani *et al.* they also reported that ZnO

NPs loaded cotton fabric during thermo gravimetric analysis showed lower degradation temperature and high char residue as compared to untreated cotton fabric [251]. In other study, Zhang *et al*. concluded that an increase in Zn contents on cellulosic fabric resulted as decrease of the degradation temperature and increase of char residues[11].

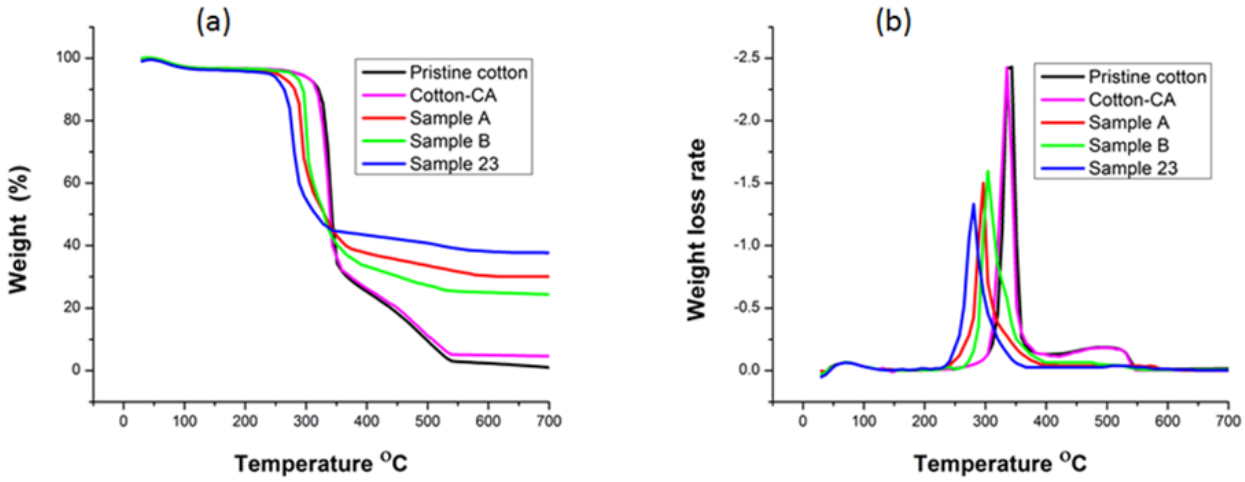

Figure 31. Thermo-oxidative behavior (a) TGA curves and (b) dTG curves.

Table 5. Thermal characteristics of pristine cotton and developed samples.

Sample	$T_{onset\ 10\%}$ (°C)	T_{max} (°C)	Residue at Tmax (%)	Residue at 600 °C (%)
Pristine cotton	319.23	343.15	47.04	2.29
Cotton-CA	317.12	335.52	62.93	4.19
Sample A	280.34	296.13	68.47	30.91
Sample B	295.18	304.32	67.11	24.25
Sample 23	266.07	280.19	70.21	38.17

5.7. Vertical flame test

The measurements of the vertical flame test of untreated and developed samples are shown in Table 6 and Figure 32. It can be seen from Table 6 and Figure 32 that MDPA has a good

effect on the flame retardancy of the cotton fabric, which further improved by the deposition of ZnO NPs.

It is evident from the results that flame retardant properties (i.e. after flame time, after glow time, char length) improved with increased deposition of ZnO NPs. The untreated sample burned intensely in contact with flame. After detaching the flame source, the burning process of the untreated sample remained continue until it completely burned out without any char formation. On the other hand, all the treated samples (MDPA treated and MDPA + ZnO NPs treated) were self-extinguished. Furthermore, char formation was observed in the case of treated samples (MDPA treated and MDPA + ZnO NPs treated). Moreover, it was observed that after flame time, after glow time, and char length of the treated samples decreased with an increased amount of Zn contents %. The best flame retardant results were observed in the case of sonochemically optimized sample 23. Sample 23 self-extinguished immediately after removal of the combustion source and had zero second after flame time, zero second after glow time, and 39 mm char length. Sample A developed by conventional magnetic stirring method had 2.13 seconds after flame time, zero second after glow time, and 76 mm char length, while sample B only treated with MDPA had 8.04 seconds after flame time, 5.21 seconds after glow time, and 127 mm char length. The char formation in the case of MDPA and MDPA + ZnO NPs treated samples was because of water removal from the fabric, the liberation of water leads to the dilution of the oxidizing gas phase, which created the insulating layer and protected the fabric after flame removal, hence increasing the flame retardancy [252]. Moreover, at elevated temperature phosphorous containing compounds release phosphate anions (pyro- and polyphosphates), these phosphate anions engage in char formation alongside the carbonized residues. This resulting carbonized layer known as char acts as a shield, effectively insulating and safeguarding the polymer from the flames while also impeding the diffusion of oxygen. Additionally, the presence of char hinders the volatilization of fuel and serves as a barrier against the generation of flammable free radicals [130], [131]. Phosphorus containing compounds are also capable of undergoing volatilization and into the gaseous state, thus leading to the creation of active radicals (such as PO_2•, PO•, and HPO•) and serve as scavengers for H• and OH• radicals[130], [131]. Furthermore, ZnO NPs acted as co-catalyst and decreased the flame spread rate; therefore, improved flame

retardancy was achieved [253]. A condensed phase mode of action through the heat barrier effect has been suggested as the foundation for flame retardancy of ZnO NPs [124].

Table 6. Experimental results for flammability test.

Sample	Zinc - acetate (M)	NaOH (M)	Sonication time (minutes)	MDPA (g/L)	Flammability test					
					After flame time		After glow time		Char length	
					(s)	Std. dev.	(s)	Std. dev.	(mm)	Std. dev.
Untreated	-	-	-	-	19.34	3.21	9.62	1.86	Completely burned	-
1	0.05	0.1	30	300	7.42	0.12	3.25	0.13	103	1.92
2	0.05	0.1	60	300	7.02	0.13	3.11	0.08	99	2.12
3	0.05	0.1	90	300	6.24	0.17	2.94	0.11	95	1.22
4	0.05	0.1	120	300	6.74	0.12	3.03	0.08	96	0.71
5	0.05	0.2	30	300	5.83	0.21	2.72	0.17	92	2.00
6	0.05	0.2	60	300	5.26	0.16	2.33	0.16	90	2.35
7	0.05	0.2	90	300	4.19	0.22	2.04	0.07	89	0.70
8	0.05	0.2	120	300	4.84	0.25	2.17	0.14	89	1.00
9	0.05	0.3	30	300	3.87	0.22	1.91	0.11	83	1.87
10	0.05	0.3	60	300	3.58	0.18	1.62	0.07	78	3.11
11	0.05	0.3	90	300	2.82	0.20	1.06	0.05	76	1.58
12	0.05	0.3	120	300	3.12	0.15	1.34	0.12	76	1.21
13	0.1	0.1	30	300	2.09	0.21	0.78	0.09	73	1.23
14	0.1	0.1	60	300	1.56	0.16	0.27	0.05	71	1.87
15	0.1	0.1	90	300	0.59	0.11	0	0	68	2.65
16	0.1	0.1	120	300	1.17	0.12	0	0	70	2.55
17	0.1	0.2	30	300	0	0	0	0	55	2.74
18	0.1	0.2	60	300	0	0	0	0	53	2.12
19	0.1	0.2	90	300	0	0	0	0	51	2.24
20	0.1	0.2	120	300	0	0	0	0	52	2.92
21	0.1	0.3	30	300	0	0	0	0	42	2.16
22	0.1	0.3	60	300	0	0	0	0	40	1.78
23	0.1	0.3	90	300	0	0	0	0	39	0.71
24	0.1	0.3	120	300	0	0	0	0	40	1.58
25	0.15	0.1	30	300	1.97	0.14	0.53	0.03	73	1.14
26	0.15	0.1	60	300	0.92	0.11	0	0	69	2.72
27	0.15	0.1	90	300	0.42	0.08	0	0	65	1.64
28	0.15	0.1	120	300	1.02	0.10	0	0	70	2.12
29	0.15	0.2	30	300	0	0	0	0	55	2.16
30	0.15	0.2	60	300	0	0	0	0	51	1.78
31	0.15	0.2	90	300	0	0	0	0	50	1.56
32	0.15	0.2	120	300	0	0	0	0	51	3.74
33	0.15	0.3	30	300	0	0	0	0	49	1.31
34	0.15	0.3	60	300	0	0	0	0	47	0.83
35	0.15	0.3	90	300	0	0	0	0	44	1.87
36	0.15	0.3	120	300	0	0	0	0	47	1.22
A	0.1	0.3	90 (magnetic stirring)	300	2.13	0.75	0	0	76	3.82
B	-	-	-	300	8.04	0.25	5.21	0.23	127	4.95

Wang *et al*. described that ZnO NPs could shield the insulating layer on the surface of the fiber, minimizing the amount of heat, fuel, and oxygen that are transferred from the flame to the fibers and, as a result, lowering the intensity as well as the rate of burning. Additionally, ZnO is already classified as a substance that suppresses the production of smoke [214]. Furthermore, these results are in accordance with Samanta *et al*., Wang *et al*., and Arputharaj *et al*. they concluded that ZnO NPs greatly enhanced the amount of char residue, decreased the char length, and reduced the after flame time as well as afterglow time[201], [214], [215].

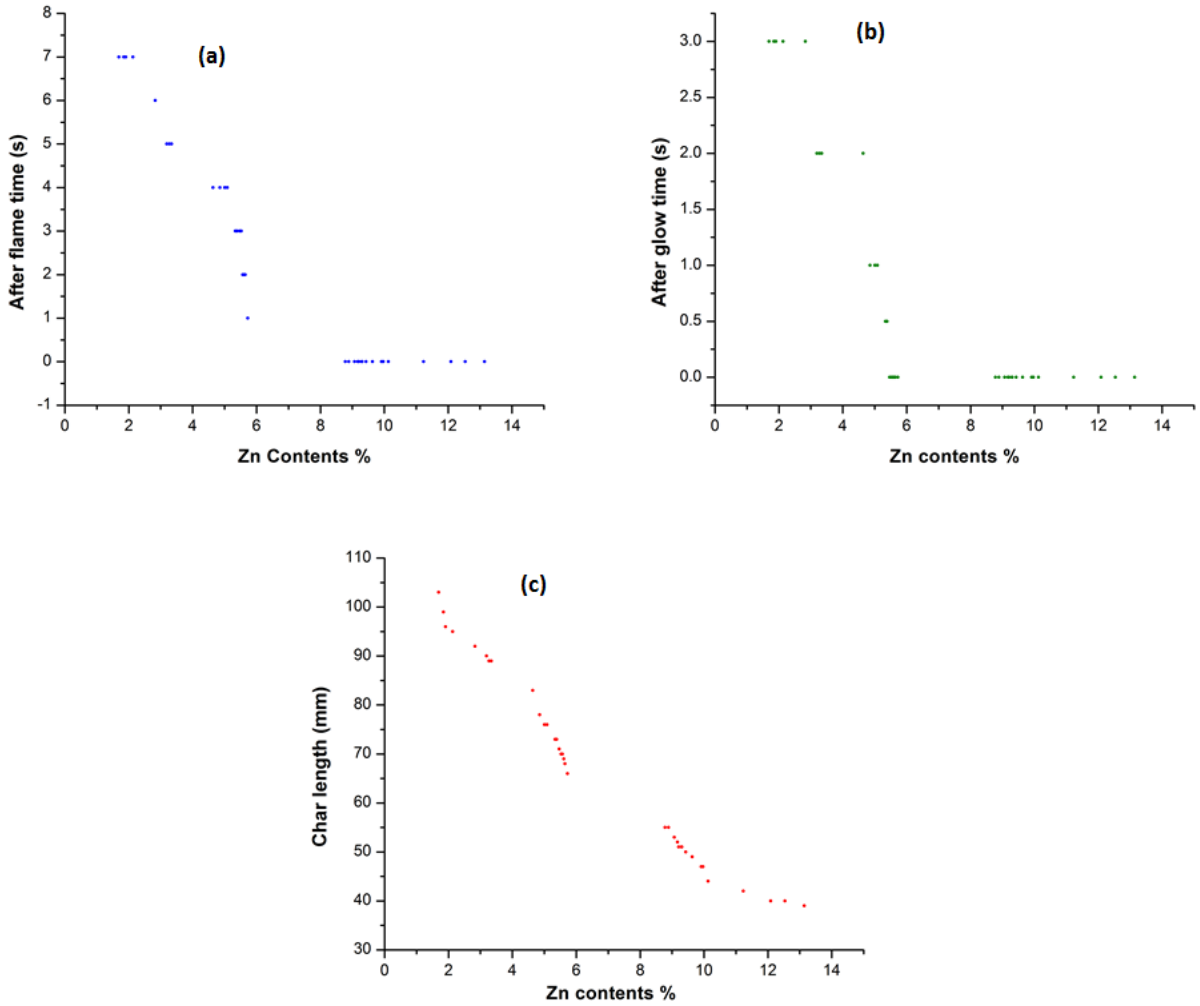

Figure 32. Flammability behavior (a) after flame time against Zn contents % (b) afterglow time against Zn contents % (c) char length against Zn contents %.

Equation (23) shows the regression model for prediction after flame time (s). The R-squared value presented in the model summary shows that the fitted model could explain 77.58 % of total variations , while p-value = 0.00 and F value = 99.78 presented in the model summary indicate that the model is significant.

After flame time (s) = 12.674 − 76.85 zinc acetate (M) − 24.90 NaOH (M) − 0.02118 sonication time (minutes) + 121.2 zinc acetate (M) × NaOH (M) + 0.0724 zinc acetate (M)×sonication time (minutes) + 0.0383 NaOH (M) × sonication time (minutes) (23)

Model summary of after flame time (s)

S = 1.17479 R-squared = 77.58% R-squared (adj) = 76.80% R-squared (pred) = 76.00%
F-value = 99.78 p-value= 0.000

The regression model for predicting after glow time (s) is depicted by equation (24). The model summary displays the R-squared value, indicating that the fitted model can account for 76.93% of the total variations. Furthermore, the model summary presents the p-value as 0.00 and the F-value as 96.17, which suggest that the model is statistically significant.

After glow time (s) = 5.964 − 40.04 zinc acetate (M) − 11.81 NaOH (M) − 0.01032 sonication time (minutes) + 73.4 zinc acetate (M) × NaOH(M) + 0.0383 zinc acetate (M) × sonication time (minutes) + 0.0153 NaOH (M) × sonication time (minutes) (24)

Model summary of after glow time (s)

S = 0.556936 R-squared = 76.93% R-squared (adj) = 76.13% R-squared (pred) = 75.32
F-value = 96.17 p-value= 0.000

The regression model for predicting char length (mm) is demonstrated by equation (25). The model summary displays an R-squared value which indicates that the fitted model can account for 77.61% of the total variations. Furthermore, the model summary presents a p-value of 0.00 and an F-value of 97.40, both of which affirm that the model is statistically significant.

Char length (mm) = 127.05 − 319.5 zinc acetate (M) − 112.8 NaOH (M) − 0.0822 sonication time (minutes) − 132 zinc acetate (M) × NaOH (M) + 0.231 zinc acetate (M) × sonication time (minutes) + 0.064 NaOH (M) × sonication time (minutes) (25)

Model summary of char length (mm)

S = 9.29748 R-squared = 77.61% R-squared (adj) = 76.37% R-squared (pred) = 75.51%
F-value = 97.40 p-value= 0.000

The analysis of variance applied to the data concerning the duration of after flame time (s) in relation to the influence of zinc acetate (M), NaOH (M), and sonication time (minutes) is displayed in Table 7. This analysis unveiled exceedingly noteworthy impacts for all the variables, as well as their interactions, on the after flame time (s), with a p-value of less than 0.001.

Table 7. Analysis of variance for after flame time.

Source of variation	Sum of squares	df	Mean square	F-value	p-value
A-Zinc acetate (M)	873.222	2	436.611	28020.30	<.001
B-NaOH (M)	125.093	2	62.546	4014.02	<.001
C-Sonication time (minutes)	13.892	3	4.631	297.18	<.001
A×B	38.015	4	9.504	609.91	<.001
A×C	3.823	6	.637	40.88	<.001
B×C	4.813	6	.802	51.48	<.001
A×B×C	3.913	12	.326	20.92	<.001
Error	2.244	144	.016		
Total	1065.014	179			

The main effects plots presented in Figure 33 illustrate the fitted mean values of after flame time (s) under various experimental variables. In the instance of zinc acetate (M), the minimum mean after flame time (s) value is 0.36 seconds, attained at a molar concentration of

0.15 (M). While for NaOH (M), the lowest mean value of after flame time (s) is 1.12 seconds, achieved at a molar concentration of 0.3 (M). Additionally, the plots indicate that the smallest mean value of after flame time (s) for sonication time (minutes) is 1.58 seconds, occurring at the duration of 90 minutes.

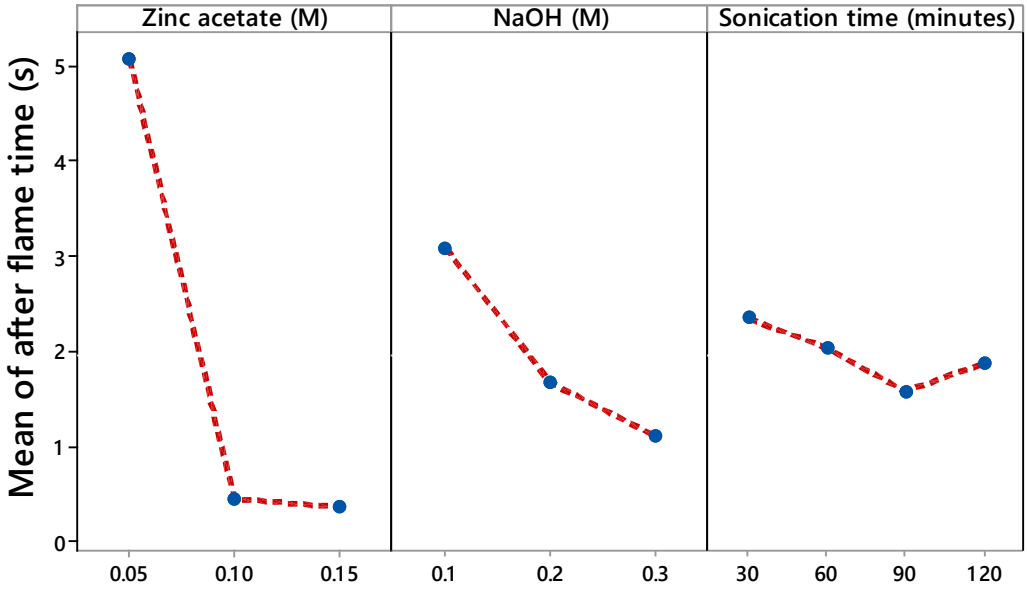

Figure 33. Main effects plots for after flame time (s).

Table 8 shows the results of the analysis of variance performed on the data pertaining to the after glow time (s) in relation to the influence of zinc acetate (M), NaOH (M), and sonication time (minutes). With a p-value of less than 0.001, this study revealed incredibly notable effects for each variable and their interactions on the after glow time (s).

The fitted mean values of after glow time (s) under different experimental factors are shown in the major effects graphs (Figure 34).With zinc acetate (M), the lowest mean after glow time (s) value is obtained at a molar concentration of 0.15 (M). This value is 0.04 seconds. The lowest mean value of after glow time (s) for NaOH (M) is 0.49 seconds, which is attained at a molar concentration of 0.3 (M). Furthermore, the plots show that the lowest mean value of after glow time (s) for sonication time (minutes) is 0.67 seconds, which happens during a 90 minutes period.

Table 8. Analysis of variance for after glow time.

Source of variation	Sum of squares	df	Mean square	F-value	p-value
A-Zinc acetate (M)	198.527	2	99.263	20384.93	<.001
B-NaOH (M)	13.388	2	6.694	1374.66	<.001
C-Sonication time (minutes)	3.186	3	1.062	218.12	<.001
A×B	13.379	4	3.345	686.89	<.001
A×C	.930	6	.155	31.83	<.001
B×C	.700	6	.117	23.95	<.001
A×B×C	1.832	12	.153	31.34	<.001
Error	.701	144	.005		
Total	232.643	179			

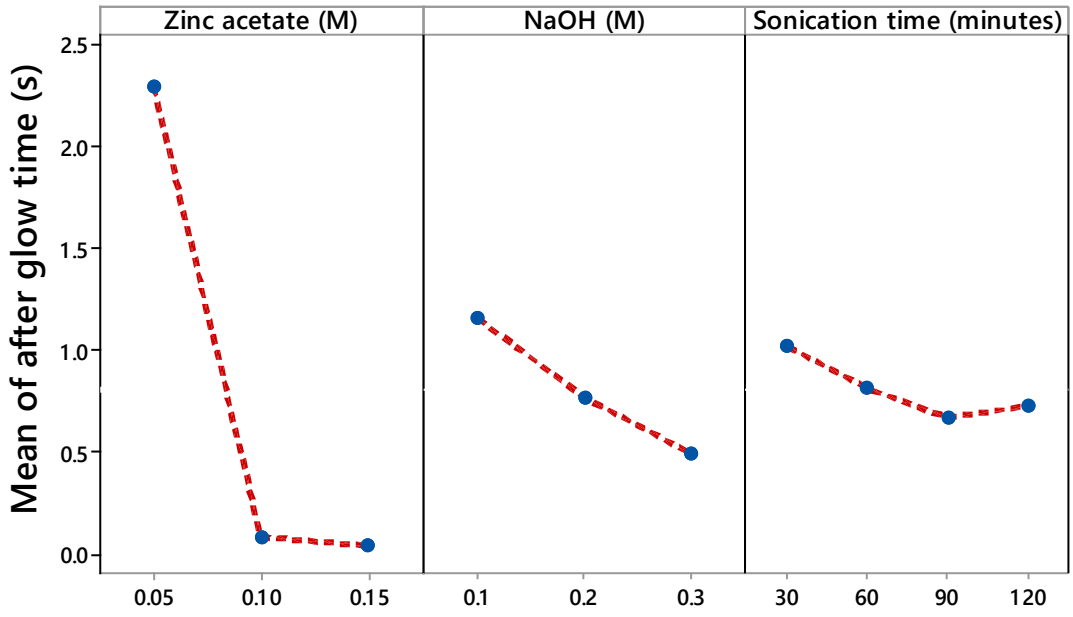

Figure 34. Main effects plots for after glow time (s).

The analysis of variance results for the char length (mm) data in connection to the effects of zinc acetate (M), NaOH (M), and sonication time (minutes) are displayed in Table 9. This

study found extremely significant impacts for each variable on the char length (mm), with a p-value of less than 0.05. However, the total interaction of all the variables and the interaction of NaOH (M) and sonication times (minutes) had non-significant effects, with p-values of 0.428 and 0.118, respectively.

Table 9. Analysis of variance for char length.

Source of variation	Sum of squares	df	Mean square	F-value	p-value
A-Zinc acetate (M)	45222.933	2	22611.467	5728.45	<.001
B-NaOH (M)	17838.533	2	8919.267	2259.63	<.001
C-Sonication time (minutes)	694.067	3	231.356	58.61	<.001
A×B	998.333	4	249.583	63.23	<.001
A×C	58.400	6	9.733	2.46	.027
B×C	40.933	6	6.822	1.72	.118
A×B×C	48.600	12	4.050	1.02	.428
Error	568.400	144	3.947		
Total	65470.200	179			

The fitted mean values of char length (mm) for various experimental factors are shown in the main effects graphs in Figure 35. The lowest mean char length (mm) value of 54.5 mm is obtained for zinc acetate (M) at a molar concentration of 0.1. In contrast, the minimum mean char length (mm) for NaOH (M) is 55.1 mm, which is achieved at a molar concentration of 0.3. Additionally, the plots show that 64.1 mm is the lowest mean value of char length (mm) for sonication time (minutes), occurring at a duration of 90 minutes.

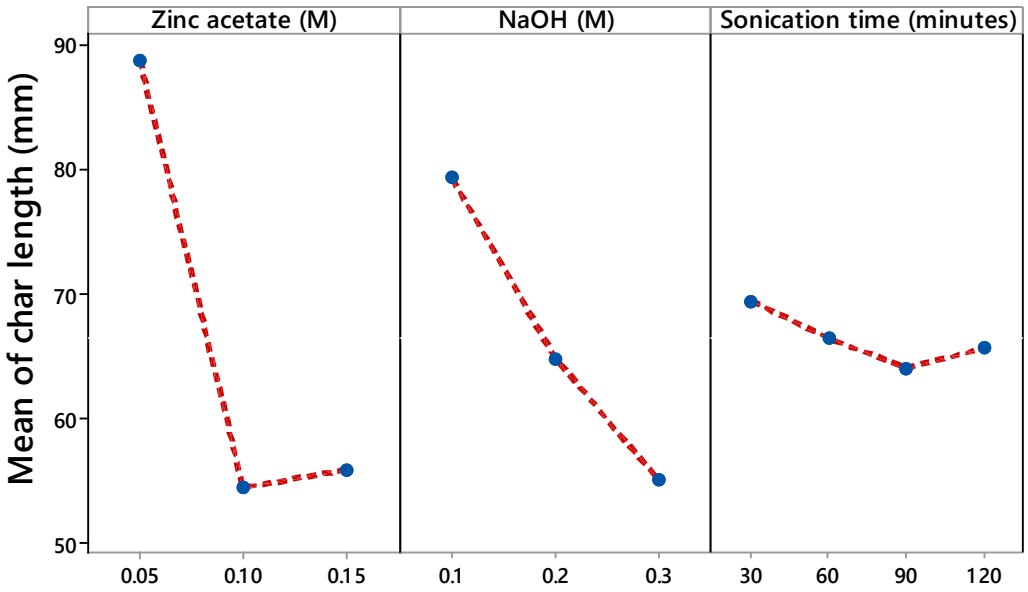

Figure 35. Main effects plots for char length (mm).

5.8. Limiting oxygen index (LOI)

LOI can be defined as the minimum available percentage amount of oxygen gas in the oxygen/nitrogen gas mixture that is necessary to continue the combustion process of a material [253]. As the LOI value of a material is increased it becomes more arduous to combustion. The LOI value of more than 27 indicates that the material is a flame retardant [253], [254]. Table 10 and Figure 36 show the values for LOI of treated and untreated fabric samples. It can be seen from Table 10 that the untreated sample has LOI value of 17.61, which indicates that pristine cotton is highly combustible. On the other hand, sample B; having flame retardant application, has LOI value of 23.81, which further increased after ZnO NPs application. Table 10 and Figure 36 show that the LOI value increased as the loaded concentration of ZnO NPs increased. These results are in accordance with Zhang *et al*. they concluded that the LOI value of cellulosic fibers increases as the loaded concentration of ZnO NPs increases [11]. The higher LOI value after ZnO NPs application might be due to the formation of a protective layer on fibers by ZnO NPs. The best LOI value was observed at 32.23 for sonochemicaly optimized sample 23. While, sample A, developed by the conventional magnetic stirring method, has the LOI value of 27.72, which is very near to the

LOI value (27.42) of sample 27, which has less ZnO NPs concentration compared to sample A. This might be due to the homogenous and smooth distribution of ZnO NPs in the case of sample 27 after the sonochemical process compared to the conventional magnetic stirring process.

Table 10. Experimental results for limiting oxygen index.

Sample	Zinc acetate (M)	NaOH (M)	Sonication time (minutes)	MDPA (g/L)	LOI	
					(%)	Std. dev.
Untreated	-	-	-	-	17.61	0.26
1	0.05	0.1	30	300	24.23	0.29
2	0.05	0.1	60	300	24.70	0.25
3	0.05	0.1	90	300	25.14	0.07
4	0.05	0.1	120	300	24.86	0.18
5	0.05	0.2	30	300	25.41	0.14
6	0.05	0.2	60	300	25.75	0.10
7	0.05	0.2	90	300	25.84	0.15
8	0.05	0.2	120	300	25.70	0.07
9	0.05	0.3	30	300	26.01	0.12
10	0.05	0.3	60	300	26.11	0.21
11	0.05	0.3	90	300	26.34	0.11
12	0.05	0.3	120	300	26.14	0.12
13	0.1	0.1	30	300	26.73	0.11
14	0.1	0.1	60	300	26.92	0.16
15	0.1	0.1	90	300	27.31	0.13
16	0.1	0.1	120	300	27.01	0.09
17	0.1	0.2	30	300	29.23	0.14
18	0.1	0.2	60	300	29.44	0.08
19	0.1	0.2	90	300	29.63	0.09
20	0.1	0.2	120	300	29.55	0.12
21	0.1	0.3	30	300	31.22	0.11
22	0.1	0.3	60	300	31.91	0.09
23	0.1	0.3	90	300	32.23	0.10
24	0.1	0.3	120	300	32.03	0.11
25	0.15	0.1	30	300	26.81	0.14
26	0.15	0.1	60	300	27.03	0.17
27	0.15	0.1	90	300	27.42	0.08
28	0.15	0.1	120	300	27.13	0.16
29	0.15	0.2	30	300	29.36	0.11
30	0.15	0.2	60	300	29.57	0.09
31	0.15	0.2	90	300	29.74	0.11
32	0.15	0.2	120	300	29.60	0.15
33	0.15	0.3	30	300	29.94	0.17
34	0.15	0.3	60	300	30.10	0.12
35	0.15	0.3	90	300	30.46	0.13
36	0.15	0.3	120	300	30.23	0.12
A	0.1	0.3	90 (magnetic stirring)	300	27.72	0.19
B	-	-	-	300	23.81	0.09

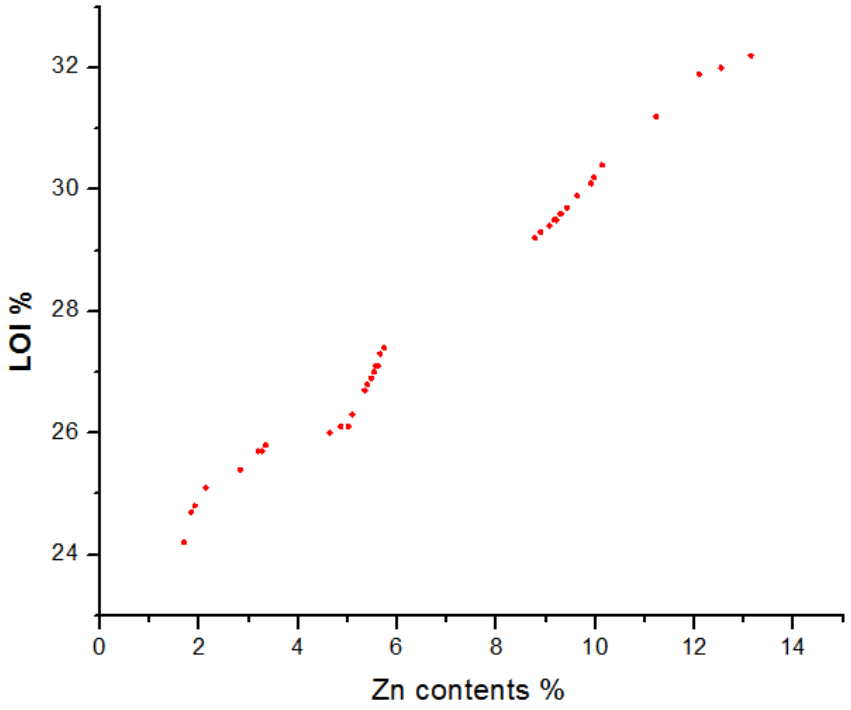

Figure 36. Graphical representation of LOI values vs Zn contents %.

The equation (26) shows the regression model for prediction of LOI %. R-squared value presented in model summary shows that the fitted model could explain 72.01 % of total variations , while p-value = 0.00 and F-value = 74.16 presented in model summary indicate that the model is significant.

$$LOI\ \% = 22.633 + 17.97\ zinc\ acetate\ (M) + 7.55\ NaOH\ (M) + 0.00535\ sonication\ time\ (minutes) + 82.0\ zinc\ acetate\ (M) \times NaOH(M) - 0.0013\ zinc\ acetate\ (M) \times sonication\ time\ (minutes) - 0.0026\ NaOH\ (M) \times sonication\ time\ (minutes) \quad (26)$$

Model summary of LOI %

S = 1.21851 R-squared = 72.01% R-squared (adj) = 72.03% R-squared (pred) = 69.88
F-Value = 74.16 p-Value = 0.000

The analysis of variance subjected to data regarding the LOI % under the effect of zinc acetate (M), NaOH (M), and sonication time (minutes) are presented in Table 11, which revealed highly significant effects for all the variables upon LOI % with p-value <.001. However interaction of zinc acetate (M) and sonication time (minutes) have significant effect upon LOI % with p-value = 0.007. While the other interactions are significant at p-value value <.001.

Table 11. Analysis of variance for limiting oxygen index.

Source of variation	Sum of squares	df	Mean square	F-value	p-value
A-Zinc acetate (M)	542.939	2	271.470	9032.25	<.001
B-NaOH (M)	296.124	2	148.062	4926.27	<.001
C-Sonication time (minutes)	7.521	3	2.507	83.40	<.001
A×B	64.851	4	16.213	539.42	<.001
A×C	.236	6	.039	1.30	.007
B×C	.360	6	.060	1.99	<.001
A×B×C	1.178	12	.098	3.26	<.001
Error	4.328	144	.030		
Total	917.537	179			

The main effects plots displayed in Figure 37 depict the fitted mean values of LOI % under different experimental variables. These plots clearly demonstrate that each value is distinct from one another. In the case of zinc acetate (M), the highest mean LOI % value is 29.39, which is achieved at a molar concentration of 0.1. On the other hand, for NaOH (M), the maximum mean value of LOI % is 29.36, obtained at a molar concentration of 0.3. Furthermore, the plots reveal that the highest mean value of LOI % for sonication time (minutes) is 28.20, which occurs at duration of 90 minutes.

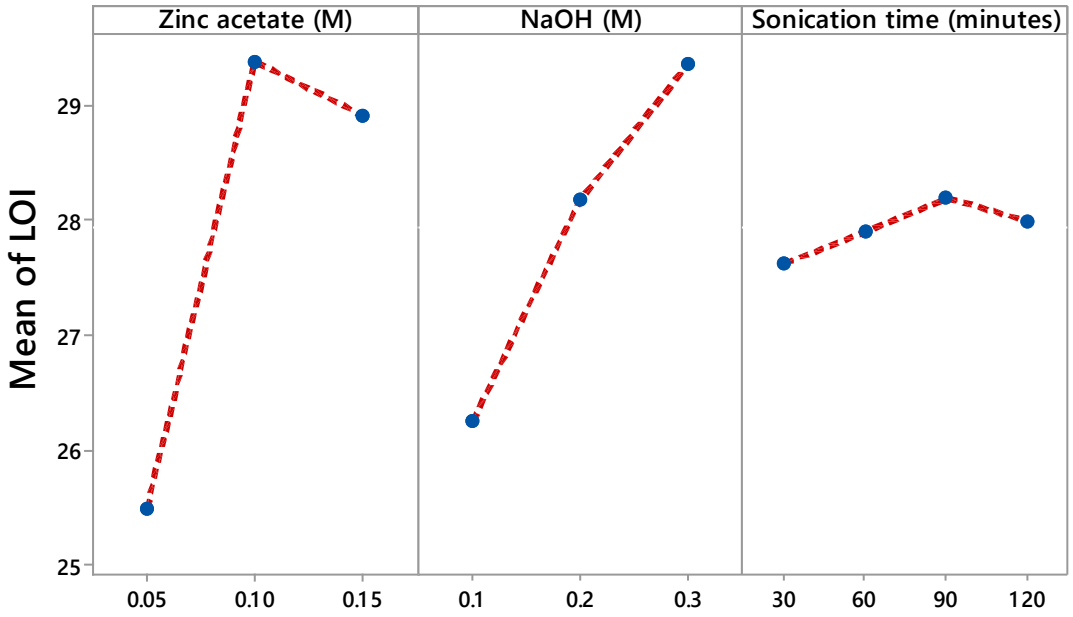

Figure 37. Main effects plots for LOI %.

5.9. Antibacterial activity

Antibacterial activity of developed samples was investigated according to the colony count test procedure and shown in Table 12 and Figure 38. The results show that treated fabrics exhibit excellent bacterial reduction for both E.coli and S.aureus bacteria. From Table 12 and Figure 38, it is evident that with an increased loaded amount of ZnO NPs, the antibacterial activity of the treated samples also increased for both E.coli and S.aureus bacteria. 100 % S.aureus reduction was achieved with 8.78 % loaded concentration of Zn contents (sample 17). While 100 % E.coli reduction was achieved with 9.07 % loaded concentration of Zn contents (sample 18). While the sample A developed by magnetic stirring showed 96.27% S.aureus reduction and 93.52% E.coli reduction. As the ZnO NPs interact with bacteria, they generate reactive oxygen species, such as H_2O_2, $\bullet OH^-$, $\bullet O_2^-$. These reactive oxygen species damage the protein and DNA of the bacterial cell, resulting in the death of a bacterial cell. Furthermore, ZnO NPs deactivate the various necessary enzymes present in a bacterial cell; it is done by the interaction between the ZnO NPs and the thiol group present in bacterial cell. Moreover, the attachment of ZnO NPs onto the cell wall of the bacteria increase the Zn^{2+} cations concentration in the cytoplasm, which results in the death of bacteria [255], [256].

Table 12. Experimental results for antibacterial activity.

Sample	Zinc acetate (M)	NaOH (M)	Sonication time (minutes)	MDPA (g/L)	Bacterial reduction %			
					S. aureus		E.coli	
					R (%)	Std. dev.	R (%)	Std. dev.
1	0.05	0.1	30	300	41.78	3.44	30.34	3.37
2	0.05	0.1	60	300	43.29	3.52	34.67	4.53
3	0.05	0.1	90	300	47.86	3.72	40.45	3.42
4	0.05	0.1	120	300	45.76	4.21	37.47	4.50
5	0.05	0.2	30	300	49.97	5.53	41.23	5.05
6	0.05	0.2	60	300	51.79	4.44	45.57	3.76
7	0.05	0.2	90	300	59.93	3.76	50.78	4.03
8	0.05	0.2	120	300	52.79	5.96	45.91	2.48
9	0.05	0.3	30	300	69.86	4.75	59.92	3.62
10	0.05	0.3	60	300	73.32	3.72	65.76	3.30
11	0.05	0.3	90	300	78.84	4.30	74.65	2.73
12	0.05	0.3	120	300	75.54	4.32	71.78	2.15
13	0.1	0.1	30	300	81.45	3.41	77.87	2.16
14	0.1	0.1	60	300	85.42	4.03	82.98	3.31
15	0.1	0.1	90	300	94.43	1.60	91.46	4.32
16	0.1	0.1	120	300	89.95	2.14	84.56	2.68
17	0.1	0.2	30	300	100	0	98.64	0.86
18	0.1	0.2	60	300	100	0	100	0
19	0.1	0.2	90	300	100	0	100	0
20	0.1	0.2	120	300	100	0	100	0
21	0.1	0.3	30	300	100	0	100	0
22	0.1	0.3	60	300	100	0	100	0
23	0.1	0.3	90	300	100	0	100	0
24	0.1	0.3	120	300	100	0	100	0
25	0.15	0.1	30	300	84.49	2.59	80.54	2.17
26	0.15	0.1	60	300	93.23	2.10	87.76	2.33
27	0.15	0.1	90	300	95.67	1.37	92.51	2.31
28	0.15	0.1	120	300	90.42	2.40	85.78	1.63
29	0.15	0.2	30	300	100	0	100	0
30	0.15	0.2	60	300	100	0	100	0
31	0.15	0.2	90	300	100	0	100	0
32	0.15	0.2	120	300	100	0	100	0
33	0.15	0.3	30	300	100	0	100	0
34	0.15	0.3	60	300	100	0	100	0
35	0.15	0.3	90	300	100	0	100	0
36	0.15	0.3	120	300	100	0	100	0
A	0.1	0.3	90 (magnetic stirring)	300	96.27	3.35	93.52	4.67

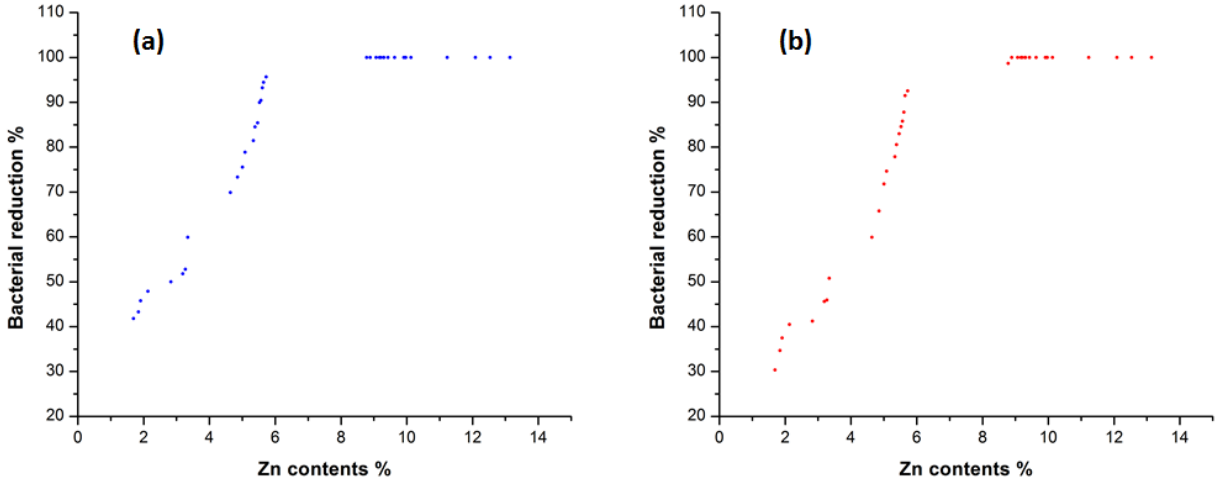

Figure 38, Graphical representation of antibacterial activity (a) S. aureus vs Zn contents % (b) E. coli vs Zn contents %.

The regression model for predicting the S.aureus bacterial reduction % is displayed in equation (27). The fitted model could explain 76.71% of the total changes, according to the R-squared value provided in the model summary. The model is significant, as indicated by the p-value of 0.00 and the F-value of 94.95 presented in the model summary.

S. aureus bacterial reduction % = − 3.63 + 630.3 zinc acetate (M) + 208.6 NaOH (M) + 0.1341 sonication time (minutes) − 1034 zinc acetate (M) × NaOH (M) − 0.392 zinc acetate (M) × sonication time (minutes) − 0.271 NaOH (M) × sonication time (minutes) (27)

Model summary of S.aureus bacterial reduction %

S = 10.0808 R-squared = 76.71% R-squared (adj) = 75.90% R-squared (pred) = 75.14%

F-Value = 94.95 p-Value = 0.000

Equation (28) shows the regression model for forecasting the E. coli bacterial reduction %. The R-squared value in the model summary indicates that 76.84% of the total changes could be explained by the fitted model. The model is significant, as shown by the model summary's F-value of 95.65 and p-value of 0.00.

E. .coli bacterial reduction % = − 17.56+704.6 zinc acetate (M) + 210.2 NaOH (M) + 0.1671 sonication time (minutes) − 946 zinc acetate (M) × NaOH (M) − 0.784 zinc acetate (M) × sonication time (minutes) − 0.177 NaOH (M) × sonication time (minutes) (28)

Model summary of E.coli reduction %

S = 11.6385 R-squared = 76.84% R-squared (adj) = 76.03% R-squared (pred) = 75.29%
F-Value = 95.65 p-Value = 0.000

Table 13 displays the results of the analysis of variance applied to the S. aureus bacterial reduction % under the influence of zinc acetate (M), NaOH (M), and sonication time (minutes). All variables had highly significant effects on the S. aureus bacterial reduction %, with a p value less than 0.001. However, interaction of zinc acetate (M) and sonication time (minutes) have significant effect upon S.aureus bacterial reduction % with p-value = 0.007. While the other interactions are signifact at p-value value less than 0.001.

Table 13. Analysis of variance for S.aureus bacterial reduction.

Source of variation	Sum of squares	df	Mean square	F-value	p-value
A-Zinc acetate (M)	60545.706	2	30272.853	3842.61	<.001
B-NaOH (M)	8752.925	2	4376.463	555.51	<.001
C-Sonication time (minutes)	686.580	3	228.860	29.05	<.001
A×B	3613.815	4	903.454	114.67	<.001
A×C	147.058	6	24.510	3.11	.007
B×C	258.365	6	43.061	5.46	<.001
A×B×C	334.035	12	27.836	3.53	<.001
Error	1134.460	144	7.878		
Total	75472.944	179			

The main effects plots for fitted mean values of S. aureus bacterial reduction % under different experimental variables are shown in Figure 39. In case of zinc acetate (M) the maximum mean value of S. aureus bacterial reduction % is 96.98 which is obtained at 0.15 molar concentration of zinc acetate, while for the NaOH (M) the maximum mean value of S. aureus bacterial reduction % is 91.46 which is obtained at 0.3 molar concentration of NaOH. The plots show that the maximum mean value of S. aureus bacterial reduction % for sonication time (minutes) is 86.30 which is obtained at 90 minutes of sonication time.

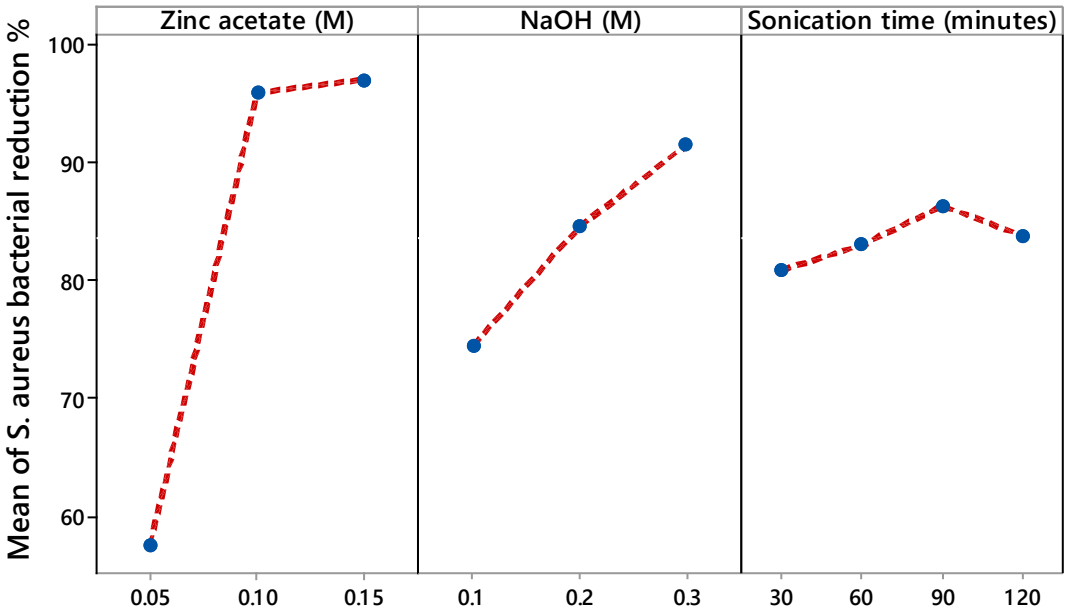

Figure 39. Main effects plots for S. aureus bacterial reduction %.

The analysis of variance subjected to data regarding the E.coli bacterial reduction % under the effect of Zinc acetate (M), NaOH (M), and sonication time (minutes) are presented in Table 14, which revealed highly significant effects for all the variables and there interactions upon E.coli bacterial reduction %with p value <.001.

Figure 40 displays the main effects plots for fitted mean values of E. coli bacterial reduction % under various experimental factors. The highest mean value of E. coli bacterial reduction % in the case of zinc acetate (M) is 95.55, obtained at a concentration of 0.15 molar zinc acetate; in the case of NaOH (M), the maximum mean value of E. coli bacterial reduction % is 89.34, obtained at a concentration of 0.3 molar NaOH. The graphs demonstrate that, at 90 minutes of

sonication time, the maximum mean value of E. coli bacterial reduction % for sonication time (minutes) is 83.33.

Table 14. Analysis of variance for E.coli bacterial reduction.

Source of variation	Sum of squares	df	Mean square	F-value	p-value
A-Zinc acetate (M)	81751.998	2	40875.999	6602.02	<.001
B-NaOH (M)	12867.526	2	6433.763	1039.14	<.001
C-Sonication time (minutes)	1070.954	3	356.985	57.65	<.001
A×B	3656.992	4	914.248	147.66	<.001
A×C	307.336	6	51.223	8.27	<.001
B×C	314.590	6	52.432	8.46	<.001
A×B×C	309.387	12	25.782	4.16	<.001
Error	891.566	144	6.191		
Total	101170.348	179			

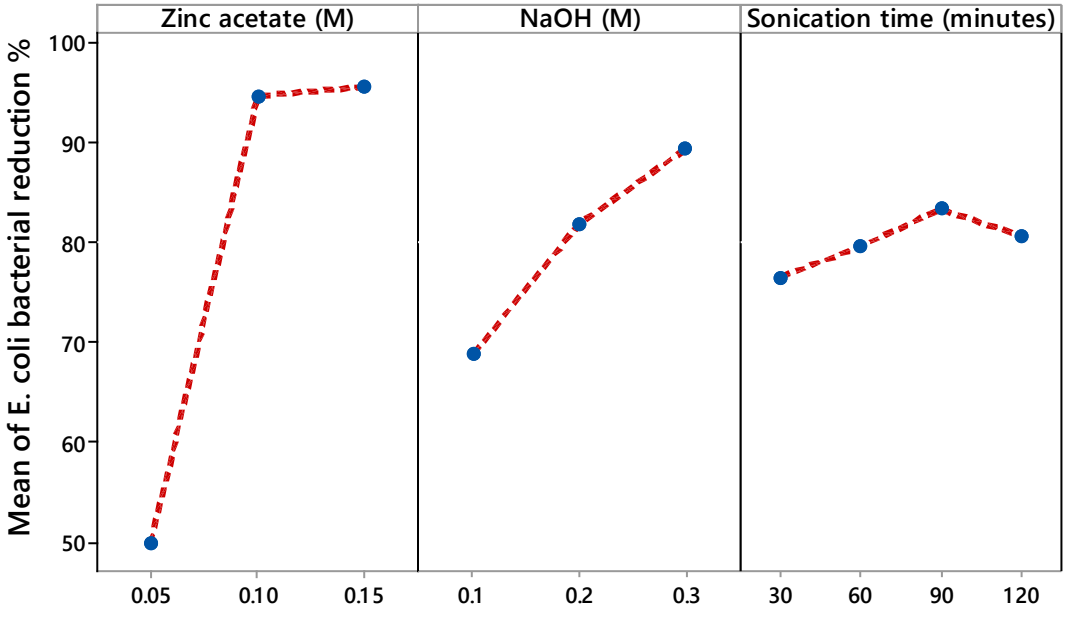

Figure 40. Main effects plots for E.coli bacterial reduction %.

5.10. Ultraviolet protection factor (UPF)

The UV protection factors (UPF values) of the untreated and developed samples are shown in Table 15 and Figure 41. It is apparent from Table 15 and Figure 41 that untreated cotton fabric has an UPF value of 4.78, while the UPF value of sonochemically synthesized optimized sample 23 has 143.76. It can also be seen from Table 15 and Figure 41 that with the increase in ZnO NPs concentration, the UPF values of the samples also increase. The study by Han and Yu supports these results; they concluded that the UV blocking ability of textile material increases with increasing the metal oxide amount in the textile matrix [257]. The higher UPF value indicates that the fabric has a higher ability to protect against UV radiations [258]. ZnO NPs have a high refractive index, which causes the UV radiations to be scattered when they interact with ZnO NPs, and not to be transmitted to the human body [231]. Furthermore, when exposed to UV rays, ZnO NPs absorb the corresponding energy through the interaction with their electrons, impeding the penetration of such radiation from the fabric into the skin. This absorption phenomenon plays a pivotal role in safeguarding the integrity of DNA within skin cells, thereby reducing the likelihood of both sunburn and long-lasting skin harm[193], [230]. Apart from absorption, ZnO NPs exhibit reflective attributes within the UV range, effectively deflecting a proportion of the incident UV radiation away from the surface of the fabric[193]. This reflective mechanism imparts an additional layer of protection against harmful UV exposure.

Table 15 shows that the sample A with 7.83 % ZnO NPs concentration has a 52.05 UPF value, and sample 27 with 5.73 % ZnO NPs has a 50.96 UPF value; the high difference in ZnO NPs concentrations and very little difference in UPF values of these samples can be explained as better and smooth distribution of ZnO NPs in case of sample 27 by the sonochemical process as compared to sample A which is prepared by the conventional stirring method.

Table 15. Experimental results for UV protection.

Sample	Zinc acetate (M)	NaOH (M)	Sonication time (minutes)	MDPA (g/L)	UV protection	
					UPF	Std. dev.
Untreated	-	-	-	-	4.78	0.11
1	0.05	0.1	30	300	19.12	0.50
2	0.05	0.1	60	300	20.31	0.36
3	0.05	0.1	90	300	20.87	0.25
4	0.05	0.1	120	300	20.64	0.14
5	0.05	0.2	30	300	20.94	0.33
6	0.05	0.2	60	300	21.53	0.39
7	0.05	0.2	90	300	21.72	0.24
8	0.05	0.2	120	300	21.67	0.35
9	0.05	0.3	30	300	32.52	0.41
10	0.05	0.3	60	300	33.71	0.29
11	0.05	0.3	90	300	34.13	0.20
12	0.05	0.3	120	300	33.98	0.24
13	0.1	0.1	30	300	34.39	0.23
14	0.1	0.1	60	300	37.17	0.37
15	0.1	0.1	90	300	49.09	1.58
16	0.1	0.1	120	300	37.98	0.90
17	0.1	0.2	30	300	67.74	1.10
18	0.1	0.2	60	300	73.89	1.62
19	0.1	0.2	90	300	93.34	2.46
20	0.1	0.2	120	300	82.98	2.61
21	0.1	0.3	30	300	134.32	3.18
22	0.1	0.3	60	300	134.87	2.77
23	0.1	0.3	90	300	143.76	3.43
24	0.1	0.3	120	300	139.93	2.64
25	0.15	0.1	30	300	36.89	0.58
26	0.15	0.1	60	300	48.04	1.03
27	0.15	0.1	90	300	50.96	1.45
28	0.15	0.1	120	300	42.74	1.21
29	0.15	0.2	30	300	71.87	1.09
30	0.15	0.2	60	300	84.45	1.46
31	0.15	0.2	90	300	97.12	3.99
32	0.15	0.2	120	300	87.92	2.03
33	0.15	0.3	30	300	104.45	2.27
34	0.15	0.3	60	300	111.56	3.07
35	0.15	0.3	90	300	124.47	5.08
36	0.15	0.3	120	300	121.34	2.71
A	0.1	0.3	90 (magnetic stirring)	300	52.05	6.09
B	-	-	-	300	13.23	0.26

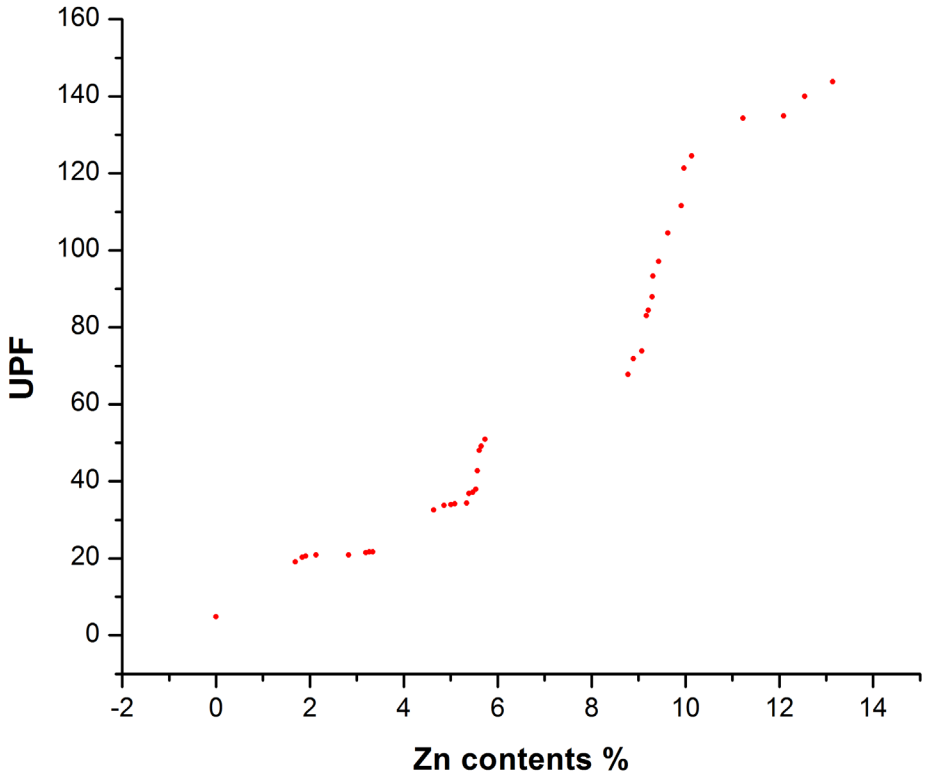

Figure 41. Graphical representation of UPF values against Zn contents %.

Equation (29) shows the regression model for the prediction of UPF value. The R-squared value presented in the model summary shows that the fitted model could explain 76.70 % of total variations , while p-value = 0.00 and F-value = 94.90 presented in the model summary indicate that the model is significant.

UPF = 11.4 −117 zinc acetate (M) - 1.8 NaOH (M) − 0.098 sonication time (minutes) + 2872 zinc acetate (M) × NaOH (M) + 1.47 zinc acetate (M) × sonication time (minutes) + 0.256 NaOH (M) × sonication time (minutes) (29)

Model summary of UPF

S = 19.973 R-squared = 76.70% R-squared (adj) = 75.89% R-squared (pred) = 74.98%

F-value = 94.90 p-value = 0.000

The analysis of variance applied to the data concerning the UPF values in relation to the influence of zinc acetate (M), NaOH (M), and sonication time (minutes) is displayed in Table 16. This analysis unveiled exceedingly significant impacts for all the variables, as well as their interactions, on the UPF values, with a p-value of less than 0.001.

Table 16. Analysis of variance for UPF.

Source of variation	Sum of squares	df	Mean square	F-value	p-value
A-Zinc acetate (M)	138348.787	2	69174.394	18576.97	<.001
B-NaOH (M)	111668.931	2	55834.465	14994.50	<.001
C-Sonication time (minutes)	3713.627	3	1237.876	332.43	<.001
A×B	39317.165	4	9829.291	2639.68	<.001
A×C	1680.934	6	280.156	75.23	<.001
B×C	434.214	6	72.369	19.43	<.001
A×B×C	456.605	12	38.050	10.21	<.001
Error	536.207	144	3.724		
Total	296156.471	179			

The main effects plots presented in Figure 42 illustrate the fitted mean values of UPF under various experimental variables. These plots clearly portray the distinctiveness of each value. In the instance of zinc acetate (M), the maximum mean UPF value is 85.79, attained at a molar concentration of 0.1 (M). While for NaOH (M), the highest mean value of UPF is 95.75, achieved at a molar concentration of 0.3 (M). Additionally, the plots indicate that the highest mean value of UPF for sonication time (minutes) is 70.61, occurring at the duration of 90 minutes.

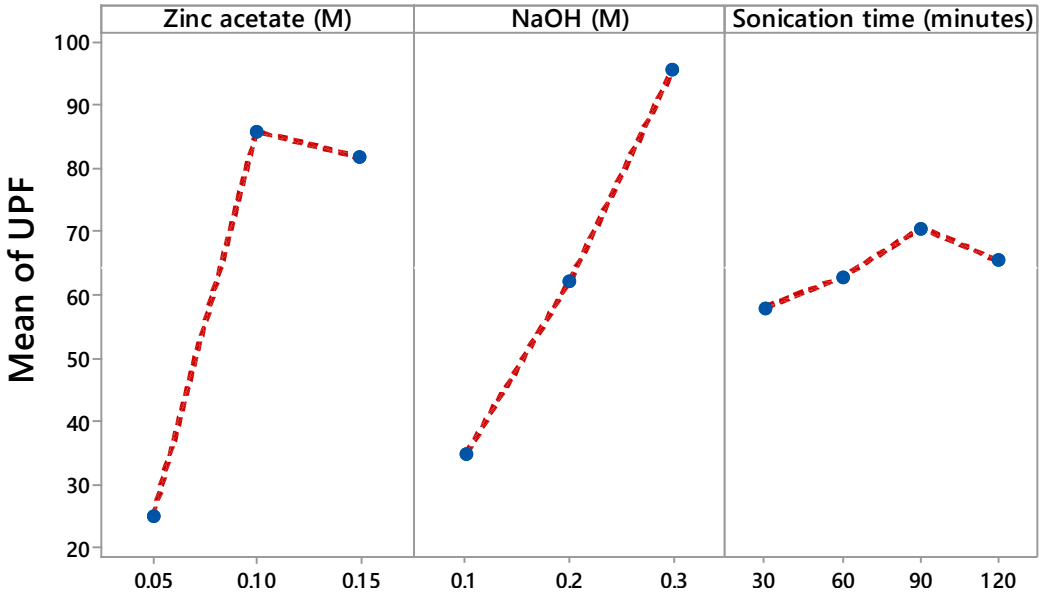

Figure 42. Main effects plots for UPF.

5.11. Self-cleaning

Cotton fabrics coated with ZnO NPs and MDPA were analyzed for self-cleaning using photocatalytic degradation of coffee stain under 8 hours of UV irradiation. Figure 44 shows the scanned images of samples before and after UV irradiation. Table 17 shows the color intensity of samples after 8 hours of UV irradiation time. In image J software black has 0 color intensity while white has 255, so greater the value of color intensity, the more the color towards the white. Figure 43 shows the relation between Zn contents % and color intensity. It is clear that color intensity increases with the increase of the loaded amount of Zn contents. Untreated sample after 8 hours of UV irradiation time has color intensity 150.51. Sample A and sample B have color intensity 214.88 and 151.42 respectively. The higher color intensity of sample A than sample B is due to the presence of ZnO NPs at the surface of fabric[23]. Sample 23 showed the excellent results having color intensity of 250.27, which is very near to the color intensity value of white color. These results are in line with Sudrajat. H work demonstrating that the higher photo catalytic activity is obtained at higher amounts of ZnO NPs[259]. When ZnO NPs exist on the top of textile fabrics, ZnO NPs has the ability to react and degrade different organic dirt stains, both colorful and colorless[220]. As compared to untreated cotton fabric, the higher photo catalytic activity of ZnO NPs loaded cotton fabrics is

because of ZnO NPs on the surface of the cotton fabrics, since ZnO NPs cause degradation of the dye molecules by photo catalytic reactions[260]. In the photo-catalytic mechanism by ZnO NPs, two photochemical reactions "oxidation and reduction" occur. During these reactions reactive oxygen species "•OH and $•O_2^-$"are produced. The •OH radical has a vital role in oxidating the dye molecules[193]. The mechanism of dye degradation can be described by Figure 45 and equations (30-33)[33].

Table 17. Experimental results for self-cleaning.

Sample	Zinc acetate (M)	NaOH (M)	Sonication time (minutes)	MDPA (g/L)	Self-cleaning	
					Color Intensity	Std. dev.
Untreated	-	-	-	-	150.51	1.47
1	0.05	0.1	30	300	158.53	3.91
2	0.05	0.1	60	300	163.05	3.21
3	0.05	0.1	90	300	177.53	2.46
4	0.05	0.1	120	300	172.29	3.31
5	0.05	0.2	30	300	180.02	4.12
6	0.05	0.2	60	300	183.41	3.14
7	0.05	0.2	90	300	186.13	2.26
8	0.05	0.2	120	300	184.29	3.30
9	0.05	0.3	30	300	191.34	2.24
10	0.05	0.3	60	300	194.51	3.24
11	0.05	0.3	90	300	199.20	4.77
12	0.05	0.3	120	300	196.27	3.62
13	0.1	0.1	30	300	203.62	4.01
14	0.1	0.1	60	300	206.54	2.58
15	0.1	0.1	90	300	210.63	3.25
16	0.1	0.1	120	300	207.19	2.91
17	0.1	0.2	30	300	222.51	4.37
18	0.1	0.2	60	300	225.05	5.58
19	0.1	0.2	90	300	229.71	3.41
20	0.1	0.2	120	300	226.86	3.29
21	0.1	0.3	30	300	246.24	1.34
22	0.1	0.3	60	300	248.06	1.01
23	0.1	0.3	90	300	250.27	1.04
24	0.1	0.3	120	300	249.49	1.29
25	0.15	0.1	30	300	204.29	4.18
26	0.15	0.1	60	300	207.97	3.80
27	0.15	0.1	90	300	212.51	2.93
28	0.15	0.1	120	300	207.80	3.84
29	0.15	0.2	30	300	224.62	6.24
30	0.15	0.2	60	300	228.35	3.77
31	0.15	0.2	90	300	232.50	3.74
32	0.15	0.2	120	300	228.83	2.81
33	0.15	0.3	30	300	235.77	3.67
34	0.15	0.3	60	300	241.46	3.76
35	0.15	0.3	90	300	243.61	1.36
36	0.15	0.3	120	300	242.47	3.42
A	0.1	0.3	90 (magnetic stirring)	300	214.88	4.53
B	-	-	-	300	151.42	1.32

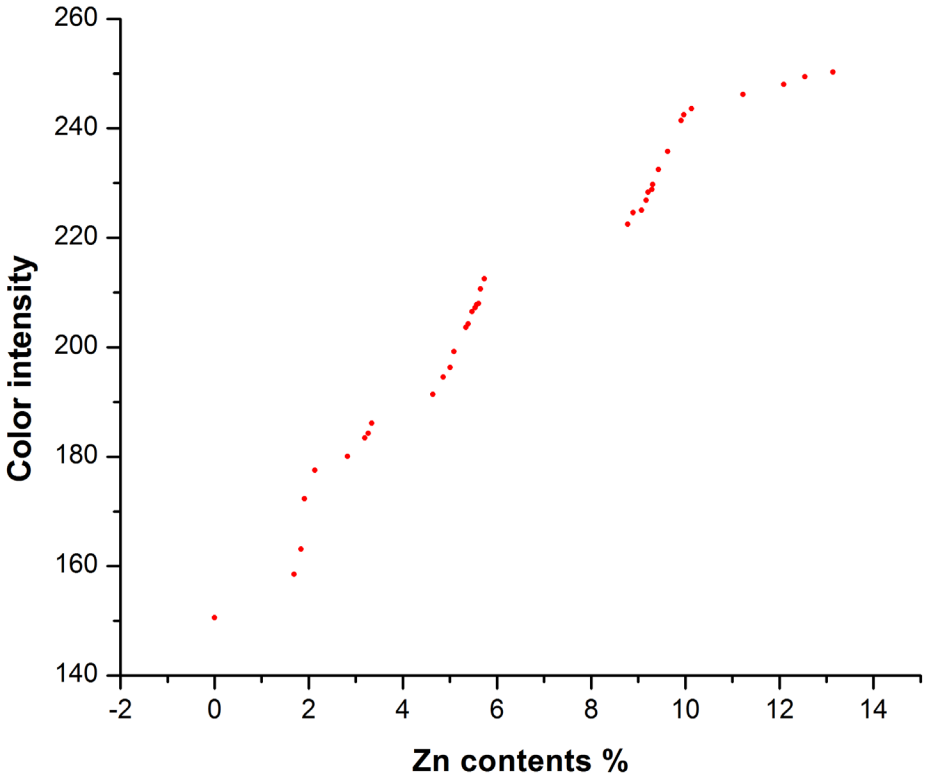

Figure 43. Graphical representation of color intensity against Zn contents %.

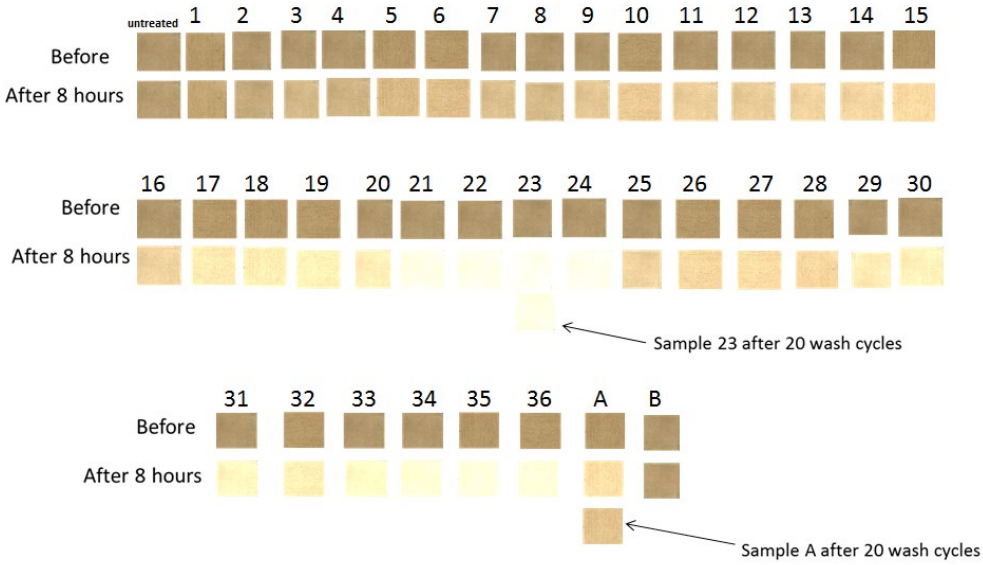

Figure 44. Degradation of coffee stain under UV-visible light irradiation.

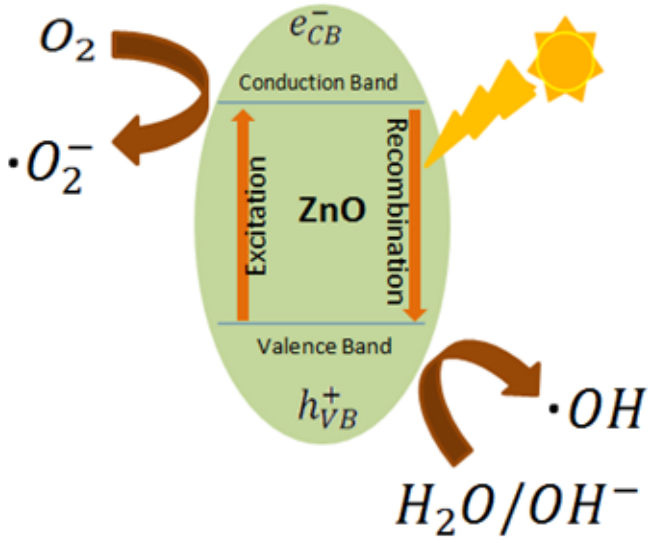

Figure 45. Schematic mechanism of photocytalytic activity.

$$ZnO + hv \rightarrow ZnO\ (2h^+ + 2e^-) \quad (30)$$

$$\frac{1}{2}O_2 + 2e^- \rightarrow H_2O + 2OH^- \quad (31)$$

$$2OH^- + h^+ \rightarrow 2\ \bullet OH \quad (32)$$

$$\bullet OH + dye \rightarrow degradation \quad (33)$$

The regression model for predicting color intensity is depicted by equation (34). The model summary displays the R-squared value, indicating that the fitted model can account for 78.49% of the total variations. Furthermore, the model summary presents the p-value as 0.00 and the F-value as 105.21, which suggests that the model is statistically significant.

Color intensity = 128.44 + 414.9 zinc acetate (M) + 156.8 NaOH (M) + 0.1464 sonication time (minutes) + 260 zinc acetate (M) × NaOH (M) − 0.407 zinc acetate (M) × sonication time (minutes) − 0.178 NaOH (M)× sonication time (minutes) (34)

Model summary of color intensity

S = 12.125 R-squared = 78.49% R-squared (adj) = 77.74% R-squared (pred) = 76.85%

F-value = 105.21 p-value = 0.000

Table 18 shows the results of the analysis of variance performed on the data pertaining to the color intensity in relation to the influence of zinc acetate (M), NaOH (M), and sonication time (minutes). With a p -value of less than 0.001, this study revealed incredibly significant effects for each variable and interactions of zinc acetate (M) with NaOH (M) on the color intensity. However all other interactions have non-significant effects on the color intensity with p-value greater than 0.05.

Table 18. Analysis of variance for color intensity.

Source of variation	Sum of squares	df	Mean square	F-value	p-value
A-Zinc acetate (M)	78560.532	2	39280.266	3293.62	<.001
B-NaOH (M)	34546.342	2	17273.171	1448.34	<.001
C-Sonication time (minutes)	1652.492	3	550.831	46.18	<.001
A×B	1236.263	4	309.066	25.91	<.001
A×C	144.860	6	24.143	2.02	.066
B×C	141.115	6	23.519	1.97	.073
A×B×C	255.916	12	21.326	1.78	.055
Error	1717.363	144	11.926		
Total	118254.883	179			

The fitted mean values of color intensity under different experimental factors are shown in the major effects graphs (Figure 46). With zinc acetate (M), the highest mean color intensity value is obtained at a molar concentration of 0.1 (M). This value is 227.18. The highest mean value of color intensity for NaOH (M) is 228.23, which is attained at a molar concentration of 0.3 (M). Furthermore, the plots show that the maximum mean value of color intensity for sonication time (minutes) is 215.79, which happens during a 90 minutes period.

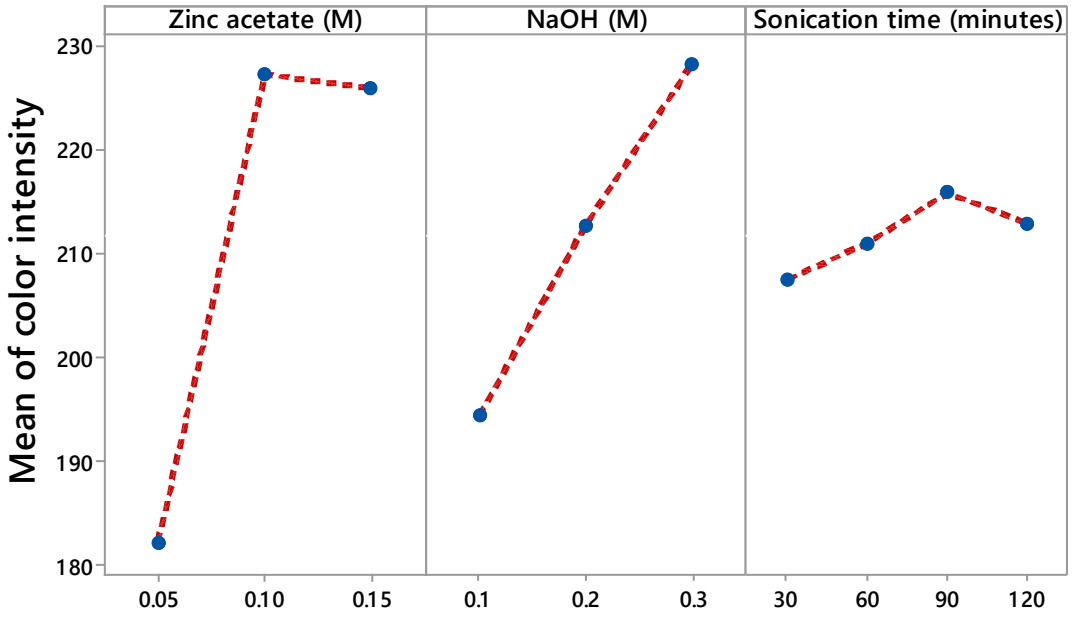

Figure 46. Main effects plots for color intensity.

5.12. Bending rigidity

Bending rigidity or stiffness is an important property of fabric which further influences fabric draping and wrinkling behavior. Each sample with a 50mm width was clamped in the instrument from one side while the other side drove through the sensor jaws, as shown in Figure 47. The measurement of each sample was repeated five times. The average bending force was obtained for each sample, and with the help of bending force the bending rigidity was calculated by using equation (35)[261].

$$B = k.Fm \quad (35)$$

Where B is bending rigidity

k is constant and k= $0.7x10^{-6}$

Fm is bending force

Figure 47. Bending Tester TH-7.

The measured values of bending force and bending rigidity are tabulated in Table 19. While Figure 48 shows the plot of bending force against Zn contents %. It is obvious from Table 19 that after MDPA coating the bending force and as well as bending rigidity of the fabric in both warp wise and weft wise directions are increased. From the results shown in Table 19 it is clear that after ZnO NPs coating the bending force and bending rigidity is further increased in both directions. Untreated fabric has warp wise and weft wise bending rigidity as 0.0581×10^{-4} Nm and 0.0392×10^{-4} Nm, respectively. While the sample B only coated with flame retardant chemical has warp wise bending rigidity 0.0787×10^{-4} Nm and weft wise bending rigidity 0.0501×10^{-4} Nm. The highest bending rigidity was recorded for sample 23 with highest amount of ZnO NPs as 0.0969×10^{-4} Nm and 0.0612×10^{-4} Nm warp wise and weft wise respectively. Figure 48 shows that with the increased amount of ZnO NPs deposition on to the fabric the bending force to bend the fabric also increased. The increase in bending force with the increase of ZnO NPs is also reported by Khan *et al.* They concluded that bending force and stiffness of the fabric have a linear increasing relationship with amount and size of ZnO nano rods[262]. In one more study, Tania and Ali also reported increase in stiffness of the cotton fabric after ZnO NPs deposition on to the cotton fabric[263].

Table 19. Experimental results for bending rigidity.

Sample	Zinc acetate (M)	NaOH (M)	Sonication time (minutes)	MDPA (g/L)	Bending force (Fm) (mN)				Bending rigidity (B) (Nm)	
					Warp wise	Std. dev.	Weft wise	Std. dev.	Warp wise	Weft wise
Untreated	-	-	-	-	8.314	0.017	5.278	0.008	0.0581×10^{-4}	0.0392×10^{-4}
1	0.05	0.1	30	300	11.328	0.031	7.206	0.018	0.0792×10^{-4}	0.0504×10^{-4}
2	0.05	0.1	60	300	11.352	0.018	7.218	0.019	0.0794×10^{-4}	0.0505×10^{-4}
3	0.05	0.1	90	300	11.412	0.017	7.250	0.016	0.0798×10^{-4}	$.0.0507\times10^{-4}$
4	0.05	0.1	120	300	11.368	0.022	7.228	0.013	0.0795×10^{-4}	0.0506×10^{-4}
5	0.05	0.2	30	300	11.466	0.020	7.294	0.023	$.0.0802\times10^{-4}$	0.0510×10^{-4}
6	0.05	0.2	60	300	11.526	0.023	7.322	0.016	$.0.0806\times10^{-4}$	0.0512×10^{-4}
7	0.05	0.2	90	300	11.592	0.016	7.366	0.019	0.0811×10^{-4}	0.0515×10^{-4}
8	0.05	0.2	120	300	11.558	0.014	7.340	0.015	0.0809×10^{-4}	0.0513×10^{-4}
9	0.05	0.3	30	300	11.730	0.020	7.452	0.019	0.0821×10^{-4}	0.0521×10^{-4}
10	0.05	0.3	60	300	11.772	0.022	7.486	0.020	0.0824×10^{-4}	0.0524×10^{-4}
11	0.05	0.3	90	300	11.824	0.018	7.510	0.015	0.0827×10^{-4}	0.0526×10^{-4}
12	0.05	0.3	120	300	11.801	0.023	7.502	0.019	0.0826×10^{-4}	0.0525×10^{-4}
13	0.1	0.1	30	300	11.860	0.025	7.532	0.013	0.0830×10^{-4}	0.0527×10^{-4}
14	0.1	0.1	60	300	11.918	0.019	7.560	0.016	0.0834×10^{-4}	0.0529×10^{-4}
15	0.1	0.1	90	300	12.014	0.021	7.628	0.013	0.0841×10^{-4}	0.0533×10^{-4}
16	0.1	0.1	120	300	11.945	0.018	7.584	0.021	0.0836×10^{-4}	0.0531×10^{-4}
17	0.1	0.2	30	300	12.630	0.026	7.992	0.019	0.0841×10^{-4}	0.0559×10^{-4}
18	0.1	0.2	60	300	12.741	0.023	8.062	0.019	0.0892×10^{-4}	0.0564×10^{-4}
19	0.1	0.2	90	300	12.842	0.028	8.132	0.013	0.0899×10^{-4}	0.0569×10^{-4}
20	0.1	0.2	120	300	12.782	0.026	8.094	0.018	0.0895×10^{-4}	0.0566×10^{-4}
21	0.1	0.3	30	300	13.322	0.022	8.428	0.019	0.0932×10^{-4}	0.0589×10^{-4}
22	0.1	0.3	60	300	13.524	0.027	8.546	0.018	0.0947×10^{-4}	0.0598×10^{-4}
23	0.1	0.3	90	300	13.848	0.035	8.756	0.016	0.0969×10^{-4}	0.0612×10^{-4}
24	0.1	0.3	120	300	13.640	0.025	8.614	0.021	0.0954×10^{-4}	0.0603×10^{-4}
25	0.15	0.1	30	300	11.882	0.028	7.548	0.017	0.0832×10^{-4}	0.0528×10^{-4}
26	0.15	0.1	60	300	11.988	0.018	7.616	0.018	0.0839×10^{-4}	0.0533×10^{-4}
27	0.15	0.1	90	300	12.042	0.019	7.640	0.016	0.0843×10^{-4}	0.0535×10^{-4}
28	0.15	0.1	120	300	11.960	0.018	7.596	0.025	0.0837×10^{-4}	0.0532×10^{-4}
29	0.15	0.2	30	300	12.694	0.029	8..034	0.018	0.0889×10^{-4}	0.0562×10^{-4}
30	0.15	0.2	60	300	12.804	0.025	8.108	0.014	0.0896×10^{-4}	0.0567×10^{-4}
31	0.15	0.2	90	300	12.874	0.038	8.150	0.016	0.0901×10^{-4}	0.0570×10^{-4}
32	0.15	0.2	120	300	12.836	0.027	8.124	0.015	0.0898×10^{-4}	0.0568×10^{-4}
33	0.15	0.3	30	300	12.912	0.024	8.164	0.018	0.0904×10^{-4}	0.0571×10^{-4}
34	0.15	0.3	60	300	13.008	0.019	8.234	0.015	0.0910×10^{-4}	0.0576×10^{-4}
35	0.15	0.3	90	300	13.114	0.024	8.292	0.017	0.0918×10^{-4}	0.0580×10^{-4}
36	0.15	0.3	120	300	13.048	0.027	8.248	0.013	0.0913×10^{-4}	0.0577×10^{-4}
A	0.1	0.3	90 (magnetic stirring)	300	12.431	0.036	7.824	0.021	0.0870×10^{-4}	0.0548×10^{-4}
B	-	-	-	300	11.246	0.023	7..146	0.011	0.0787×10^{-4}	0.0501×10^{-4}

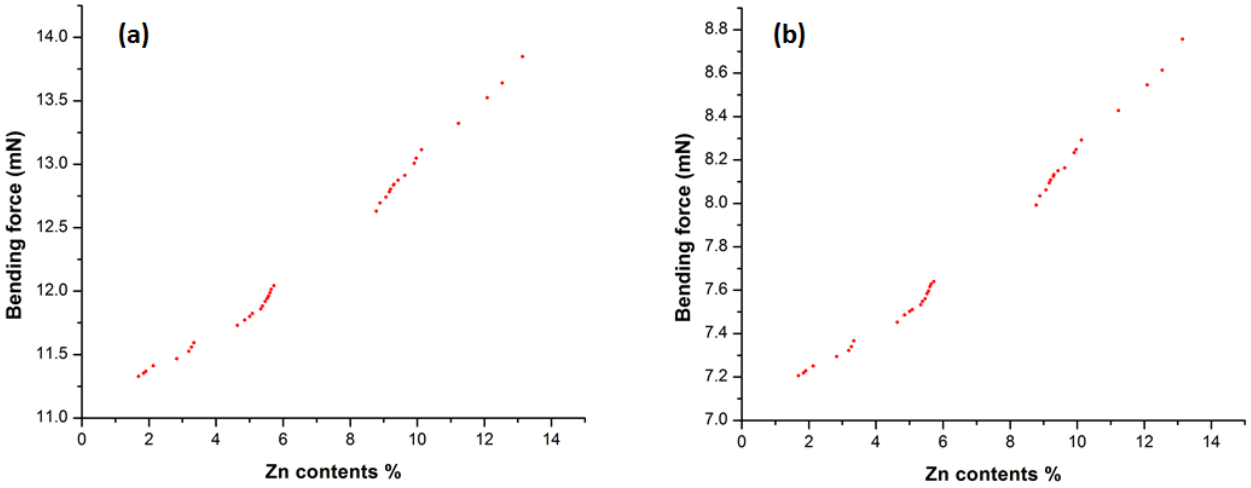

Figure 48. Graphical representation of bending force against Zn contents % (a) warp wise (b) weft wise.

Equations (36) and (37) show the regression model used to determine bending force warp wise and weft wise respectively. According to the model summary, for warp wise bending force the fitted model can explain 72.18% of the total variances based on its R-squared value. Furthermore, the model summary for warp wise bending force indicates the model's significance with a p-value of 0.000 and an F-value of 74.81. According to the model summary, for weft wise bending force the fitted model can explain 71.96% of the total variances based on its R-squared value. Furthermore, the model summary for weft wise bending force indicates the model's significance with a p-value of 0.000 and an F-value of 74.00.

The analysis of variance subjected to data regarding the bending force warp wise and weft wise under the effect of zinc acetate (M), NaOH (M), and sonication time (minutes) are presented in Tables 20 and 21 respectively, which revealed highly significant effects for all the variables and there interactions upon warp wise and weft wise bending force with p-values at <.001.

The main effects plots for fitted mean values of bending force warp wise and weft wise under different experimental variables are shown in Figures 49 and 50. In the case of zinc acetate (M) the maximum mean value of warp wise bending force is 12.754 mN and the mean value

of weft wise bending force is 8.077 mN, both are obtained at 0.1 molar concentration of zinc acetate. While for the NaOH (M) the maximum mean value of warp wise bending force is 12.795 mN and mean value of weft wise bending force is 8.102 mN, both are obtained at 0.3 molar concentration of NaOH. The plots show that the maximum mean value of warp wise bending force for sonication time (minutes) is 12.395 mN and weft wise bending force is 7.858 mN, which are obtained at 90 minutes of sonication time.

Bending force (mN) (warp wise) = 10.892 + 3.57 zinc acetate (M) + 1.50 NaOH (M) − 0.00037 sonication time (minutes) + 31.80 zinc acetate (M) × NaOH (M) + 0.0057 zinc acetate (M) × sonication time (minutes) + 0.0069 NaOH (M) × sonication time (minutes) (36)

Model summary for bending force warp wise

S = 0.387 R-squared = 72.18% R-squared (adj) = 71.22% R-squared (pred) =70.15%
F-value = 74.81 p-value = 0.00

Bending force (mN) (weft wise) = 6.926 + 2.31 zinc acetate (M) + 0.998 NaOH (M) − 0.00025 sonication time (minutes) + 18.62 zinc acetate (M) × NaOH (M) + 0.0037 zinc acetate (M) × sonication time (minutes) + 0.00423 NaOH (M) × sonication time (minutes) (37)

Model summary for bending force weft wise

S = 0.237 R-squared = 71.96% R-squared (adj) =70.99% R-squared (pred) = 69.91%
F-value =74.00 p-value = 0.000

Table 20. Analysis of variance for warp wise bending force.

Source of variation	Sum of squares	df	Mean square	F-value	p -value
A-Zinc acetate (M)	50.4928	2	25.2464	44421.81	<.001
B-NaOH (M)	32.7253	2	16.3627	28790.62	<.001
C-Sonication time (minutes)	0.8730	3	0.2910	512.01	<.001
A×B	8.5954	4	2.1488	3780.95	<.001
A×C	0.1592	6	0.0265	46.69	<.001
B×C	0.0973	6	0.0162	28.53	<.001
A×B×C	0.1318	12	0.0110	19.32	<.001
Error	0.0818	144	0.0006		
Total	93.1566	179			

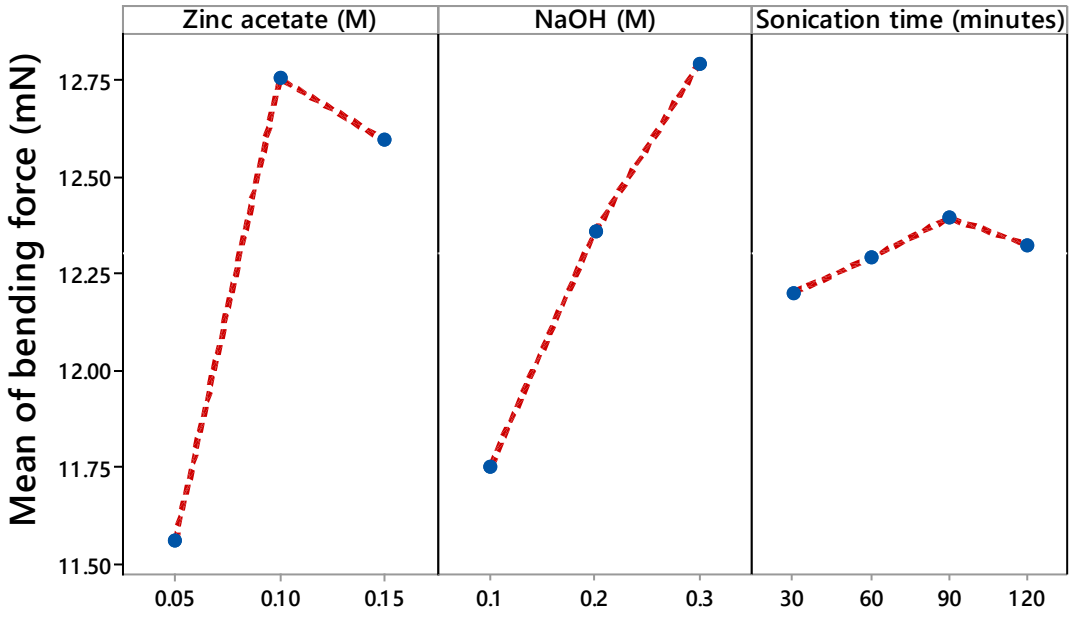

Figure 49. Main effects plots for warp wise bending force.

Table 21. Analysis of variance for warp wise bending force.

Source of variation	Sum of squares	df	Mean square	F-value	p-value
A-Zinc acetate (M)	18.814	2	9.407	30103.82	<.001
B-NaOH (M)	12.215	2	6.107	19544.76	<.001
C-Sonication time (minutes)	0.330	3	0.110	352.89	<.001
A×B	3.173	4	0.793	2538.80	<.001
A×C	0.072	6	0.012	38.52	<.001
B×C	0.038	6	0.006	20.67	.<.001
A×B×C	0.048	12	0.004	12.87	<.001
Error	0.045	144	0.0003		
Total	34.739	179			

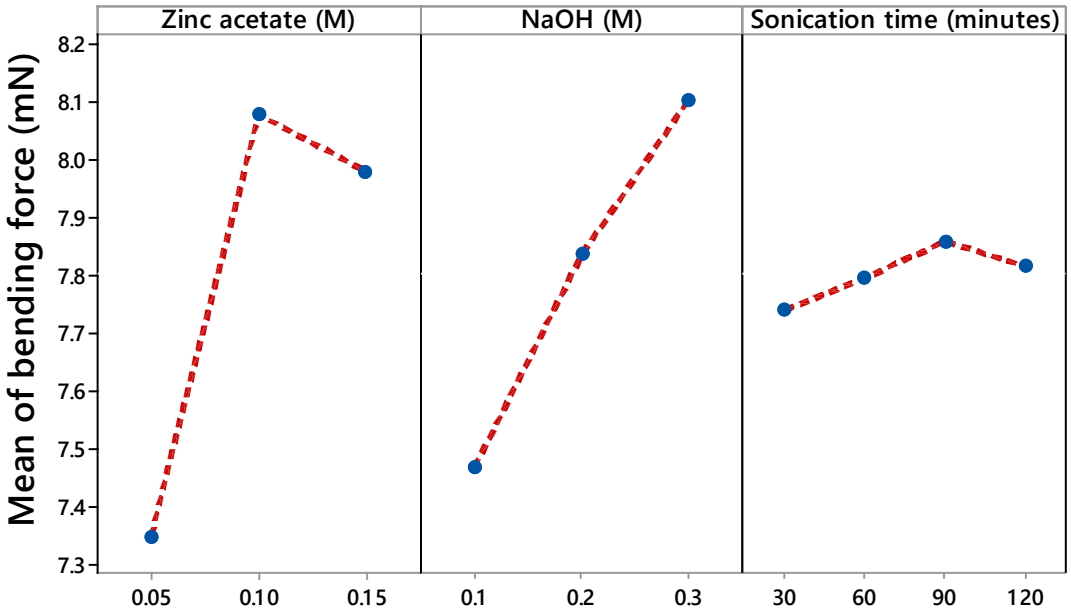

Figure 50. Main effects plots for weft wise bending force.

5.13. Air permeability

The air permeability of a fabric is dependent on factors such as its porosity, cross-section, shape of the fabric, and number of channels. Additionally, the thermal properties of the fabric are primarily influenced by its air permeability[264]. The air permeability of textile fabrics holds significance as a comfort attribute. Moreover, it is crucial to examine the impact of coating on the fabric's air permeation. Table 22 shows the results for air permeability of the untreated and treated samples. While the Figure 51 shows the relation between the synthesized amount of ZnO NPs and air permeability. It can be seen from Table 22 that air permeability of the fabric is decreased after flame retardant MDPA coating, which is further decreased after ZnO NPs deposition. The untreated sample has an air permeability 701.40 mm/s, while sample B after MDPA treatment has an air permeability of 676.44 mm/s. The minimum air permeability was recorded for sample 23 which is 508.64 mm/s. Figure 51 shows that there is a gradual decrease in the air permeability with the increase in ZnO NPs deposition. The decrease in the permeability of air may have been a result of the reduction in the sizes of the pores in the fabric, which was caused by the development of ZnO NPs on the surface of the cotton fibers. However, there is no major collapse of air permeability. This range of air permeability is commercially acceptable.

The regression model for predicting air permeability is depicted by equation (38). In order to assess the model's fit to the data, the R-squared value can be utilized. The model summary reveals that the R-squared value indicates a capability of the fitted model to account for 73.76% of the total variations. Additionally, the model summary presents a p-value of 0.000 and an F-value of 81.06, implying the significance of the model.

The analysis of variance subjected to data regarding the air permeability of the fabric under the effect of zinc acetate (M), NaOH (M), and sonication time (minutes) are presented in Table 23, which revealed highly significant effects for all the variables and there interactions upon air permeability with p-value at significant level.

The main effects plots for fitted mean values of air permeability under different experimental variables are shown in Figure 52. In the case of zinc acetate (M) the minimum mean value of air permeability is 574.55 mm/s which is obtained at 0.1 molar concentration of zinc acetate,

while for the NaOH (M) the minimum mean value of air permeability is 570.38 mm/s which is obtained at 0.3 molar concentration of NaOH. The plots show that the minimum mean value of air permeability for sonication time (minutes) is 595.20 mm/s, which is obtained at 90 minutes of sonication time.

Table 22. Experimental results for air permeability.

Sample	Zinc acetate (M)	NaOH (M)	Sonication time (minutes)	MDPA (g/L)	Air permeability	
					mm/s	Std. dev.
Untreated	-	-	-	-	701.40	1.14
1	0.05	0.1	30	300	674.81	2.16
2	0.05	0.1	60	300	671.60	1.52
3	0.05	0.1	90	300	661.84	2.38
4	0.05	0.1	120	300	666.60	2.30
5	0.05	0.2	30	300	653.62	2.61
6	0.05	0.2	60	300	648.20	3.49
7	0.05	0.2	90	300	641.44	2.70
8	0.05	0.2	120	300	644.60	3.21
9	0.05	0.3	30	300	632.22	2.59
10	0.05	0.3	60	300	628.82	2.77
11	0.05	0.3	90	300	625.62	2.41
12	0.05	0.3	120	300	626.40	2.07
13	0.1	0.1	30	300	622.64	2.30
14	0.1	0.1	60	300	618.88	2.86
15	0.1	0.1	90	300	613.80	3.42
16	0.1	0.1	120	300	617.60	2.88
17	0.1	0.2	30	300	589.21	3.27
18	0.1	0.2	60	300	582.82	3.35
19	0.1	0.2	90	300	572.40	2.61
20	0.1	0.2	120	300	581.43	3.57
21	0.1	0.3	30	300	539.47	3.05
22	0.1	0.3	60	300	528.85	3.11
23	0.1	0.3	90	300	508.64	3.13
24	0.1	0.3	120	300	521.40	3.21
25	0.15	0.1	30	300	620.86	3.70
26	0.15	0.1	60	300	616.00	3.46
27	0.15	0.1	90	300	609.66	2.41
28	0.15	0.1	120	300	616.87	3.63
29	0.15	0.2	30	300	586.60	2.97
30	0.15	0.2	60	300	575.05	1.58
31	0.15	0.2	90	300	569.25	2.39
32	0.15	0.2	120	300	573.22	2.28
33	0.15	0.3	30	300	564.68	3.65
34	0.15	0.3	60	300	559.40	3.36
35	0.15	0.3	90	300	554.41	3.91
36	0.15	0.3	120	300	557.2	3.11
A	0.1	0.3	90 (magnetic stirring)	300	602.12	4.27
B	-	-	-	300	676.44	2.85

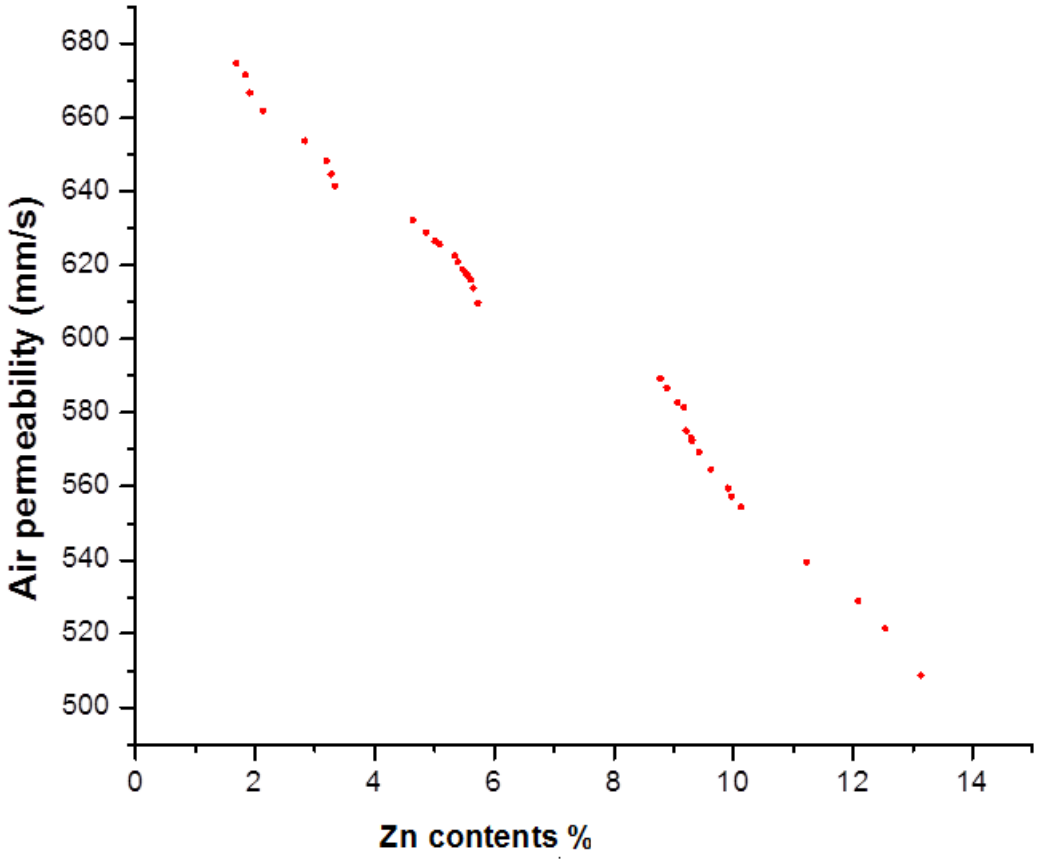

Figure 51. Graphical representation of air permeability against Zn contents %.

Air permeability (mm/s) = 717.8 − 477 zinc acetate (M) − 214.3 NaOH (M) − 0.052 sonication time (minutes) − 822 zinc acetate (M) × NaOH (M) − 0.03 zinc acetate (M) × sonication time (minutes) − 0.303 NaOH (M) × sonication time (minutes) (38)

Model summary for air permeability

S = 22.713 R-squared = 73.76% R-squared (adj) = 72.86% R-squared (pred) = 71.82%

F-vale= 81.06 p-value = 0.000

Table 23. Analysis of variance for air permeability.

Source of variation	Sum of squares	df	Mean square	F-value	p-value
A-Zinc acetate (M)	192373	2	96186.7	11349.46	<.001
B-NaOH (M)	122333	2	61166.5	7217.29	<.001
C-Sonication time (minutes)	4665	3	1555.1	183.49	<.001
A×B	18318	4	4579.6	540.37	<.001
A×C	325	6	54.2	6.40	<.001
B×C	172	6	28.6	3.38	0.004
A×B×C	785	12	65.4	7.72	<.001
Error	1220	144	8.5		
Total	340193	179			

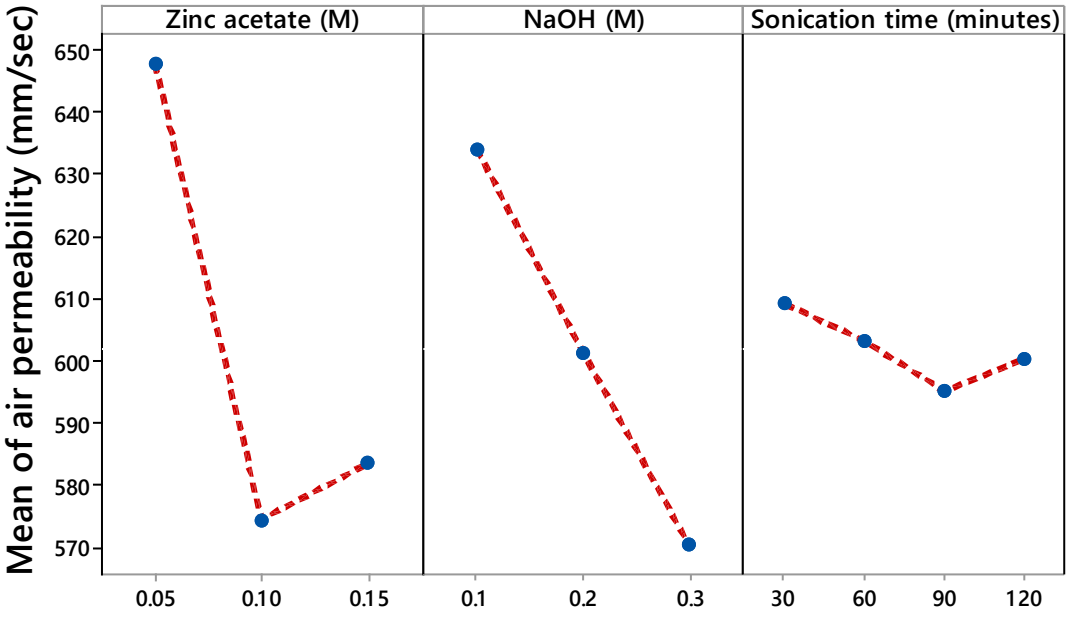

Figure 52. Main effects plots for air permeability.

5.14. Tensile strength

The measured values of tensile strength are shown in Table 24. It is apparent from Table 24 that after MDPA coating, both warp wise and weft wise tensile strength decreased. Furthermore, results presented in Table 24 show that after sonochemical treatment tensile strength further reduced in both warp wise and weft wise directions. Untreated fabric has warp wise and weft wise tensile strengths as 323.30 N and 247.83 N, respectively. While the sample B only coated with flame retardant chemical has warp wise tensile strength 284.78 N and weft wise tensile strength 216.12 N. The lowest tensile strength was recorded for sample 24 as 231.64 N and 182.06 N warp wise and weft wise respectively. Obtained results revealed that flame retardant coating, sonication time, and amount of Zn contents % all have a negative impact upon the tensile strength of the fabric. The decrease in tensile strength after the flame retardant application is due to the ester crosslinking of BTCA crosslinker present in the recipe with cellulose and acid degradation of cellulose due to BTCA[85], [265], [266]. Yang and Wei also reported that BTCA crosslinker reduces the strength of the cotton fabric due to acid-catalyzed depolymenzation[267]. In another study Sadr and Montazer synthesized TiO_2 NPs on to the cotton fabric by sonochemical process and reported 3% loss in the fabric strength due to the effect of ultrasonic waves upon cellulose chains[34]. In one more research work Perincek *et al.* applied the ultrasonic method for cotton finishing and observed a little decrease in breaking strength of the fabric[268]. Parsad *et al.* investigated that ZnO NPs coating on to the cotton fabric increase the fabric friction and hence decrease the tensile strength[269]. Tania and Ali concluded that with increased amount of ZnO NPs deposition on to the cotton fabric resulted in decreased tensile strength[270]. The results are further in accordance with Attia *et al.* they reported a decrease in tensile strength of cotton/polyester blended fabric after ZnO NPs treatment[271].

Equations (39) and (40) show the regression model used to determine tensile strength warp wise and weft wise respectively. According to the model summary, for warp wise tensile strength the fitted model can explain 82.42% of the total variances based on its R-squared value. Furthermore, the model summary for warp wise tensile strength indicates the model's significance with a p-value of 0.00 and an F-value of 135.15. According to the model summary, for weft wise tensile strength the fitted model can explain 77.27% of the total

variances based on its R-squared value. The model summary for weft wise tensile strength indicates the model's significance with a p-value of 0.00 and an F-value of 98.03.

Table 24. Experimental results for tensile strength.

Sample	Zinc acetate (M)	NaOH (M)	Sonication time (minutes)	MDPA (g/L)	Tensile strength (N)			
					Warp wise	Std. dev.	Weft wise	Std. dev.
Untreated	-	-	-	-	323.30	3.62	247.83	2.39
1	0.05	0.1	30	300	271.35	4.22	207.44	2.40
2	0.05	0.1	60	300	259.54	3.83	201.98	2.86
3	0.05	0.1	90	300	248.66	4.04	197.70	2.33
4	0.05	0.1	120	300	240.40	2.11	193.31	3.67
5	0.05	0.2	30	300	267.97	3.15	206.36	3.07
6	0.05	0.2	60	300	254.64	4.44	199.96	3.94
7	0.05	0.2	90	300	246.13	3.41	195.28	2.52
8	0.05	0.2	120	300	239.97	3.77	192.64	2.76
9	0.05	0.3	30	300	266.19	3.57	204.66	3.72
10	0.05	0.3	60	300	252.47	2.28	199.30	3.76
11	0.05	0.3	90	300	244.02	5.51	192.29	3.17
12	0.05	0.3	120	300	238.44	3.55	191.07	2.88
13	0.1	0.1	30	300	264.99	3.90	203.97	3.45
14	0.1	0.1	60	300	250.30	3.33	197.58	2.57
15	0.1	0.1	90	300	241.22	2.19	190.93	2.03
16	0.1	0.1	120	300	236.46	3.87	190.35	2.01
17	0.1	0.2	30	300	258.49	4.68	199.78	3.29
18	0.1	0.2	60	300	244.62	2.94	194.38	2.03
19	0.1	0.2	90	300	237.81	3.25	186.51	2.41
20	0.1	0.2	120	300	233.11	2.84	185.33	2.02
21	0.1	0.3	30	300	254.79	3.41	194.84	2.19
22	0.1	0.3	60	300	241.85	3.78	190.91	3.23
23	0.1	0.3	90	300	234.43	3.09	183.40	2.61
24	0.1	0.3	120	300	231.64	3.41	182.06	2.63
25	0.15	0.1	30	300	263.86	4.50	202.07	3.25
26	0.15	0.1	60	300	247.40	2.39	196.52	2.26
27	0.15	0.1	90	300	240.50	3.18	190.48	2.52
28	0.15	0.1	120	300	234.21	3.27	189.90	2.05
29	0.15	0.2	30	300	255.16	3.57	198.35	2.42
30	0.15	0.2	60	300	242.40	4.41	193.94	3.05
31	0.15	0.2	90	300	235.99	4.78	185.70	2.39
32	0.15	0.2	120	300	232.64	3.16	184.88	2.19
33	0.15	0.3	30	300	256.32	3.22	196.78	2.66
34	0.15	0.3	60	300	244.34	3.32	193.57	2.78
35	0.15	0.3	90	300	239.53	2.87	185.53	2.14
36	0.15	0.3	120	300	235.45	3.47	184.68	1.96
A	0.1	0.3	90 (magnetic stirring)	300	278.58	3.49	213.34	3.24
B	-	-	-	300	284.78	4.18	216.12	3.68

Tensile strength (N) (warp wise) = 290.90 − 128.30 zinc acetate (M) − 52.60 NaOH (M) − 0.3939 sonication time (minutes) + 71.00 zinc acetate (M) × NaOH (M) + 0.421 zinc acetate (M) × sonication time (minutes) + 0.295 NaOH (M) × sonication time (minutes) (39)

Model summary for tensile strength warp wise

S = 4.997 R-squared = 82.42% R-squared (adj) = 81.81% R-squared (pred) = 80.99% F-value = 135.15 p-value = 0.000

Tensile strength (N) (weft wise) = 216.62-57.0 zinc acetate (M) − 19.6 NaOH (M) − 0.1610 sonication time (minutes) − 66.5 zinc acetate (M) × NaOH (M) + 0.053 zinc acetate (M) × sonication time (minutes) + 0.0034 NaOH (M) × sonication time (minutes) (40)

Model summary for tensile strength weft wise

S = 3.452 R-squared = 77.27% R-squared (adj) =76.48% R-squared (pred) = 75.14% F-value = 98.03 p-value = 0.000

The analysis of variance subjected to data regarding the tensile strength warp wise and weft wise under the effect of zinc acetate (M), NaOH (M), and sonication time (minutes) are presented in Tables 25 and 26 respectively, p-values presented in Tables 25 and 26 revealed highly significant effects for all the variables and interaction of zinc acetate (M) with NaOH (M) upon warp wise and weft wise tensile strength. While all other interactions are non-significant, having a p-value higher than 0.05.

Table 25. Analysis of variance for warp wise tensile strength.

Source of Variation	Sum of Squares	df	Mean Square	F Value	p Value
A-Zinc acetate (M)	2783.8	2	1391.90	85.97	<.001
B-NaOH (M)	735.8	2	367.91	22.72	<.001
C-Sonication time (minutes)	18195.1	3	6065.02	374.59	<.001
A×B	165.5	4	41.37	2.56	0.041
A×C	161.0	6	26.83	1.66	0.136
B×C	134.2	6	22.37	1.38	0.226
A×B×C	69.3	12	5.27	0.33	0.984
Error	2331.5	144	16.19		
Total	24570.1	179			

Table 26. Analysis of variance for warp wise tensile strength.

Source of Variation	Sum of Squares	df	Mean Square	F Value	p Value
A-Zinc acetate (M)	1799.36	2	899.68	116.61	<.001
B-NaOH (M)	830.92	2	415.46	53.85	<.001
C-Sonication time (minutes)	5123.91	3	1707.97	221.37	<.001
A×B	129.88	4	32.47	2.56	0.003
A×C	31.04	6	5.17	0.67	0.674
B×C	20.66	6	3.44	0.45	0.847
A×B×C	25.25	12	2.10	0.27	0.993
Error	1111.05	144	7.72		
Total	9072.07	179			

The main effects plots for fitted mean values of tensile strength warp wise and weft wise under different experimental variables are shown in Figures 53 and 54. In the case of zinc

acetate (M) the minimum mean value of warp wise tensile strength is 244.145 N and mean value of weft wise tensile strength is 191.724 N, both are obtained at 0.1 molar concentration of zinc acetate. While for the NaOH (M) the minimum mean value of warp wise tensile strength is 245.126 N and mean value of weft wise tensile strength is 191.645 N, both are obtained at 0.3 molar concentration of NaOH. The plots show that the minimum mean value of warp wise tensile for sonication time (minutes) is 235.817 N and weft wise tensile is 188.318 N, which are obtained at 120 minutes of sonication time.

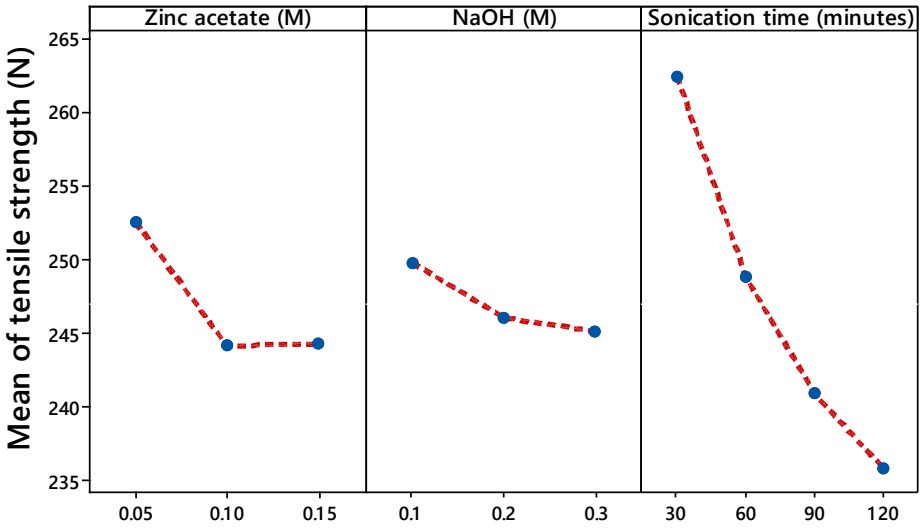

Figure 53. Main effects plots for warp wise tensile strength.

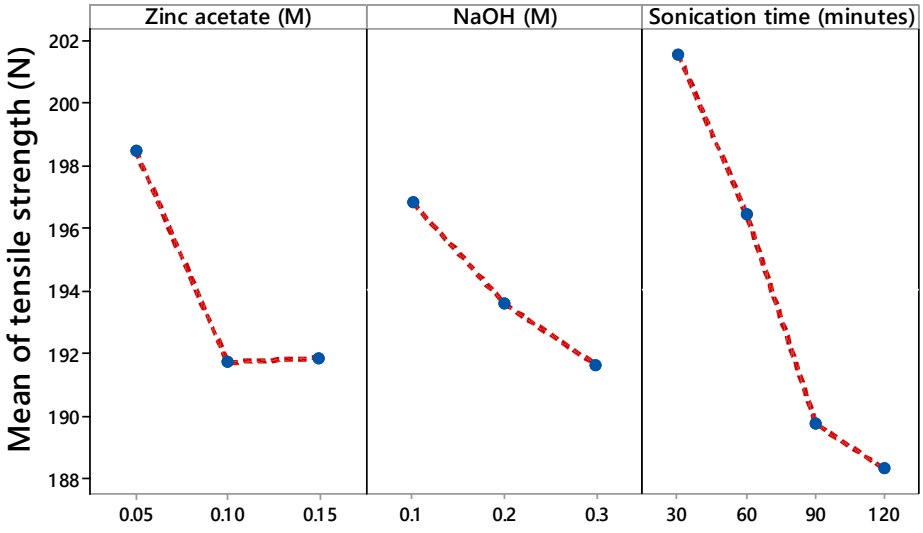

Figure 54. Main effects plots for weft wise tensile strength.

5.15. Wash durability

Tables 27, 28, and 29 show the wash durability results after 5, 10 and 20 wash cycles for samples A, B and 23. The results show that there is a gradual decrease in Zn contents %, P contents %, flame retardancy, and functional properties of the sample after each wash cycle. However, in the case of ultrasonically optimized sample 23, there is enough Zn and P contents % even after 20 wash cycles. Although char length increased to 52 mm and LOI decreased to 29.61 after 20 wash cycles for sample 23, however, these values are excellent for flame retardancy. Sample 23 retained enough amounts of Zn contents % after 20 wash cycles and showed 100 % bacterial reduction for both S.aureus and E.coli bacteria. Sample 23 showed an excellent UPF value of 123.16 and color intensity 244.73 even after 20 wash cycles.

Table 27. Results of contents analysis after washing.

Contents (%)				
After 5 wash cycles				
Sample	**Zn contents (%)**	**Std. dev.**	**P contents (%)**	**Std. dev.**
Sample A	5.76	0.13	3.30	0.05
Sample B	-	-	3.48	0.06
Sample 23	11.38	0.08	3.11	0.05
After 10 wash cycles				
Sample	**Zn contents (%)**	**Std. dev.**	**P contents (%)**	**Std. dev.**
Sample A	4.74	0.17	3.13	0.04
Sample B	-	-	3.32	0.06
Sample 23	10.61	0.06	2.99	0.04
After 20 wash cycles				
Sample	**(%)**	**Std. dev.**	**(%)**	**Std. dev.**
Sample A	3.97	0.10	3.04	0.07
Sample B	-	-	3.24	0.05
Sample 23	10.17	0.12	2.93	0.04

Table 28. Results of flammability test and LOI after washing

Flammability test and LOI								
After 5 wash cycles								
Sample	**After flame time (s)**	**Std. dev.**	**After glow time (s)**	**Std. dev.**	**Char length (mm)**	**Std. dev.**	**LOI**	**Std. dev.**
Sample A	5.94	0.91	3.15	0.68	89	4.02	26.70	0.21
Sample B	10.32	0.37	5.47	0.28	134	5.24	22.11	0.18
Sample 23	0	0	0	0	46	0.94	30.32	0.13
After 10 wash cycles								
Sample	**After flame time (s)**	**Std. dev.**	**After glow time (s)**	**Std. dev.**	**Char length (mm)**	**Std. dev.**	**LOI**	**Std. dev.**
Sample A	7.03	1.01	3.52	0.74	93	4.36	24.91	0.32
Sample B	10.72	0.41	5.89	0.32	145	5.57	21.60	0.24
Sample 23	0	0	0	0	49	1.03	29.83	0.17
After 20 wash cycles								
Sample	**After flame time (s)**	**Std. dev.**	**After glow time (s)**	**Std. dev.**	**Char length (mm)**	**Std. dev.**	**LOI**	**Std. dev.**
Sample A	7.82	1.12	4.23	0.88	96	5.24	23.52	0.27
Sample B	11.29	0.69	6.08	0.51	149	5.93	20.41	0.23
Sample 23	0	0	0	0	52	1.36	29.61	0.11

Table 29. Results of antibacterial activity, UV protection, and self-cleaning after washing.

Bacterial reduction (%), UPF and color intensity								
After 5 wash cycles								
Sample	**S. aureus reduction %**	**Std. dev.**	**E.coli reduction %**	**Std. dev.**	**UPF**	**Std. dev.**	**Color intensity**	**Std. dev.**
Sample A	72.43	6.38	70.28	4.81	41.37	5.29	209.53	6.42
Sample B	-	-	-	-	11.81	1.08	-	-
Sample 23	100	0	100	0	132.92	4.36	247.08	2.24
After 10 wash cycles								
Sample	**S. aureus reduction %**	**Std. dev.**	**E.coli reduction %**	**Std. dev.**	**UPF**	**Std. dev.**	**Color intensity**	**Std. dev.**
Sample A	63.23	3.69	60.96	4.16	34.87	3.35	190.24	5.12
Sample B	-	-	-	-	11.09	1.21	-	-
Sample 23	100	0	100	0	125.53	3.86	245.19	3.43
After 20 wash cycles								
Sample	**S. aureus reduction %**	**Std. dev.**	**E.coli reduction %**	**Std. dev.**	**UPF**	**Std. dev.**	**Color intensity**	**Std. dev.**
Sample A	54.47	4.65	50.52	3.73	30.76	2.57	187.39	4.71
Sample B	-	-	-	-	10.61	0.94	-	-
Sample 23	100	0	100	0	123.16	3.47	244.73	2.86

CHAPTER 6

Summary and Future Prospective

In this research study, cotton fabric was modified by the ultrasonically assisted in-situ synthesis of ZnO NPs and MDPA application by the conventional pad dry cure method. BTCA was used as a crosslinker for the crosslinking of MDPA with cellulose, so halogen and formaldehyde free ecological flame retardant treatment was done. The study revealed that MDPA greatly affects the flame retardant performance of the cotton fabric, which is further increases by the deposition of ZnO NPs. For the deposition of ZnO NPs onto the cotton fabric, sonication time and concentrations of the chemical reagents were varied. The optimized conditions at 0.1 M zinc acetate, 0.3 M of NaOH, and 90 minutes of sonication time produced 13.14 % Zn contents. The pure hexagonal wurtzite crystalline structure of ZnO NPs was confirmed by XRD. The grafting and presence of ZnO NPs was confirmed by ICP AES, FTIR and SEM. While the presence of phosphorous contents was confirmed by ICP AES, and the grafting of phosphorous and amide group onto the cellulose structure was confirmed by FTIR. This research work disclosed that the concentration of ZnO NPs deposited onto the fabric has a direct correlation with flame retardancy and other functional properties. The optimized sample 23 showed excellent performance for flame retardancy before and after washing. A 100 % bacterial reduction for both S. aureus and E. coli bacteria was observed even after 20 wash cycles. The sample with the highest concentration of ZnO NPs showed UPF value of 143.76 initially and 123.16 after 20 wash cycles. Developed samples showed good photocatalytic self-cleaning before and after washing. The results obtained in this research work proved that ultrasonically developed fabric samples showed better flame retardancy and functional properties as compared to fabric sample developed by conventional magenetic stirring method. SEM analysis showed that the ultrasonic method deposits ZnO NPs onto the cotton fabric more uniformly and homogeneously as compared to the conventional magnetic stirring method. Moreover, statistical analysis showed the significant effects of all the process parameters upon the flame retardancy and functioinal properties of the developed samples. This research study revealed that MDPA application increased the bending rigidity of the fabric which was further increased by the deposition of

ZnO NPs. On the other hand MDPA application resulted in a decrease in air permeability which further decrease after ZnO NPs deposition. In the case of tensile strength the developed samples showed less tensile strength as compared to the untreated sample, which was due to the ester crosslinking of BTCA crosslinker, the effect of ultrasonic waves upon cellulose chains, and the increase in the friction between the fabric structure due to the presence of ZnO NPs. However results showed that the air permeability and tensile strength of the developed samples are in an acceptable range.

Flame retardant multifunctional textiles at hand these days are the outcome of only chemical treatments; at present, the technology that has been developed for producing flame retardant textiles based on nanomaterial is still at the lab scale. The uses of nanoparticles impart some other desired properties. In future research should be center of attention on the application of nanoparticles as stuffing material, as their nano sizes let them penetrate into the interiors of polymer chains, hence imparting multifunctional properties. Along with ZnO NPs in the future other metal oxides NPs (e.g. TiO_2, CuO, MgO etc.) and the nano clay should also be used in combination with MDPA to obtain the best FR/NPs system.

REFERENCES

[1] S. Hall and B. Evarts, “Fire Loss in the United States During 2021 (NFPA ®) Key Findings,” no. September, 2022.

[2] J. H. Troitzsch, “Fires, statistics, ignition sources, and passive fire protection measures,” *J. Fire Sci.*, vol. 34, no. 3, pp. 171–198, 2016, doi: 10.1177/0734904116636642.

[3] A. N. Zhang *et al.*, “Construction of durable eco-friendly biomass-based flame-retardant coating for cotton fabrics,” *Chem. Eng. J.*, vol. 410, no. January, p. 128361, 2021, doi: 10.1016/j.cej.2020.128361.

[4] V. Babrauskas, D. Lucas, D. Eisenberg, V. Singla, M. Dedeo, and A. Blum, “Flame retardants in building insulation: a case for re-evaluating building codes,” *Build. Res. Inf.*, vol. 40, no. 6, pp. 738–755, 2012.

[5] S. A. H. Ravandi and M. Valizadeh, “Properties of fibers and fabrics that contribute to human comfort,” in *Improving comfort in clothing*, Elsevier, 2011, pp. 61–78.

[6] J. Yip and W.-Y. Chan, “Textile fibers and fabrics,” in *Latest Material and Technological Developments for Activewear*, Elsevier, 2020, pp. 47–72.

[7] H. A. Cheema, A. El-Shafei, and P. J. Hauser, “Conferring flame retardancy on cotton using novel halogen-free flame retardant bifunctional monomers: Synthesis, characterizations and applications,” *Carbohydr. Polym.*, vol. 92, no. 1, pp. 885–893, 2013, doi: 10.1016/j.carbpol.2012.09.081.

[8] T. Mayer-Gall *et al.*, “A green water-soluble cyclophosphazene as a flame retardant finish for textiles,” *Molecules*, vol. 24, no. 17, pp. 26–28, 2019, doi: 10.3390/molecules24173100.

[9] M. L. Rahman Liman, M. T. Islam, M. R. Repon, M. M. Hossain, and P. Sarker, “Comparative dyeing behavior and UV protective characteristics of cotton fabric treated with polyphenols enriched banana and watermelon biowaste,” *Sustain. Chem. Pharm.*, vol. 21, no. March, p. 100417, 2021, doi: 10.1016/j.scp.2021.100417.

[10] Z. Fan, L. Di, X. Zhang, and H. Wang, "A surface dielectric barrier discharge plasma for preparing cotton-fabric-supported silver nanoparticles," *Nanomaterials*, vol. 9, no. 7, 2019, doi: 10.3390/nano9070961.

[11] K. K. Zhang *et al.*, "Improve the flame retardancy of cellulose fibers by grafting zinc ion," *Carbohydr. Polym.*, vol. 136, pp. 121–127, 2016, doi: 10.1016/j.carbpol.2015.09.026.

[12] S. Saleemi *et al.*, "Surface functionalization of cotton and pc fabrics using SiO2 and ZnO nanoparticles for durable flame retardant properties," *Coatings*, vol. 10, no. 2, 2020, doi: 10.3390/coatings10020124.

[13] S. Yang, Y. Hu, and Q. Zhang, "Synthesis of a phosphorus–nitrogen-containing flame retardant and its application in epoxy resin," *High Perform. Polym.*, vol. 31, no. 2, pp. 186–196, 2019, doi: 10.1177/0954008318756496.

[14] T. N. Rao, T. M. Naidu, M. S. Kim, B. Parvatamma, Y. Prashanthi, and B. H. Koo, "Influence of zinc oxide nanoparticles and char forming agent polymer on flame retardancy of intumescent flame retardant coatings," *Nanomaterials*, vol. 10, no. 1, 2020, doi: 10.3390/nano10010042.

[15] T. M. Nguyen, S. Chang, B. Condon, R. Slopek, E. Graves, and M. Yoshioka-Tarver, "Structural effect of phosphoramidate derivatives on the thermal and flame retardant behaviors of treated cotton cellulose," *Ind. Eng. Chem. Res.*, vol. 52, no. 13, pp. 4715–4724, 2013, doi: 10.1021/ie400180f.

[16] J. Li, W. Jiang, and M. Liu, "Durable phosphorus/nitrogen flame retardant for cotton fabric," *Cellulose*, vol. 29, no. 8, pp. 4725–4751, 2022, doi: 10.1007/s10570-022-04558-x.

[17] Y. Chen, L. Xu, X. Wu, and B. Xu, "The influence of nano ZnO coated by phosphazene/triazine bi-group molecular on the flame retardant property and mechanical property of intumescent flame retardant poly (lactic acid) composites," *Thermochim. Acta*, vol. 679, no. 11, 2019, doi: 10.1016/j.tca.2019.178336.

[18] N. T. Huong, V. T. H. Khanh, and N. P. D. Linh, "Optimizing content of Pyrovatex CP New and Knittex FFRC in flame retardant treatment for cotton fabric," *Ind. Textila*, vol. 72, no. 3, pp. 315–323, 2021, doi: 10.35530/IT.072.03.1648.

[19] S. C. Chang, B. Condon, J. Smith, and S. Nam, "Flame Resistant Cotton Fabric Containing Casein and Inorganic Materials Using an Environmentally-Friendly Microwave Assisted Technique," *Fibers Polym.*, vol. 21, no. 10, pp. 2246–2252, 2020, doi: 10.1007/s12221-020-9965-x.

[20] I. Yaqoob, Asim ALI Parveen, Tabassum Umar, Khalid Nasir, Mohammad Nasir, "Role of Nanomaterials in the Treatment of waste water," *Water 2020,* vol. 12, p. 495, 2020.

[21] A. A. Yaqoob *et al.*, "Recent Advances in Metal Decorated Nanomaterials and Their Various Biological Applications: A Review," *Front. Chem.*, vol. 8, no. May, pp. 1–23, 2020, doi: 10.3389/fchem.2020.00341.

[22] A. R. Galaly and N. Dawood, "Non-Thermal Plasma Treatment Coupled with a Photocatalyst for Antimicrobial Performance of Ihram Cotton Fabric," *Nanomaterials*, vol. 12, no. 6, pp. 1–14, 2022, doi: 10.3390/nano12061004.

[23] A. Javed *et al.*, "One step in-situ synthesis of zinc oxide nanoparticles for multifunctional cotton fabrics," *Materials (Basel).*, vol. 14, no. 14, p. 3956, 2021.

[24] A. V. Abramova *et al.*, "Strong antibacterial properties of cotton fabrics coated with ceria nanoparticles under high-power ultrasound," *Nanomaterials*, vol. 11, no. 10, 2021, doi: 10.3390/nano11102704.

[25] M. Fernandes *et al.*, "Polysaccharides and Metal Nanoparticles for Functional Textiles: A Review," *Nanomaterials*, vol. 12, no. 6, p. 1006, 2022, doi: 10.3390/nano12061006.

[26] M. A. Tănase *et al.*, "Facile in situ synthesis of zno flower-like hierarchical nanostructures by the microwave irradiation method for multifunctional textile coatings," *Nanomaterials*, vol. 11, no. 10, 2021, doi: 10.3390/nano11102574.

[27] H. T. P. Nguyen *et al.*, "Characterization and photocatalytic activity of new

photocatalysts based on Ag, F-modified ZnO nanoparticles prepared by thermal shock method," *Arab. J. Chem.*, vol. 13, no. 1, pp. 1837–1847, 2020, doi: 10.1016/j.arabjc.2018.01.018.

[28] P. J. P. Espitia, N. de F. F. Soares, J. S. dos R. Coimbra, N. J. de Andrade, R. S. Cruz, and E. A. A. Medeiros, "Zinc Oxide Nanoparticles: Synthesis, Antimicrobial Activity and Food Packaging Applications," *Food Bioprocess Technol.*, vol. 5, no. 5, pp. 1447–1464, 2012, doi: 10.1007/s11947-012-0797-6.

[29] A. Moezzi, A. M. McDonagh, and M. B. Cortie, "Zinc oxide particles: Synthesis, properties and applications," *Chem. Eng. J.*, vol. 185–186, pp. 1–22, 2012, doi: 10.1016/j.cej.2012.01.076.

[30] R. D. Kale, M. Soni, and T. Potdar, "A flame retardant, antimicrobial and UV protective polyester fabric by solvent crazing route," *J. Polym. Res.*, vol. 26, no. 8, 2019, doi: 10.1007/s10965-019-1849-7.

[31] M. M. A. El-Hady, A. Farouk, and S. Sharaf, "Flame retardancy and UV protection of cotton based fabrics using nano ZnO and polycarboxylic acids," *Carbohydr. Polym.*, vol. 92, no. 1, pp. 400–406, 2013, doi: 10.1016/j.carbpol.2012.08.085.

[32] E. Magovac, B. Vončina, I. Jordanov, J. C. Grunlan, and S. Bischof, "Layer-by-Layer Deposition: A Promising Environmentally Benign Flame-Retardant Treatment for Cotton, Polyester, Polyamide and Blended Textiles," *Materials (Basel).*, vol. 15, no. 2, 2022, doi: 10.3390/ma15020432.

[33] A. Javed, M. Azeem, J. Wiener, M. Thukkaram, J. Saskova, and T. Mansoor, "Ultrasonically Assisted In Situ Deposition of ZnO Nano Particles on Cotton Fabrics for Multifunctional Textiles," *Fibers Polym.*, 2021, doi: 10.1007/s12221-021-0051-9.

[34] F. Akhavan Sadr and M. Montazer, "In situ sonosynthesis of nano TiO2 on cotton fabric," *Ultrason. Sonochem.*, vol. 21, no. 2, pp. 681–691, 2014, doi: 10.1016/j.ultsonch.2013.09.018.

[35] C. F. Putri and N. Tjahjono, "Counseling and application of personal protective

equipment to reduce work accidents in welding workshops," *Abdimas J. Pengabdi. Masy. Univ. Merdeka Malang*, vol. 7, no. 3, pp. 460–470, 2022, doi: 10.26905/abdimas.v7i3.7016.

[36] H. Nakashima, A. Utsunomiya, J. Takahashi, N. Fujii, and T. Okuno, "Hazard of ultraviolet radiation emitted in gas metal arc welding of mild steel," *J. Occup. Health*, vol. 58, no. 5, pp. 452–459, 2016, doi: 10.1539/joh.16-0065-OA.

[37] Y. Qin, "A brief description of textile fibers," *Med. Text. Mater.*, vol. 3, pp. 23–42, 2016.

[38] J. Egan and S. Salmon, "Strategies and progress in synthetic textile fiber biodegradability," *SN Appl. Sci.*, vol. 4, pp. 1–36, 2022.

[39] J. Hu, M. A. Jahid, N. H. Kumar, and V. Harun, *Fundamentals of the fibrous materials*, vol. 1–2, no. July. 2020.

[40] A. El Nemr, *From natural to synthetic fibers*, no. January 2012. 2012.

[41] R. Sinclair, *Understanding Textile Fibres and Their Properties: What is a Textile Fibre?* Elsevier Ltd, 2015.

[42] I. Elfaleh *et al.*, "A comprehensive review of natural fibers and their composites: An eco-friendly alternative to conventional materials," *Results Eng.*, vol. 19, no. June, p. 101271, 2023, doi: 10.1016/j.rineng.2023.101271.

[43] A. Seguin and J. Crassous, "Twist-Controlled Force Amplification and Spinning Tension Transition in Yarn," *Phys. Rev. Lett.*, vol. 128, no. 7, 2022, doi: 10.1103/PhysRevLett.128.078002.

[44] S. Islam, S. Chowdhury, and S. Akter, "The Experiential Analysis of Woven Fabric for Reproduction," *J. Text. Sci. Technol.*, vol. 04, no. 01, pp. 18–48, 2018, doi: 10.4236/jtst.2018.41002.

[45] J.-L. Wertz, O. Bédué, and J. P. Mercier, *Cellulose science and technology*. EPFL press, 2010.

[46] T. Heinze, "Cellulose: structure and properties," *Cellul. Chem. Prop. fibers, nanocelluloses Adv. Mater.*, pp. 1–52, 2016.

[47] T. Heinze, O. A. El Seoud, and A. Koschella, *Cellulose derivatives: synthesis, structure, and properties*. Springer, 2018.

[48] P. K. Gupta *et al.*, "An update on overview of cellulose, its structure and applications," *Cellulose*, vol. 201, no. 9, p. 84727, 2019.

[49] N. B. Erdal and M. Hakkarainen, "Degradation of Cellulose Derivatives in Laboratory, Man-Made, and Natural Environments," *Biomacromolecules*, vol. 23, no. 7, pp. 2713–2729, 2022, doi: 10.1021/acs.biomac.2c00336.

[50] V. V. Revin *et al.*, "Bacterial Cellulose-Based Polymer Nanocomposites: A Review," *Polymers (Basel).*, vol. 14, no. 21, pp. 1–35, 2022, doi: 10.3390/polym14214670.

[51] C. Felgueiras, N. G. Azoia, C. Gonçalves, M. Gama, and F. Dourado, "Trends on the Cellulose-Based Textiles: Raw Materials and Technologies," *Front. Bioeng. Biotechnol.*, vol. 9, no. March, pp. 1–20, 2021, doi: 10.3389/fbioe.2021.608826.

[52] Y. Habibi, L. A. Lucia, and O. J. Rojas, "Cellulose nanocrystals: Chemistry, self-assembly, and applications," *Chem. Rev.*, vol. 110, no. 6, pp. 3479–3500, 2010, doi: 10.1021/cr900339w.

[53] A. S. Gross, A. T. Bell, and J.-W. Chu, "Preferential interactions between lithium chloride and glucan chains in N, N-dimethylacetamide drive cellulose dissolution," *J. Phys. Chem. B*, vol. 117, no. 12, pp. 3280–3286, 2013.

[54] H. Seddiqi *et al.*, *Cellulose and its derivatives: towards biomedical applications*, vol. 28, no. 4. Springer Netherlands, 2021.

[55] E. Rudnik, "Compostable polymer materials — definitions, structures and methods of preparation," *Compost. Polym. Mater.*, no. 2008, pp. 10–36, 2008, doi: 10.1016/b978-008045371-2.50004-4.

[56] L. Liu, M. J. Levin, F. Klimscha, and D. Rosenberg, "The earliest cotton fibers and

Pan-regional contacts in the Near East," *Front. Plant Sci.*, vol. 13, no. December, pp. 1–15, 2022, doi: 10.3389/fpls.2022.1045554.

[57] J. A. Lee and D. D. Fang, "Cotton as a world crop: origin, history, and current status," *Cotton*, vol. 57, pp. 1–23, 2015.

[58] S. Radoor, J. Karayil, J. M. Shivanna, A. Jayakumar, J. Parameswaranpillai, and S. Siengchin, "Cotton fibers, their composites and applications," in *Plant Fibers, their Composites, and Applications*, Elsevier, 2022, pp. 379–390.

[59] R. Maiti, C. A. Kumari, A. K. S. Huda, D. Mandal, and S. Begum, *Advances in Cotton Science: Botany, Production, and Crop Improvement*. CRC Press, 2020.

[60] U. Cotton *et al.*, "Effects of Environment and Sowing Time on Growth[J]," *Plants*, vol. 9, no. 1209, pp. 1–21, 2020.

[61] R. Oswaldo, V. Torres, and B. Oviedo, "Genus Gossypium : history , economy , genetic origin , computational genomics and Ecuador as a reservoir of long staple cotton genetic resources," no. July, 2023, doi: 10.14704/nq.2022.20.8.NQ44674.

[62] S. Shakir *et al.*, "Non-cultivated cotton species (Gossypium spp.) act as a reservoir for cotton leaf curl begomoviruses and associated satellites," *Plants*, vol. 8, no. 5, 2019, doi: 10.3390/plants8050127.

[63] V. Dabrowski *et al.*, "A tale of new crops in the arid Arabian Peninsula oasis from antiquity to the early Islamic period," *Veg. Hist. Archaeobot.*, no. 0123456789, 2024, doi: 10.1007/s00334-023-00976-4.

[64] C. Yu, "Natural textile fibres: vegetable fibres," in *Textiles and fashion*, Elsevier, 2015, pp. 29–56.

[65] M. Dochia, C. Sirghie, R. M. Kozłowski, and Z. Roskwitalski, "Cotton fibres," in *Handbook of natural fibres*, Elsevier, 2012, pp. 11–23.

[66] H. Wang, M. Q. Siddiqui, and H. Memon, "Physical Structure, properties and quality of cotton," *Cott. Sci. Process. Technol. Gene, ginning, garment green Recycl.*, pp. 79–

97, 2020.

[67] P. Kumar, C. S. Ram, J. P. Srivastava, A. K. Behura, and A. Kumar, "Synthesis of Cotton Fiber and Its Structure," *Nat. Synth. Fiber Reinf. Compos. Synth. Prop. Appl.*, pp. 17–36, 2021, doi: 10.1002/9783527832996.ch2.

[68] V. K. Thakur, *Cellulose-based graft copolymers: structure and chemistry*. CRC Press, 2015.

[69] K. C. Schuster, F. Suchomel, J. Männer, M. Abu-Rous, and H. Firgo, "Functional and Comfort Properties of Textiles from TENCEL® Fibres Resulting from the Fibres' Water-Absorbing Nanostructure: A Review," in *Macromolecular Symposia*, 2006, vol. 244, no. 1, pp. 149–165.

[70] R. R. Mather, S. Rana, and R. H. Wardman, *The chemistry of textile fibres*. Royal Society of chemistry, 2023.

[71] F. Parvin, S. Islam, Z. Urmy, and S. Ahmed, "a Study on the Textile Materials Applied in Human Medical Treatment," *Eur. J. Physiother. Rehabil. Stud.*, vol. 1, p. 57, 2020, doi: 10.5281/zenodo.3779236.

[72] M. A. Imran, M. Q. Khan, A. Salam, and A. Ahmad, "Cotton in nonwoven products," *Cott. Sci. Process. Technol. Gene, Ginning, Garment Green Recycl.*, pp. 305–332, 2020.

[73] S. F. Grgac, A. Tarbuk, T. Dekanic, W. Sujka, and Z. Draczynski, "The chitosan implementation into cotton and polyester/cotton blend fabrics," *Materials (Basel).*, vol. 13, no. 7, pp. 1–19, 2020, doi: 10.3390/ma13071616.

[74] L. Li and Q. Li, "Combined scouring and bleaching of cotton/linen blends by a near-neutral activated peroxide system," *Fibres Text. East. Eur.*, vol. 28, no. 6–144, pp. 104–109, 2020, doi: 10.5604/01.3001.0014.3805.

[75] Z. Ma, R. Xu, W. Wang, and D. Yu, "A wearable, anti-bacterial strain sensor prepared by silver plated cotton/spandex blended fabric for human motion monitoring," *Colloids Surfaces A Physicochem. Eng. Asp.*, vol. 582, no. September, p. 123918, 2019, doi:

10.1016/j.colsurfa.2019.123918.

[76] F. Naeem, F. Asim, and M. Tufail, "Performance Evaluation of Anti Pilling and Easy-Care Finished Rayon and Rayon/Cotton Satin Fabric," *J. Nat. Fibers*, vol. 19, no. 3, pp. 1–15, 2020, doi: 10.1080/15440478.2020.1787912.

[77] F. Hosseinali and J. A. Thomasson, "Multiscale frictional properties of cotton fibers: A review," *Fibers*, vol. 6, no. 3, 2018, doi: 10.3390/fib6030049.

[78] M. Tausif, A. Jabbar, M. S. Naeem, A. Basit, F. Ahmad, and T. Cassidy, "Cotton in the new millennium: advances, economics, perceptions and problems," *Text. Prog.*, vol. 50, no. 1, pp. 1–66, 2018, doi: 10.1080/00405167.2018.1528095.

[79] L. Xie *et al.*, "Flammability and combustion behavior of the polyester/cotton blended fabric via an independent flame-retardation for two components strategy," *Polym. Degrad. Stab.*, vol. 220, no. December 2023, p. 110638, 2024, doi: 10.1016/j.polymdegradstab.2023.110638.

[80] P. Chauhan, A. Kumar, and B. Bhushan, "Self-cleaning, stain-resistant and anti-bacterial superhydrophobic cotton fabric prepared by simple immersion technique," *J. Colloid Interface Sci.*, vol. 535, pp. 66–74, 2019, doi: 10.1016/j.jcis.2018.09.087.

[81] M. K. Imrith, S. Rosunee, and R. Unmar, "Structural modelling of 100% cotton single jersey fabrics for optimum UV protection," *Res. J. Text. Appar.*, vol. 27, no. 3, pp. 343–365, 2023, doi: 10.1108/RJTA-02-2022-0016.

[82] S. K. Sela, A. K. M. Nayab-Ul-Hossain, M. S. I. Rakib, and M. K. H. Niloy, "Improving the functionality of raw cotton: simultaneous strength increases and additional multi-functional properties," *Heliyon*, vol. 6, no. 8, 2020, doi: 10.1016/j.heliyon.2020.e04607.

[83] S. U. Islam and B. S. Butola, *Advances in Functional and Protective Textiles*. Woodhead Publishing, 2020.

[84] T. M. Abou Elmaaty, H. Elsisi, G. Elsayad, H. Elhadad, and M. R. Plutino, "Recent Advances in Functionalization of Cotton Fabrics with Nanotechnology," *Polymers*

(Basel)., vol. 14, no. 20, pp. 1–17, 2022, doi: 10.3390/polym14204273.

[85] J. Wa1. Wang, J.; Fang, K.; Liu, X.; Zhang, S.; Qiao, X.; Liu, D. A Review on the Status of Formaldehyde-Free Anti-Wrinkle Cross-Linking Agents for Cotton Fabrics: Mechanisms and Applications. Ind. Crops Prod. 2023, 200, , no. PB, p. 116831, 2023, doi: 10.1016/j.indcrop.2023.116831.

[86] W. Nie, J. Wu, J. Yang, and L. Hu, "Fabrication of sustainable hydrophobic cotton fabrics with fluorescence-emitting performance using novel 1, 8-naphthalimide functional molecules," *ACS Sustain. Chem. Eng.*, vol. 11, no. 9, pp. 3873–3881, 2023.

[87] V. Trovato *et al.*, "How to Address Flame-Retardant Technology on Cotton Fabrics by Using Functional Inorganic Sol–Gel Precursors and Nanofillers: Flammability Insights, Research Advances, and Sustainability Challenges," *Inorganics*, vol. 11, no. 7, 2023, doi: 10.3390/inorganics11070306.

[88] A. Mahmood, B. Tomkova, and J. Militky, *Incorporation of Cellulose ‐ Based Aerogels into Textile Structures*. 2024.

[89] M. Kert *et al.*, "Application of fragrance microcapsules onto cotton fabric after treatment with oxygen and nitrogen plasma," *Coatings*, vol. 11, no. 10, 2021, doi: 10.3390/coatings11101181.

[90] D. Song *et al.*, "Soluble and colorless polyimide coated cotton fabric with attractive multifunction: Warmth retention, breathable, antifouling, UV and acid resistance," *Chem. Eng. J.*, vol. 455, no. August 2022, p. 140755, 2023, doi: 10.1016/j.cej.2022.140755.

[91] S. Nasrin, S. Mandal, M. M. Islam, A. Petrova, R. J. Agnew, and L. M. Boorady, "Factors Affecting the Sweat-Drying Performance of Active Sportswear—A Review," *Textiles*, vol. 3, no. 3, pp. 319–338, 2023, doi: 10.3390/textiles3030022.

[92] E. Ahmed, D. Maamoun, M. S. Abdelrahman, T. M. Hassan, and T. A. Khattab, "Imparting cotton textiles glow-in-the-dark property along with other functional properties: photochromism, flame-retardant, water-repellency, and antimicrobial

activity," *Cellulose*, vol. 30, no. 6, pp. 4041–4055, 2023, doi: 10.1007/s10570-023-05125-8.

[93] B. Murugesan, A. Dessie Wolela, and R. V. Mahendragowda, "Investigation on the Flammability and Washing Durability of Trevira CS and Its Blends with Cotton, Modal, and Acrylic Fabrics," *J. Chem.*, vol. 2023, 2023, doi: 10.1155/2023/1619577.

[94] X. Ao, A. Vázquez-López, D. Mocerino, C. González, and D. Y. Wang, "Flame retardancy and fire mechanical properties for natural fiber/polymer composite: A review," *Compos. Part B Eng.*, vol. 268, no. October 2023, 2024, doi: 10.1016/j.compositesb.2023.111069.

[95] A. L. Mohamed and A. G. Hassabo, *Flame Retardant of Cellulosic Materials and Their Composites*, no. i. 2015.

[96] D. Price and A. R. Horrocks, "Polymer degradation and the matching of FR chemistry to degradation," *Fire Retard. Polym. Mater. Wilkie, CA, Morgan, AB, Eds*, pp. 15–43, 2009.

[97] A. Witkowski, A. A. Stec, and T. R. Hull, "Thermal decomposition of polymeric materials," *SFPE Handb. fire Prot. Eng.*, pp. 167–254, 2016.

[98] S. Ma and D. C. Webster, "Degradable thermosets based on labile bonds or linkages: A review," *Prog. Polym. Sci.*, vol. 76, pp. 65–110, 2018, doi: 10.1016/j.progpolymsci.2017.07.008.

[99] R. Thandavamoorthy, Y. Devarajan, and S. Thanappan, "Analysis of the characterization of NaOH-treated natural cellulose fibre extracted from banyan aerial roots," *Sci. Rep.*, vol. 13, no. 1, pp. 1–8, 2023, doi: 10.1038/s41598-023-39229-9.

[100] V. Mamleev, S. Bourbigot, and J. Yvon, "Kinetic analysis of the thermal decomposition of cellulose: The main step of mass loss," *J. Anal. Appl. Pyrolysis*, vol. 80, no. 1, pp. 151–165, 2007, doi: 10.1016/j.jaap.2007.01.013.

[101] A. G. W. Bradbury, Y. Sakai, and F. Shafizadeh, "A kinetic model for pyrolysis of cellulose," *J. Appl. Polym. Sci.*, vol. 23, no. 11, pp. 3271–3280, 1979, doi:

10.1002/app.1979.070231112.

[102] Q. Liu, S. Wang, K. Wang, X. Guo, Z. Luo, and K. Cen, "Mechanism of formation and consequent evolution of active cellulose during cellulose pyrolysis," *Acta Physico-Chimica Sin.*, vol. 24, no. 11, pp. 1957–1963, 2008.

[103] D. Price, A. R. Horrocks, M. Akalin, and A. A. Faroq, "Influence of flame retardants on the mechanism of pyrolysis of cotton (cellulose) fabrics in air," *J. Anal. Appl. Pyrolysis*, vol. 40–41, pp. 511–524, 1997, doi: 10.1016/S0165-2370(97)00043-0.

[104] F. Shafizadeh, "Introduction to pyrolysis of biomass," *J. Anal. Appl. Pyrolysis*, vol. 3, no. 4, pp. 283–305, 1982.

[105] M. J. Antal Jr, H. L. Friedman, and F. E. Rogers, "Kinetics of cellulose pyrolysis in nitrogen and steam," *Combust. Sci. Technol.*, vol. 21, no. 3–4, pp. 141–152, 1980.

[106] U.-J. Kim, S. H. Eom, and M. Wada, "Thermal decomposition of native cellulose: influence on crystallite size," *Polym. Degrad. Stab.*, vol. 95, no. 5, pp. 778–781, 2010.

[107] D. Shen, R. Xiao, S. Gu, and H. Zhang, "The overview of thermal decomposition of cellulose in lignocellulosic biomass," *Cellul. Convers.*, pp. 193–226, 2013.

[108] J. Alongi and G. Malucelli, "Thermal degradation of cellulose and cellulosic substrates," *React. Mech. Therm. Anal. Adv. Mater.*, vol. 14, pp. 301–332, 2015.

[109] S. Xin *et al.*, "Chemical structure evolution of char during the pyrolysis of cellulose," *J. Anal. Appl. Pyrolysis*, vol. 116, pp. 263–271, 2015.

[110] J. Alongi and G. Malucelli, "Cotton flame retardancy: state of the art and future perspectives," *Rsc Adv.*, vol. 5, no. 31, pp. 24239–24263, 2015.

[111] E. Picheau, S. Amar, A. Derré, A. Pénicaud, and F. Hof, "An Introduction to the Combustion of Carbon Materials," *Chem. - A Eur. J.*, vol. 28, no. 54, 2022, doi: 10.1002/chem.202200117.

[112] K. Kohse-Höinghaus, "Combustion in the future: The importance of chemistry," *Proc. Combust. Inst.*, vol. 38, no. 1, pp. 1–56, 2021.

[113] P. J. Wakelyn, "Environmentally friendly flame resistant textiles," in *Advances in fire retardant materials*, Elsevier, 2008, pp. 188–212.

[114] R. E. Lyon, *Solid-state thermochemistry of flaming combustion*. Marcel Dekker, Inc., NY, 2000.

[115] M. A. Santoso, E. G. Christensen, J. Yang, and G. Rein, "Review of the transition from smouldering to flaming combustion in wildfires," *Front. Mech. Eng.*, vol. 5, p. 49, 2019.

[116] Z. Wang *et al.*, "Smouldering and its transition to flaming combustion of polyurethane foam: An experimental study," *Fuel*, vol. 309, no. November 2021, p. 122249, 2022, doi: 10.1016/j.fuel.2021.122249.

[117] M. A. Santoso, E. G. Christensen, and G. Rein, "The effects of pulsating wind on the transition from smouldering to flaming combustion," *Fire Saf. J.*, vol. 141, no. June, p. 103993, 2023, doi: 10.1016/j.firesaf.2023.103993.

[118] K. Pielichowski, J. Njuguna, and T. M. Majka, *Thermal degradation of polymeric materials*. Elsevier, 2022.

[119] R. Ogabi, B. Manescau, K. Chetehouna, and and N. Gascoin, "Composites and Their Gaseous Emission Assessment," *Energy*, vol. 14, pp. 1–32, 2021.

[120] N. Ramadan, M. Taha, A. D. La Rosa, and A. Elsabbagh, "Towards selection charts for epoxy resin, unsaturated polyester resin and their fibre-fabric composites with flame retardants," *Materials (Basel).*, vol. 14, no. 5, p. 1181, 2021.

[121] B. Liu, H. Zhao, and Y. Wang, "Advanced flame-retardant methods for polymeric materials," *Adv. Mater.*, vol. 34, no. 46, p. 2107905, 2022.

[122] J. Shen, J. Liang, X. Lin, H. Lin, J. Yu, and S. Wang, "The flame-retardant mechanisms and preparation of polymer composites and their potential application in construction engineering," *Polymers (Basel).*, vol. 14, no. 1, 2022, doi: 10.3390/polym14010082.

[123] R. Wolf and B. L. Kaul, "Plastics, Additives," *Ullmann's Encycl. Ind. Chem.*, 2000, doi: 10.1002/14356007.a20_459.

[124] J. Alongi, *Update on flame retardant textiles*. Smithers Rapra, 2013.

[125] B. Camino and G. Camino, "The chemical kinetics of the polymer combustion allows for inherent fire retardant synergism," *Polym. Degrad. Stab.*, vol. 160, pp. 142–147, 2019, doi: 10.1016/j.polymdegradstab.2018.12.018.

[126] W. Gwenzi, N. Chaukura, N. Muisa-Zikali, K. Musiyiwa, and C. Teta, "Occurrence and behaviour of emerging organic contaminants in aquatic systems," in *Emerging Contaminants in the Terrestrial-Aquatic-Atmosphere Continuum:*, Elsevier, 2022, pp. 67–86.

[127] Y. Hu and Y. Zhang, "Mechanisms and modes of action in flame retardancy of polymers," in *Flame Retardant Polymeric Materials*, CRC Press, 2019, pp. 13–34.

[128] F. Laoutid, L. Bonnaud, M. Alexandre, J.-M. Lopez-Cuesta, and P. Dubois, "New prospects in flame retardant polymer materials: From fundamentals to nanocomposites," *Mater. Sci. Eng. R Reports*, vol. 63, no. 3, pp. 100–125, 2009.

[129] W. Zhao, C. Kumar Kundu, Z. Li, X. Li, and Z. Zhang, "Flame retardant treatments for polypropylene: Strategies and recent advances," *Compos. Part A Appl. Sci. Manuf.*, vol. 145, no. February, p. 106382, 2021, doi: 10.1016/j.compositesa.2021.106382.

[130] S. Gaan, G. Sun, K. Hutches, and M. H. Engelhard, "Effect of nitrogen additives on flame retardant action of tributyl phosphate: phosphorus–nitrogen synergism," *Polym. Degrad. Stab.*, vol. 93, no. 1, pp. 99–108, 2008.

[131] A. R. Horrocks, B. K. Kandola, P. J. Davies, S. Zhang, and S. A. Padbury, "Developments in flame retardant textiles–a review," *Polym. Degrad. Stab.*, vol. 88, no. 1, pp. 3–12, 2005.

[132] A. Bartošová, M. Soldán, M. Sirotiak, and M. Prachová, "Novel environmental friendly fire retardants," *Adv. Sci. Eng.*, vol. 11, no. 1, pp. 1–8, 2019.

[133] F. M. de Souza, R. K. Gupta, and P. K. Kahol, "Recent development on flame retardants for polyurethanes," in *Polyurethane Chemistry: Renewable Polyols and Isocyanates*, ACS Publications, 2021, pp. 187–223.

[134] J. Zhou, M. Xu, X. Zhang, Y. Leng, Y. He, and B. Li, "Preparation of highly efficient flame retardant unsaturated polyester resin by exerting the fire resistant effect in gaseous and condensed phase simultaneously," *Polym. Adv. Technol.*, vol. 30, no. 7, pp. 1684–1695, 2019.

[135] M. S. Özer and S. Gaan, "Recent developments in phosphorus based flame retardant coatings for textiles: Synthesis, applications and performance," *Prog. Org. Coatings*, vol. 171, no. July, 2022, doi: 10.1016/j.porgcoat.2022.107027.

[136] A. Hochół, M. Flejszar, and P. Chmielarz, "Advances and opportunities in synthesis of flame retardant polymers via reversible deactivation radical polymerization," *Polym. Degrad. Stab.*, vol. 214, no. April, 2023, doi: 10.1016/j.polymdegradstab.2023.110414.

[137] L. Wan, C. Deng, Z.-Y. Zhao, H. Chen, and Y.-Z. Wang, "Flame retardation of natural rubber: Strategy and recent progress," *Polymers (Basel).*, vol. 12, no. 2, p. 429, 2020.

[138] X. Lin, W. Feng, and L. Xu, "Study on fl ame retardant ABS," pp. 1–10, 2017.

[139] R. Sauerwein, "Mineral filler flame retardants," *Non-Halogenated Flame Retard. Handb.*, pp. 101–168, 2021.

[140] M. Murariu *et al.*, "Pathways to biodegradable flame retardant polymer (nano) composites," in *Polymer green flame retardants*, Elsevier, 2014, pp. 709–773.

[141] P. Kiliaris and C. D. Papaspyrides, "Polymers on fire," in *Polymer green flame retardants*, Elsevier, 2014, pp. 1–43.

[142] H. Nabipour and Y. Hu, "Introduction to flame retardants for polymeric materials," in *Bio-Based Flame-retardant Technology for Polymeric Materials*, Elsevier, 2022, pp. 1–27.

[143] P. R. Hornsby and R. N. Rothon, "Fire retardant fillers for polymers," *Fire Retard.*

Polym. New Appl. Miner. Fill., pp. 19–41, 2005.

[144] K. K. Shen, "Boron-based flame retardants in non-halogen based polymers," *Non-Halogenated Flame Retard. Handb.*, pp. 309–336, 2021.

[145] L. Wang *et al.*, "Flame retardant properties of a guanidine phosphate–zinc borate composite flame retardant on wood," *ACS omega*, vol. 6, no. 16, pp. 11015–11024, 2021.

[146] W. Dukarski, I. Rykowska, P. Krzyżanowski, and M. Gonsior, "Flame Retardant Additives Used for Polyurea-Based Elastomers—A Review," *Fire*, vol. 7, no. 2, p. 50, 2024.

[147] M. E. Mngomezulu, M. J. John, V. Jacobs, and A. S. Luyt, "Review on flammability of biofibres and biocomposites," *Carbohydr. Polym.*, vol. 111, pp. 149–182, 2014.

[148] A. B. Morgan, *Non-halogenated flame retardant handbook*. John Wiley & Sons, 2021.

[149] N. Mazumder and M. T. Islam, "Flame retardant finish for textile fibers," *Innov. Emerg. Technol. Text. Dye. Finish.*, pp. 373–405, 2021.

[150] S. Y. Tawfik, "Flame retardants: Additives in plastic technology," *Polym. Polym. Compos. a Ref. Ser.*, pp. 1–27, 2017.

[151] C. J. Hager, C. D. McMillen, R. Sachdeva, A. W. Martin, and J. S. Thrasher, "New Fluorine-Containing Diamine Monomers for Potentially Improved Polyimides," *Molecules*, vol. 28, no. 19, pp. 1–15, 2023, doi: 10.3390/molecules28196855.

[152] K. A. Szychowski, K. Rybczyńska-Tkaczyk, M. L. Leja, A. K. Wójtowicz, and J. Gmiński, "Tetrabromobisphenol A (TBBPA)-stimulated reactive oxygen species (ROS) production in cell-free model using the 2′, 7′-dichlorodihydrofluorescein diacetate (H 2 DCFDA) assay—limitations of method," *Environ. Sci. Pollut. Res.*, vol. 23, pp. 12246–12252, 2016.

[153] P. P. Unit, "National implementation plan for reduc-tion and elimination of Persistent Organic Pollutants in the Republic of Macedonia–NIP Update," 2017.

[154] M. Alaee, P. Arias, A. Sjödin, and Å. Bergman, "An overview of commercially used brominated flame retardants, their applications, their use patterns in different countries/regions and possible modes of release," *Environ. Int.*, vol. 29, no. 6, pp. 683–689, 2003.

[155] J. M. Nzangya, E. N. Ndunda, G. O. Bosire, B. S. Martincigh, and V. O. Nyamori, "Polybrominated diphenyl ethers (PBDEs) as emerging environmental pollutants: Advances in sample preparation and detection techniques," *Emerg. Contam.*, pp. 1–22, 2021.

[156] T. R. Hull, R. J. Law, and Å. Bergman, "Environmental drivers for replacement of halogenated flame retardants," *Polym. Green Flame Retard.*, pp. 119–179, 2014.

[157] S. D. Jadhav, "A review of non-halogenated flame retardant," *Pharma Innov.*, vol. 7, no. 5, Part F, p. 380, 2018.

[158] N. Arastehnejad, M. R. Sulaiman, and R. K. Gupta, "Nitrogen-based ecofriendly flame retardants for polyurethane foams," in *Polyurethane Chemistry: Renewable Polyols and Isocyanates*, ACS Publications, 2021, pp. 167–185.

[159] S. V Levchik, "Introduction to flame retardancy and polymer flammability," *Flame Retard. Polym. nanocomposites*, pp. 1–29, 2007.

[160] A. B. Morgan and M. Klatt, "Nitrogen-Based Flame Retardants," *Non-Halogenated Flame Retard. Handb.*, pp. 236–270, 2021.

[161] H. Feuchter, F. Poutch, and A. Beard, "The impact of halogen free phosphorus, inorganic and nitrogen flame retardants on the toxicity and density of smoke from 10 common polymers," *Fire Mater.*, 2023.

[162] L. Passauer, "Thermal characterization of ammonium starch phosphate carbamates for potential applications as bio-based flame-retardants," *Carbohydr. Polym.*, vol. 211, no. January, pp. 69–74, 2019, doi: 10.1016/j.carbpol.2019.01.100.

[163] S. Levchik, "Phosphorus-Based Flame Retardants," *Non-Halogenated Flame Retard. Handb.*, pp. 23–99, 2021.

[164] O. Y. Wen, M. Z. M. Tohir, T. C. S. Yeaw, M. A. Razak, H. S. Zainuddin, and M. R. A. Hamid, "Fire-resistant and flame-retardant surface finishing of polymers and textiles: A state-of-the-art review," *Prog. Org. Coatings*, vol. 175, p. 107330, 2023.

[165] K.-S. Lim *et al.*, "A review of application of ammonium polyphosphate as intumescent flame retardant in thermoplastic composites," *Compos. Part B Eng.*, vol. 84, pp. 155–174, 2016.

[166] S. Fu, P. Song, and X. Liu, "Thermal and flame retardancy properties of thermoplastics/natural fiber biocomposites," in *Advanced High Strength Natural Fibre Composites in Construction*, Elsevier, 2017, pp. 479–508.

[167] A. Kushwaha, K. Chaudhary, S. Singh, and C. Prakash, "Application of ammonium polyphosphate as intumescent flame retardant on Varanasi brocade pineapple fabric," *Biomass Convers. Biorefinery*, pp. 1–12, 2023.

[168] M. Martí, C. Alonso, A. Manich, I. De Vilder, and L. Coderch, "Flame retardant textile finishing: thermal analysis and dermal security," *Text. Res. J.*, vol. 94, no. 1–2, pp. 69–81, 2024.

[169] N. T. Huong and V. T. H. Khanh, "Study on contents of Pyrovatex CP New and Knittex FFRC in flame retardant treatment for cotton fabrics," in *Proceeding Book of Proceeding Indonesian Textile Conference: textile 4.0 clothing and beyond (international conference)*, 2019, vol. 3.

[170] R. Shen, Y. Quan, and Q. Wang, "Thermal Stability and Flame Retardancy of Epoxy/Synthetic Fiber Composites," in *Handbook of Epoxy/Fiber Composites*, Springer, 2022, pp. 193–227.

[171] S. Hamdani, C. Longuet, D. Perrin, J.-M. Lopez-Cuesta, and F. Ganachaud, "Flame retardancy of silicone-based materials," *Polym. Degrad. Stab.*, vol. 94, no. 4, pp. 465–495, 2009.

[172] X. Song, D. Xu, Z. Luo, and B. Wang, "A silicone diphenylsulfonate for improving the flame retardancy of polycarbonate," *J. Appl. Polym. Sci.*, vol. 139, no. 46, p. e53152,

2022.

[173] A. B. Morgan and M. Kilinc, "Silicon-Based Flame Retardants," *Non-Halogenated Flame Retard. Handb.*, pp. 271–308, 2021.

[174] M. Zielecka, A. Rabajczyk, Ł. Pastuszka, and L. Jurecki, "Flame resistant silicone-containing coating materials," *Coatings*, vol. 10, no. 5, pp. 1–14, 2020, doi: 10.3390/COATINGS10050479.

[175] X. Qiu *et al.*, "A simple and universal strategy for construction and application of silica-based flame-retardant nanostructure," *Compos. Part B Eng.*, vol. 238, p. 109887, 2022.

[176] "Silicon Dioxide," *Dict. Gems Gemol.*, vol. 22683, pp. 779–779, 2009, doi: 10.1007/978-3-540-72816-0_19855.

[177] S. Wang *et al.*, "Biobased Phosphorus Siloxane-Containing Polyurethane Foam with Flame-Retardant and Smoke-Suppressant Performances," *ACS Sustain. Chem. Eng.*, vol. 9, no. 25, pp. 8623–8634, 2021, doi: 10.1021/acssuschemeng.1c02273.

[178] S. Sun, X. Peng, H. Pang, and H. Niu, "Synthesis and flame retardant behavior of siloxane functionalized polyethylene," *J. Appl. Polym. Sci.*, vol. 139, no. 36, p. e52850, 2022.

[179] K. Mojsiewicz-Pieńkowska, M. Jamrógiewicz, and K. Szymkowska, "Direct human contact with siloxanes (silicones)–safety or risk part 1. Characteristics of siloxanes (silicones)," *Front. Pharmacol.*, vol. 7, p. 198329, 2016.

[180] A. Dowbysz, M. Samsonowicz, B. Kukfisz, and P. Koperniak, "Recent Developments of Nano Flame Retardants for Unsaturated Polyester Resin," *Materials (Basel).*, vol. 17, no. 4, p. 852, 2024.

[181] D. Kačíková *et al.*, "The influence of nanoparticles on fire retardancy of pedunculate oak wood," *Nanomaterials*, vol. 11, no. 12, p. 3405, 2021.

[182] O. Öhrn *et al.*, "Surface coated ZnO powder as flame retardant for wood: A short

communication," *Sci. Total Environ.*, vol. 897, p. 165290, 2023.

[183] S. M. Fayyadh and A. Ben Ahmed, "A comparative study between the use of nanoparticles of magnesium oxide and zinc oxide as coating for polymeric surfaces a flame retardant and corrosion resistance," *Mater. Chem. Phys.*, vol. 314, p. 128899, 2024.

[184] S. Perera, D. Wijesekara, G. Thiripuranathar, and F. Menaa, "The Use of Nanoparticles to Enhance Performance in the Textile Industry-A Concise Review," *Curr. Nanosci.*, vol. 18, no. 3, pp. 319–335, 2022.

[185] M. M. Rashid *et al.*, "In situ tailoring of Ag-doped-TiO2/TPMP/cotton nanocomposite with UV-protective, self-sterilizing and flame-retardant performance for advanced technical textiles," *Polym. Degrad. Stab.*, vol. 216, p. 110504, 2023.

[186] Q. Li and Y.-T. Pan, "Flame retardant properties of metal oxide/polymer nanocomposites," in *Flame Retardant Nanocomposites*, Elsevier, 2024, pp. 201–224.

[187] C. K. Kundu, L. Song, and Y. Hu, "Chitosan-metal oxide nanoparticle hybrids in developing bi-functional polyamide 66 textiles with enhanced flame retardancy and wettability," *Appl. Surf. Sci. Adv.*, vol. 7, p. 100202, 2022.

[188] C. I. Idumah, "Recent advancements in fire retardant mechanisms of carbon nanotubes, graphene, and fullerene polymeric nanoarchitectures," *J. Anal. Appl. Pyrolysis*, p. 106113, 2023.

[189] J. Chen and J. Han, "Comparative performance of carbon nanotubes and nanoclays as flame retardants for epoxy composites," *Results Phys.*, vol. 14, p. 102481, 2019.

[190] A. Kausar, "Flame retardant potential of clay nanoparticles," in *Clay Nanoparticles*, Elsevier, 2020, pp. 169–184.

[191] Z. Xu, H. Zhou, L. Yan, and H. Jia, "Comparative study of the fire protection performance and thermal stability of intumescent fire-retardant coatings filled with three types of clay nano-fillers," *Fire Mater.*, vol. 44, no. 1, pp. 112–120, 2020.

[192] Y. Demirhan, R. Yurtseven, and N. Usta, "The effect of boric acid on flame retardancy of intumescent flame retardant polypropylene composites including nanoclay," *J. Thermoplast. Compos. Mater.*, vol. 36, no. 3, pp. 1187–1214, 2023.

[193] A. Verbič, M. Gorjanc, and B. Simončič, "Zinc oxide for functional textile coatings: Recent advances," *Coatings*, vol. 9, no. 9, pp. 17–23, 2019, doi: 10.3390/coatings9090550.

[194] S. Ghayempour and M. Montazer, "Ultrasound irradiation based in-situ synthesis of star-like Tragacanth gum/zinc oxide nanoparticles on cotton fabric," *Ultrason. Sonochem.*, vol. 34, pp. 458–465, 2017.

[195] A. Srivastava and A. Katiyar, "Zinc oxide nanostructures," in *Ceramic Science and Engineering*, Elsevier, 2022, pp. 235–262.

[196] H. Morkoç and Ü. Özgür, *Zinc oxide: fundamentals, materials and device technology*. John Wiley & Sons, 2008.

[197] S. Hackenberg, A. Scherzed, A. Technau, K. Froelich, R. Hagen, and N. Kleinsasser, "Functional responses of human adipose tissue-derived mesenchymal stem cells to metal oxide nanoparticles in vitro," *J. Biomed. Nanotechnol.*, vol. 9, no. 1, pp. 86–95, 2013.

[198] M. Z. Khan *et al.*, "Growth of ZnO nanorods on cotton fabrics via microwave hydrothermal method: effect of size and shape of nanorods on superhydrophobic and UV-blocking properties," *Cellulose*, vol. 27, no. 17, pp. 10519–10539, 2020, doi: 10.1007/s10570-020-03495-x.

[199] A. Kolodziejczak-Radzimska and T. Jesionowski, "Zinc oxide-from synthesis to application: A review," *Materials (Basel).*, vol. 7, no. 4, pp. 2833–2881, 2014, doi: 10.3390/ma7042833.

[200] V. Parihar, M. Raja, and R. Paulose, "A brief review of structural, electrical and electrochemical properties of zinc oxide nanoparticles," *Rev. Adv. Mater. Sci.*, vol. 53, no. 2, pp. 119–130, 2018, doi: 10.1515/rams-2018-0009.

[201] A. K. Samanta, R. Bhattacharyya, S. Jose, G. Basu, and R. Chowdhury, "Fire retardant finish of jute fabric with nano zinc oxide," *Cellulose*, vol. 24, no. 2, pp. 1143–1157, 2017, doi: 10.1007/s10570-016-1171-z.

[202] P. Ramamurthy, K. P. Chellamani, B. Dhurai, S. P. ThankaRajan, B. Subramanian, and E. Santhini, "Antimicrobial characteristics of pulsed laser deposited metal oxides on polypropylene hydroentangled nonwovens for medical textiles," *Fibres Text. East. Eur.*, 2017.

[203] A. Amani, M. Montazer, and M. Mahmoudirad, "Synthesis of applicable hydrogel corn silk/ZnO nanocomposites on polyester fabric with antimicrobial properties and low cytotoxicity," *Int. J. Biol. Macromol.*, vol. 123, pp. 1079–1090, 2019.

[204] M. Sheshama, H. Khatri, M. Suthar, S. Basak, and W. Ali, "Bulk vs. Nano ZnO: Influence of fire retardant behavior on sisal fibre yarn," *Carbohydr. Polym.*, vol. 175, pp. 257–264, 2017.

[205] L. Cai *et al.*, "Spectrally selective nanocomposite textile for outdoor personal cooling," *Adv. Mater.*, vol. 30, no. 35, p. 1802152, 2018.

[206] W.-T. Chiu *et al.*, "Fabrication and photocatalytic performance of Au/ZnO layered structure on silk textile for flexible device applications," *Electrochim. Acta*, vol. 253, pp. 39–46, 2017.

[207] H. Wan, P. Han, S. Ge, F. Li, S. Zhang, and H. Li, "Development zinc oxide–cotton fibers as anode materials for lithium-ion batteries," *Int. J. Electrochem. Sci*, vol. 13, pp. 4115–4122, 2018.

[208] S. Karthik, P. Siva, K. S. Balu, R. Suriyaprabha, V. Rajendran, and M. Maaza, "Acalypha indica–mediated green synthesis of ZnO nanostructures under differential thermal treatment: Effect on textile coating, hydrophobicity, UV resistance, and antibacterial activity," *Adv. Powder Technol.*, vol. 28, no. 12, pp. 3184–3194, 2017.

[209] S. Pal, S. Mondal, and J. Maity, "Synthesis, characterization and photocatalytic properties of ZnO nanoparticles and cotton fabric modified with ZnO nanoparticles via

in-situ hydrothermal coating technique: Dual response," *Mater. Technol.*, vol. 33, no. 14, pp. 884–891, 2018.

[210] V. H. T. Thi and B.-K. Lee, "Development of multifunctional self-cleaning and UV blocking cotton fabric with modification of photoactive ZnO coating via microwave method," *J. Photochem. Photobiol. A Chem.*, vol. 338, pp. 13–22, 2017.

[211] M. Ashraf, M. I. Siyal, A. Nazir, and A. Rehman, "Single-step antimicrobial and moisture management finishing of PC fabric using ZNO nanoparticles," *Autex Res. J.*, vol. 17, no. 3, pp. 259–262, 2017.

[212] O. Sacco *et al.*, "Crystal violet and toxicity removal by adsorption and simultaneous photocatalysis in a continuous flow micro-reactor," *Sci. Total Environ.*, vol. 644, pp. 430–438, 2018.

[213] O. Sacco, V. Vaiano, and M. Matarangolo, "ZnO supported on zeolite pellets as efficient catalytic system for the removal of caffeine by adsorption and photocatalysis," *Sep. Purif. Technol.*, vol. 193, pp. 303–310, 2018.

[214] Y.-W. Wang, R. Shen, Q. Wang, and Y. Vasquez, "ZnO microstructures as flame-retardant coatings on cotton fabrics," *ACS omega*, vol. 3, no. 6, pp. 6330–6338, 2018.

[215] A. Arputharaj, V. Nadanathangam, and S. R. Shukla, "A simple and efficient protocol to develop durable multifunctional property to cellulosic materials using in situ generated nano-ZnO," *Cellulose*, vol. 24, pp. 3399–3410, 2017.

[216] A. Javed, J. Wiener, J. Saskova, and J. Müllerová, "Zinc Oxide Nanoparticles (ZnO NPs) and N-Methylol Dimethyl Phosphonopropion Amide (MDPA) System for Flame Retardant Cotton Fabrics," *Polymers (Basel).*, vol. 14, no. 16, 2022, doi: 10.3390/polym14163414.

[217] A. K. Samanta, R. Bhattacharyay, A. Bagchi, and R. Chowdhuri, "Statistical optimisation of nano-zinc oxide-based fire-protective finish on jute fabric," in *Functional textiles and clothing*, 2019, pp. 167–191.

[218] Y. Li, C. Liao, and S. C. Tjong, "Recent advances in zinc oxide nanostructures with

antimicrobial activities," *Int. J. Mol. Sci.*, vol. 21, no. 22, p. 8836, 2020.

[219] W. He, H.-K. Kim, W. G. Wamer, D. Melka, J. H. Callahan, and J.-J. Yin, "Photogenerated charge carriers and reactive oxygen species in ZnO/Au hybrid nanostructures with enhanced photocatalytic and antibacterial activity," *J. Am. Chem. Soc.*, vol. 136, no. 2, pp. 750–757, 2014.

[220] J. Bedia, V. Muelas-Ramos, M. Peñas-Garzón, A. Gómez-Avilés, J. J. Rodríguez, and C. Belver, "A review on the synthesis and characterization of metal organic frameworks for photocatalytic water purification," *Catalysts*, vol. 9, no. 1, p. 52, 2019.

[221] M. Salat, P. Petkova, J. Hoyo, I. Perelshtein, A. Gedanken, and T. Tzanov, "Durable antimicrobial cotton textiles coated sonochemically with ZnO nanoparticles embedded in an in-situ enzymatically generated bioadhesive," *Carbohydr. Polym.*, vol. 189, pp. 198–203, 2018.

[222] Z. Khabir, "Transdermal Penetration of Photoluminescent Nanoparticles in Human Skin." Macquarie University, 2022.

[223] A. S. Bhosale, K. K. Abitkar, P. S. Sadalage, K. D. Pawar, and K. M. Garadkar, "Photocatalytic and antibacterial activities of ZnO nanoparticles synthesized by chemical method," *J. Mater. Sci. Mater. Electron.*, vol. 32, pp. 20510–20524, 2021.

[224] B. Abebe, E. A. Zereffa, A. Tadesse, and H. C. A. Murthy, "A review on enhancing the antibacterial activity of ZnO: Mechanisms and microscopic investigation," *Nanoscale Res. Lett.*, vol. 15, pp. 1–19, 2020.

[225] A. H. Hammadi, S. A. Habeeb, L. F. Al-Jibouri, and F. H. Hussien, "Synthesis, Characterization and Biological Activity of Zinc Oxide Nanoparticles (ZnO NPs)," *Syst. Rev. Pharm.*, vol. 11, no. 5, pp. 431–439, 2020.

[226] B. D. Wilson, S. Moon, and F. Armstrong, "Comprehensive review of ultraviolet radiation and the current status on sunscreens," *J. Clin. Aesthet. Dermatol.*, vol. 5, no. 9, p. 18, 2012.

[227] R. D. Piacentini, "The Importance of the use of Clothes with Solar UV Protection,"

Curr. Trends Fash. Technol. Text. Eng., vol. 3, no. 5, pp. 96–100, 2018, doi: 10.19080/ctftte.2018.03.555623.

[228] P. Gies *et al.*, *Australian/New Zealand Standard, AS/NZS 4399: 2017: sun protective clothing–evaluation and classification*. Standards Australia, 2017.

[229] R. Huang, S. Zhang, W. Zhang, and X. Yang, "Progress of zinc oxide-based nanocomposites in the textile industry," *IET Collab. Intell. Manuf.*, vol. 3, no. 3, pp. 281–289, 2021.

[230] A. Bashari, M. Shakeri, and A. R. Shirvan, "UV-protective textiles," in *The impact and prospects of green chemistry for textile technology*, Elsevier, 2019, pp. 327–365.

[231] O. K. Alebeid and T. Zhao, "Review on: developing UV protection for cotton fabric," *J. Text. Inst.*, vol. 108, no. 12, pp. 2027–2039, 2017, doi: 10.1080/00405000.2017.1311201.

[232] J. Ran, M. He, W. Li, D. Cheng, and X. Wang, "Growing ZnO nanoparticles on polydopamine-templated cotton fabrics for durable antimicrobial activity and UV protection," *Polymers (Basel).*, vol. 10, no. 5, 2018, doi: 10.3390/polym10050495.

[233] J. Wojnarowicz, T. Chudoba, and W. Lojkowski, "A Review of Microwave Synthesis of Zinc Oxide Nanomaterials : Reactants , Process Parameters and Morphologies," 2020.

[234] A. Mohajerani *et al.*, "Nanoparticles in construction materials and other applications, and implications of nanoparticle use," *Materials (Basel).*, vol. 12, no. 19, p. 3052, 2019.

[235] A. C. Dodd, A. J. McKinley, M. Saunders, and T. Tsuzuki, "Effect of particle size on the photocatalytic activity of nanoparticulate zinc oxide," *J. Nanoparticle Res.*, vol. 8, no. 1, pp. 43–51, 2006, doi: 10.1007/s11051-005-5131-z.

[236] L. Jiao, J. Ma, and H. Dai, "Preparation and characterization of self-reinforced antibacterial and oil-resistant paper using a NaOH/Urea/ZnO solution," *PLoS One*, vol. 10, no. 10, pp. 1–16, 2015, doi: 10.1371/journal.pone.0140603.

[237] X. Z. Sun, D. H. Bremner, N. Wan, and X. Wang, "Development of antibacterial ZnO-loaded cotton fabric based on in situ fabrication," *Appl. Phys. A Mater. Sci. Process.*, vol. 122, no. 11, pp. 1–9, 2016, doi: 10.1007/s00339-016-0482-0.

[238] D. Shao, Y. Gao, K. Cao, and Q. Wei, "Rapid surface functionalization of cotton fabrics by modified hydrothermal synthesis of ZnO," *J. Text. Inst.*, vol. 108, no. 8, pp. 1391–1397, 2017.

[239] P. M. Sivakumar, S. Balaji, V. Prabhawathi, R. Neelakandan, P. T. Manoharan, and M. Doble, "Effective antibacterial adhesive coating on cotton fabric using ZnO nanorods and chalcone," *Carbohydr. Polym.*, vol. 79, no. 3, pp. 717–723, 2010, doi: 10.1016/j.carbpol.2009.09.027.

[240] C. Chung, M. Lee, and E. K. Choe, "Characterization of cotton fabric scouring by FT-IR ATR spectroscopy," *Carbohydr. Polym.*, vol. 58, no. 4, pp. 417–420, 2004, doi: 10.1016/j.carbpol.2004.08.005.

[241] H. Zhao, Q. Liang, and Y. Lu, "Microstructure and properties of copper plating on citric acid modified cotton fabric," *Fibers Polym.*, vol. 16, no. 3, pp. 593–598, 2015, doi: 10.1007/s12221-015-0593-9.

[242] F. Xu, G. Zhang, P. Wang, and F. Dai, "Durable and high-efficiency casein-derived phosphorus-nitrogen-rich flame retardants for cotton fabrics," *Cellulose*, vol. 29, no. 4, pp. 2681–2697, 2022, doi: 10.1007/s10570-022-04430-y.

[243] P. Bazant, I. Kuritka, L. Munster, and L. Kalina, "Microwave solvothermal decoration of the cellulose surface by nanostructured hybrid Ag/ZnO particles: a joint XPS, XRD and SEM study," *Cellulose*, vol. 22, no. 2, pp. 1275–1293, 2015, doi: 10.1007/s10570-015-0561-y.

[244] Ö. Ceylan, L. Van Landuyt, H. Rahier, and K. De Clerck, "The effect of water immersion on the thermal degradation of cotton fibers," *Cellulose*, vol. 20, no. 4, pp. 1603–1612, 2013, doi: 10.1007/s10570-013-9936-0.

[245] H. Barani, "Surface activation of cotton fiber by seeding silver nanoparticles and in situ

synthesizing ZnO nanoparticles," *New J. Chem.*, vol. 38, no. 9, pp. 4365–4370, 2014, doi: 10.1039/c4nj00547c.

[246] S. Gaan and G. Sun, "Effect of phosphorus and nitrogen on flame retardant cellulose: a study of phosphorus compounds," *J. Anal. Appl. Pyrolysis*, vol. 78, no. 2, pp. 371–377, 2007.

[247] M. H. Fallah, S. A. Fallah, and M. A. Zanjanchi, "Synthesis and characterization of nano-sized zinc oxide coating on cellulosic fibers: Photoactivity and flame-retardancy study," *Chinese J. Chem.*, vol. 29, no. 6, pp. 1239–1245, 2011, doi: 10.1002/cjoc.201190230.

[248] W. Wu, X. Zhen, and C. Q. Yang, "Correlation between Limiting Oxygen Index and Phosphorus Content of the Cotton Fabric Treated with a Hydroxy-functional Organophosphorus Flame Retarding Finish and Melamine-Formaldehyde," *J. Fire Sci.*, vol. 22, no. 1, pp. 11–23, 2004, doi: 10.1177/0734904104035253.

[249] S. Wang *et al.*, "Durable flame retardant finishing of cotton fabrics with organosilicon functionalized cyclotriphosphazene," *Polym. Degrad. Stab.*, vol. 128, pp. 22–28, 2016, doi: 10.1016/j.polymdegradstab.2016.02.009.

[250] X. Qian *et al.*, "Combustion and thermal degradation mechanism of a novel intumescent flame retardant for epoxy acrylate containing phosphorus and nitrogen," *Ind. Eng. Chem. Res.*, vol. 50, no. 4, pp. 1881–1892, 2011.

[251] P. Dhandapani, A. S. Siddarth, S. Kamalasekaran, S. Maruthamuthu, and G. Rajagopal, "Bio-approach: Ureolytic bacteria mediated synthesis of ZnO nanocrystals on cotton fabric and evaluation of their antibacterial properties," *Carbohydr. Polym.*, vol. 103, no. 1, pp. 448–455, 2014, doi: 10.1016/j.carbpol.2013.12.074.

[252] A. Siriviriyanun, E. A. O'Rear, and N. Yanumet, "Self-extinguishing cotton fabric with minimal phosphorus deposition," *Cellulose*, vol. 15, no. 5, pp. 731–737, 2008, doi: 10.1007/s10570-008-9223-7.

[253] E. D. Tomak and A. D. Cavdar, "Limited oxygen index levels of impregnated Scots

pine wood," *Thermochim. Acta*, vol. 573, pp. 181–185, 2013, doi: 10.1016/j.tca.2013.09.022.

[254] K. Xie, A. Gao, and Y. Zhang, "Flame retardant finishing of cotton fabric based on synergistic compounds containing boron and nitrogen," *Carbohydr. Polym.*, vol. 98, no. 1, pp. 706–710, 2013.

[255] L. Wang, C. Hu, and L. Shao, "The antimicrobial activity of nanoparticles: Present situation and prospects for the future," *Int. J. Nanomedicine*, vol. 12, pp. 1227–1249, 2017, doi: 10.2147/IJN.S121956.

[256] S. Shaikh *et al.*, "Mechanistic insights into the antimicrobial actions of metallic nanoparticles and their implications for multidrug resistance," *Int. J. Mol. Sci.*, vol. 20, no. 10, pp. 1–15, 2019, doi: 10.3390/ijms20102468.

[257] K. Han and M. Yu, "Study of the preparation and properties of UV-blocking fabrics of a PET/TiO2 nanocomposite prepared by in situ polycondensation," *J. Appl. Polym. Sci.*, vol. 100, no. 2, pp. 1588–1593, 2006.

[258] S. Mondal, "Nanomaterials for UV protective textiles," *J. Ind. Text.*, vol. 0, no. 0, pp. 1–30, 2021, doi: 10.1177/1528083721988949.

[259] H. Sudrajat, "Superior photocatalytic activity of polyester fabrics coated with zinc oxide from waste hot dipping zinc," *J. Clean. Prod.*, vol. 172, pp. 1722–1729, 2018, doi: 10.1016/j.jclepro.2017.12.024.

[260] M. Shaban, S. Abdallah, and A. A. Khalek, "Characterization and photocatalytic properties of cotton fibers modified with ZnO nanoparticles using sol–gel spin coating technique," *Beni-Suef Univ. J. Basic Appl. Sci.*, vol. 5, no. 3, pp. 277–283, 2016, doi: 10.1016/j.bjbas.2016.08.003.

[261] L. Fridrichová, "A new method of measuring the bending rigidity of fabrics and its application to the determination of the their anisotropy," *Text. Res. J.*, vol. 83, no. 9, pp. 883–892, 2013, doi: 10.1177/0040517512467133.

[262] M. Z. Khan *et al.*, "Ultra-fast growth of ZnO nanorods on cotton fabrics and their self-

cleaning and physiological comfort properties," *Coatings*, vol. 11, no. 11, p. 1309, 2021.

[263] I. S. Tania and M. Ali, "Coating of ZnO nanoparticle on cotton fabric to create a functional textile with enhanced mechanical properties," *Polymers (Basel).*, vol. 13, no. 16, p. 2701, 2021.

[264] L. Hes and M. de Araujo, "Simulation of the effect of air gaps between the skin and a wet fabric on resulting cooling flow," *Text. Res. J.*, vol. 80, no. 14, pp. 1488–1497, 2010.

[265] W. Sricharussin, W. Ryo-Aree, W. Intasen, and S. Poungraksakirt, "Effect of boric acid and BTCA on tensile strength loss of finished cotton fabrics," *Text. Res. J.*, vol. 74, no. 6, pp. 475–480, 2004.

[266] B. Ji, C. Zhao, K. Yan, and G. Sun, "Effects of acid diffusibility and affinity to cellulose on strength loss of polycarboxylic acid crosslinked fabrics," *Carbohydr. Polym.*, vol. 144, pp. 282–288, 2016.

[267] C. Q. Yang, W. Wei, and G. C. Lickfield, "Mechanical strength of durable press finished cotton fabric: Part II: Comparison of crosslinking agents with different molecular structures and reactivity," *Text. Res. J.*, vol. 70, no. 2, pp. 143–147, 2000.

[268] S. Perincek, I. Bahtiyari, A. Korlu, and K. Duran, "New techniques in cotton finishing," *Text. Res. J.*, vol. 79, no. 2, pp. 121–128, 2009.

[269] A. Yadav *et al.*, "Functional finishing in cotton fabrics using zinc oxide nanoparticles," *Bull. Mater. Sci.*, vol. 29, pp. 641–645, 2006.

[270] I. S. Tania and M. Ali, "Effect of the coating of zinc oxide (ZnO) nanoparticles with binder on the functional and mechanical properties of cotton fabric," *Mater. Today Proc.*, vol. 38, pp. 2607–2611, 2020, doi: 10.1016/j.matpr.2020.08.171.

[271] N. F. Attia, M. Moussa, A. M. F. Sheta, R. Taha, and H. Gamal, "Effect of different nanoparticles based coating on the performance of textile properties," *Prog. Org. Coatings*, vol. 104, pp. 72–80, 2017, doi: 10.1016/j.porgcoat.2016.12.007.

List of Publications

As a first author

1. Javed, A., Wiener, J., Saskova, J., & Müllerová, J. (2022). Zinc Oxide Nanoparticles (ZnO NPs) and N-Methylol Dimethyl Phosphonopropion Amide (MDPA) System for Flame Retardant Cotton Fabrics. Polymers, 14(16), 3414. (Impact Factor 5.0)

2. Javed, A., Wiener, J., Tamulevičienė, A., Tamulevičius, T., Lazauskas, A., Saskova, J., & Račkauskas, S. (2021). One step in-situ synthesis of zinc oxide nanoparticles for multifunctional cotton fabrics. Materials, 14(14), 3956. (Impact Factor 3.748)

3. Javed, A., Azeem, M., Wiener, J., Thukkaram, M., Saskova, J., & Mansoor, T. (2021). Ultrasonically Assisted In Situ Deposition of ZnO Nano Particles on Cotton Fabrics for Multifunctional Textiles. Fibers and Polymers, 22(1), 77-86. (Impact Factor 2.5)

4. Javed, A., Wiener, J., &Saskova, J. (2023). Sonochemical Route to Develop Flame Retardant Cotton Fabrics with Multifunctional Properties. In Proceedings of The Fiber Society 2023 Fall Meeting and Technical Conference Sustainability, Scalability, and Society: Advanced Fibers and Textiles. October 25–27, 2023, Drexel University, Philadelphia, Pennsylvania, USA. (Conference Proceedings)

5. Javed, A., Wiener, J., Saskova, J., & Militky, J. (2022). In-situ green synthesis of zinc oxide nanoparticles (ZnO NPs) onto the cotton fabrics by neem (azadirachta indica) leaf extract. In Proceedings of the 21th World Textile Conference-Autex 2022. Lodz, Poland. (Conference Proceedings)

6. Javed, A., Wiener, J., Saskova, J., & Militky, J. (2021). In-situ sonochemical synthesis of ZnO on cotton fabrics for antibacterial and self-cleaning properties. In Proceedings of the 20th World Textile Conference-Autex 2021. Guimarães, Portugal. (Conference Proceedings)

7. Javed, A., Musaddaq, A., & Šašková, J. (2019). UV protective fabrics by application of ball milled Neem tree leaves. In Proceedings the 19th World Textile Conference-Autex

2019. Ghent, Belgium. (Conference Proceedings)

As a co-author

8. Khan, M. Z., Militky, J., Petru, M., Tomková, B., Ali, A., Javed, A., ... & Křemenáková, D. (2021). Ultra-Fast Growth of ZnO Nanorods on Cotton Fabrics and Their Self-Cleaning and Physiological Comfort Properties. Coatings, 11(11), 1309. (Impact Factor 3.4)

9. Azeem, M., Javed, A., Morikawa, H., Noman, M. T., Khan, M. Q., Shahid, M., & Wiener, J. (2021). Hydrophilization of polyester textiles by nonthermal plasma. Autex Research Journal, 21(2), 142-149. (Impact Factor 1.944)

10. Mansoor, T., Hes, L., Skenderi, Z., Siddique, H. F., Hussain, S., & Javed, A. (2019). Effect of preheat setting process on heat, mass and air transfer in plain socks. The journal of the Textile Institute, 110(2), 159-170. (Impact Factor 2.17).

11. Fraz, A., Azeem, M., & Javed, A. (2018). Effect of Dyeing Temperature on the Shrinkage and Fastness Properties of Polyester/Acrylic Fabric. Pakistan Journal of Scientific & Industrial Research Series A: Physical Sciences, 61(2), 100-105. (Impact Factor 0.679)

12. Azeem, M., Javed, A., & Wiener, J. (2019). Hydrophilization of PETusing DBD plasma. In proceedings: ICCM22 2019. Melbourne, VIC: Engineers Australia, 2019: 430-436. (Conference Proceedings)

13. Mansoor, T., Hes, L., Skenderi, Z. S., & Javed, A. (2018). Effect of moisture content on thermophysiological properties of plain knitted socks followed by thermal resistance comparison among different skin models. In proceedings 22nd STRUTEX conference 2018, Liberec, Czech Republic. (Conference Proceedings)